Université Ferhat ABBAS Sétif 1

UNIVERSITÉ FERHAT ABBAS - SÉTIF 1

FACULTÉ DE TECHNOLOGIE

THÈSE

Présentée au Département de Génie des Procédés

Pour l'obtention du diplôme de

DOCTORAT EN SCIENCES

Option: Génie des Polymères
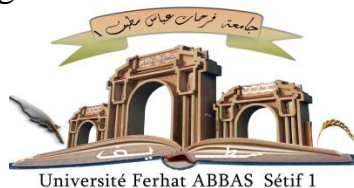
Par

BENABID Samira

THÈME

Polycondensation of an Elastomeric Polyester with an Antibacterial Activity in a Deep Eutectic Solvent : Numerical Study

Soutenue le 26/02/2022 devant le Jury:

BENACHOUR Djafer	**Professeur**	**Univ. Ferhat Abbas Sétif 1**	**Président**
HADDAOUI Nacereddine	**Professeur**	**Univ. Ferhat Abbas Sétif 1**	**Directeur de thèse**
BENGUERBA Yacine	**Professeur M.C.A.**	**Univ. Ferhat Abbas Sétif 1**	**Co-Directeur**
Hellati Abdelhak	**M.C.A.**	**Univ. BBA**	**Examinateur**
BOUKERROU Ammar	**Professeur**	**Univ. Bejaïa**	**Examinateur**
BAOUZ Toufik	**M.C.A.**	**Univ. Bejaïa**	**Examinateur**

الجمهورية الجزائرية الديمقراطية الشعبية

People's Democratic Republic of Algeria

Ministry of Higher Education and Scientific Research

Université Ferhat ABBAS Sétif 1

Ferhat ABBAS University Setif-1

Faculty of Technology

Department of Process Engineering

Option: Polymer Engineering

PhD Science

Presented by

BENABID Samira

Polycondensation of an Elastomeric Polyester with an Antibacterial Activity in a Deep Eutectic Solvent: Numerical Study

Presented and publicly supported on: 26 / 02 / 2022 to the jury Committee of :

BENACHOUR Djafer	Professor	Univ. Ferhat Abbas Sétif 1	President
HADDAOUI Nacereddine	Professor	Univ. Ferhat Abbas Sétif 1	Supervisor
BENGUERBA Yacine	Professor	Univ. Ferhat Abbas Sétif 1	Co-Supervisor
HELLATI Abdelhak	MCA	Univ. BBA	External Examiner
BOUKERROU Ammar	Professor	Univ. Béjaïa	External Examiner
BAOUZ Toufik	MCA	Univ. Béjaïa	External Examiner

In the memory of my parents

À la mémoire de mes parents

Acknowledgements

Abbreviations

B3LYP	Becke, 3-parameter, Lee–Yang–Parr
CA	Citric acid
Caf. A	Caffeic acid
CFCs	Chlorofluorocarbons
ChCl	Choline chloride ((2-Hydroxyethyl) trimethylammonium chloride)
COSMO-RS	Conductor-like Screening Model for Real Solvents
CSMs	Continuum Solvation Models
DDBAC	Dodecyldimethylbenzyl ammonium chloride
$D_{10}DO$	1,10-decanediol
DES	Deep eutectic solvent
DFT	Density functional theory
DNP	Double numerical polarization
HBA	Hydrogen bond acceptor
HBD	Hydrogen bond donor
HDES	Hydrophobic deep eutectic solvent
HES	Hydrophobic eutectic solvent
HOMO	Higher occupied molecular orbital
ILs	Ionic liquids
L.R.T.	Liquid at Room Temperature
LUMO	Lower unoccupied molecular orbital
NADES	Natural deep eutectic solvents
PBE	Perdew–Burke–Ernzerhof
PDCA	Poly (diol-citric acid) or Poly (diol-citrate)
$PD_{10}CA$	Poly (1,10-decanediol-citrate)
PVP	Poly (vinyl pyrrolidone)
QACs	Quaternary Ammonium Compounds
QCM	Quantum Chemical Methods
QSPR	Quantitative Structure Property Relationships
SCD	Surface Charge Density
SCF	Self-consistent field
SDF	Standard database format
SLE	Solid-liquid equilibrium
TMAC	Tetramethyl ammonium chloride

Nomenclature

γ_i^∞	activity coefficient at infinite dilution
η	chemical hardness
μ_x	electronic chemical potential
$\mu(\sigma)$	*σ-potentials*
$\rho(r)$	electronic density
σ	polarization charge density
σ_{hb}	threshold for hydrogen bonding
τ_{VdW}	van der Waals' fitting parameter
χ	Flory-Huggins' interaction parameter
ω	electrophilicity index
a_{eff}	effective contact area
c_{HB}	hydrogen bonding strength coefficient
E_{blend}	blend binding energy
E_{ij}	binding energy between constituents *i* and *j*
E_{HOMO}	higher occupied molecular orbital energy
E_{LUMO}	lower unoccupied molecular orbital energy
E_{HB}	hydrogen bonding energy
E_{MF}	electrostatic misfit energy
E_{VdW}	van der Waals' energy
E_{mix}	total mixture energy
$f(r)$	Fukui function
f^+	Cationic Fukui function
f^-	Anionic Fukui function
N	number of electrons
P^{x^i}	*σ-profile* of component *i*
R	gas constant
T	Temperature
$V(r)$	electronic potential
x_i	mole fraction of component *i*
Z	coordination number

General Introduction

The rapid growth of human civilization and industry over the past century has resulted in negative impacts on the environment due to excessive pollution and energy usage (Clarke et al., 2018). Solutions to these undeniable impacts are of paramount importance as means to reduce their effects on the planet. One of the leading origins of pollution is the excessive consumption of solvents in the chemical industry that are harmful and hazardous, hence being unsustainable (Clarke et al., 2018; Pollet et al., 2014). Conventionally, chemical processes rely on a disproportionate amount of organic solvents for several applications, which include: separation and purification, extraction, solvation, etc. (Clarke et al., 2018). Previous studies have estimated that these conventional organic solvents account for approximately eighty percent (80 %) of the total amount of chemicals utilized in generic processes (Anastas & Kirchhoff, 2002). Even though organic solvents have numerous advantages, they still have several unsustainable drawbacks that include high volatility, toxicity, flammability, and their inherent non-biodegradable nature, which pose risks to both environment and human health (Clarke et al., 2018; Francisco et al., 2013). In this sense, investigations and developments focusing on the design of new green and sustainable solvents became a hot research topic (Clarke et al., 2018; Pollet et al., 2014). They include the application of "designer solvents" like ionic liquids (ILs) (Petkovic et al., 2011) and, more recently, deep eutectic solvents (DESs) (Abbott et al., 2003; Smith et al., 2014).

ILs are generally defined as salts consisting of organic cations and anions having a freezing point below 100 $^{\circ}$C. In contrast, as with any relatively young field, a clear definition of DESs has not been settled on in the literature as of yet (Martins et al., 2019; Van Osch et al., 2020). According to MARTINS *et al.*, "a 'deep eutectic solvent' is a mixture of two or more pure compounds for which the eutectic point is below that of an ideal liquid mixture, presenting significant negative deviations from ideality (Martins et al., 2019). Additionally, the temperature depression should be such that the mixture is liquid at the operating temperature for a specific molar composition. DESs are generally described as a mixture of a hydrogen bond acceptor (HBA) and a hydrogen bond donor (HBD), and their formation occurs via a combination of entropy of mixing, VAN DER WAALS' interactions, and hydrogen bonding (Abbott et al., 2003; Smith et al., 2014). DESs possess several advantageous characteristics over conventional solvents, which have been extensively reported in the literature that include their simple synthesis, biodegradability, low volatility, and high tunability (Smith et al., 2014). In fact, their high tunability enables the preparation of natural eutectic solvents (NADESs) (Liu et al., 2018; Vanda et al., 2018), which can be prepared by simply mixing natural constituents together, such as sugars, organic acids, amino acids, or

choline derivatives. It has been estimated that the cost of preparing a NADES is generally about 80% lower than that of a typical IL (Gorke et al., 2010; Xu et al., 2016).

The characteristics of DESs which define their application field depend not only on the choice of their constituents, but also on their synergetic mixing effects (Hayyan et al., 2013, 2015; Mbous et al., 2017). Since their inception in 2003, DESs have been effectively explored in numerous fields that include separation (Hatab et al., 2020; Lemaoui et al., 2021; Warrag, Darwish, Abuhatab, et al., 2020; Warrag, Darwish, Adeyemi, et al., 2020), catalysis (Sapir et al., 2016), electrochemistry (Lemaoui et al., 2020), biochemistry (Pätzold et al., 2019), and polymer chemistry (Jablonský et al., 2019). However, originally, DES studies were focused only on hydrophilic DESs (Smith et al., 2014; Zhang et al., 2012). Nonetheless, a novel type of DESs coined as Hydrophobic DESs (HESs) has recently been discovered by VAN OSCH *et al.* in 2015 enabling the use of these novel solvents in a variety of new applications (Van Osch et al., 2015; Dwamena, 2019; van Osch et al., 2020).

There are many potential applications of DESs, for example, they can be used in the electrochemical treatment of metals, as reaction media for various industrial processes, biochemical processes, drug delivery, etc. Since DESs serve as an environmentally friendly alternative to organic solvents, their field of applications can be potentially further enlarged in the next years. Figure 1 bellow shows the publication numbers by a percentage in each research field from Scopus.
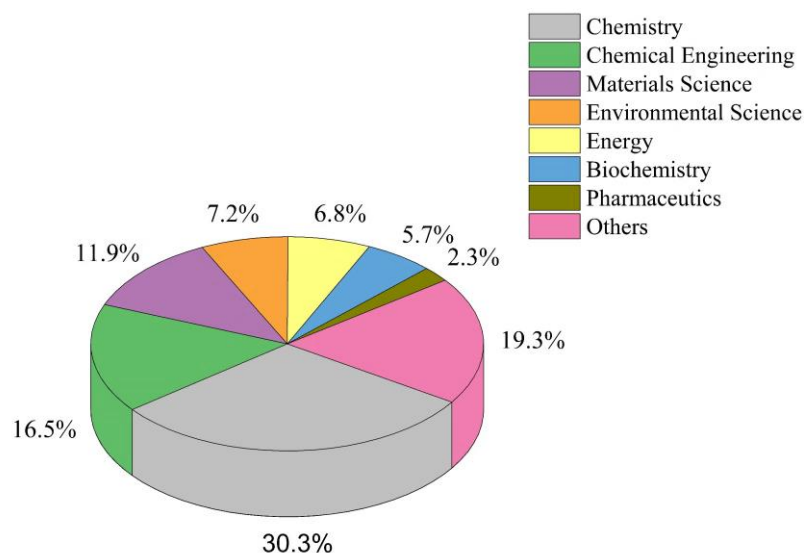
Figure 1. The publication number by percentage in each research field (Roda et al., 2019).

In polymer technology, the role of DESs can be summarized in two main ways: the DES functions as an inert solvent without influencing the conversion of the monomer to a polymer, but instead, affecting the kinetics of conversion, and one of the DES constituents can polymerize with an external monomer, while the other constituent role is to act as an additive enhancing a specific property of the resulting polymer. Hence, the use of DESs may provide flexibility to the polymer as they can essentially be utilized as monomers (Mota-Morales et al., 2018), additives/modifiers (Jablonský et al., 2019), synthesis media (Stefanovic et al., 2019), and synthesis initiators (García-Argüelles et al., 2015).

Despite the recent birth of DESs, their application in green polymer chemistry is developing at a fast pace (Jablonský et al., 2019; Roda et al., 2019). Details on the utilization of DESs in polymer technology are reported in the literature (Jablonský et al., 2019).

In this framework, the present study attempts to numerically study the feasibility of developing an antibacterial floor coating film for food trays made of benzalkonium salt-filled biodegradable polyester. The synthesis modelled is supposed to occur in a DES that plays not only the role of green medium and catalyst for the polymerization process, but also provides the antibacterial filler through the HBA moiety, and the second monomer for the polyester through the HBD part.

Since the use of DESs is recent in polymer technology, making them not well known, the first chapter of the present manuscript was dedicated to fundamentals on DESs. Followed by a second chapter in which polycondensation and DES-assisted polycondensation are viewed to highlight the advantages gained by the polymerization process when using DESs.

In chapter three, the numerical approaches and methods governing the molecular modeling applied for the geometry optimization of molecules are described. The energies contributing at sub-atomic, atomic and molecular scale are determined, and the laws for calculating of appropriate physicochemical properties of DESs, polymers and composites are given to help understand their thermodynamic behavior.

In the fourth and last chapter, the numerical data and equations provided in chapter three, are exploited applying continuum solvation models (CSMs) as a class of the Quantum Chemical Methods (QCM), and the Density Functional Theory (DFT) on:

i) First, some DESs selected to make their knowledge easier (since the use of DESs in polymer technology is recent);

ii) Then, a (1:3) ratio (dodecyldimethylbenzyl ammonium chloride:1,10-decanediol (DDBAC:D10DO)) DES, and poly(1,10-decanediol-citrate)/DDBAC composite, specifically

chosen as antibacterial biodegradable coating film for food trays, to understand the DES-assisted green synthesis step mechanism. The modelling results have been exploited to highlight the advantage of the use of DESs over conventional organic solvents.

References

Abbott, A. P., Capper, G., Davies, D. L., Rasheed, R. K., & Tambyrajah, V. (2003). Novel solvent properties of choline chloride/urea mixtures. *Chemical Communications*, *1*, 70–71. https://doi.org/10.1039/b210714g

Anastas, P. T., & Kirchhoff, M. M. (2002). Origins, current status, and future challenges of green chemistry. *Accounts of Chemical Research*, *35*(9), 686–694. https://doi.org/10.1021/ar010065m

Clarke, C. J., Tu, W. C., Levers, O., Bröhl, A., & Hallett, J. P. (2018). Green and Sustainable Solvents in Chemical Processes. *Chemical Reviews*, *118*(2), 747–800. https://doi.org/10.1021/acs.chemrev.7b00571

Dwamena, A. K. (2019). Recent advances in hydrophobic deep eutectic solvents for extraction. *Separations*, *6*(1), 9-23. https://doi.org/10.3390/separations6010009

Francisco, M., Van Den Bruinhorst, A., & Kroon, M. C. (2013). Low-transition-temperature mixtures (LTTMs): A new generation of designer solvents. *Angewandte Chemie - International Edition*, *52*(11), 3074–3085. https://doi.org/10.1002/anie.201207548

García-Argüelles, S., García, C., Serrano, M. C., Gutiérrez, M. C., Ferrer, M. L., & Del Monte, F. (2015). Near-to-eutectic mixtures as bifunctional catalysts in the low-temperature-ring-opening-polymerization of ε-caprolactone. *Green Chemistry*, *17*(6), 3632–3643. https://doi.org/10.1039/c5gc00348b

Gorke, J. T., Srienc, F., & Kazlauskas, R. J. (2010). Deep eutectic solvents for Candida antarctica lipase B-catalyzed reactions. *ACS Symposium Series*, *1038*, 169–180. https://doi.org/10.1021/bk-2010-1038.ch014

Hatab, F. A., Darwish, A. S., Lemaoui, T., Warrag, S. E. E., Benguerba, Y., Kroon, M. C., & Alnashef, I. M. (2020). *Extraction of Thiophene , Pyridine , and Toluene from n‑Decane as a Diesel Model Using Betaine-Based Natural Deep Eutectic Solvents*. https://doi.org/10.1021/acs.jced.0c00579

Hayyan, M., Hashim, M. A., Hayyan, A., Al-Saadi, M. A., AlNashef, I. M., Mirghani, M. E. S., & Saheed, O. K. (2013). Are deep eutectic solvents benign or toxic? *Chemosphere*, *90*(7), 2193–2195. https://doi.org/10.1016/j.chemosphere.2012.11.004

Hayyan, M., Looi, C. Y., Hayyan, A., Wong, W. F., & Hashim, M. A. (2015). In Vitro and in Vivo toxicity profiling of ammonium-based deep eutectic solvents. *PLoS ONE*, *10*(2), 1–18. https://doi.org/10.1371/journal.pone.0117934

Jablonský, M., Škulcová, A., & Šima, J. (2019). Use of deep eutectic solvents in polymer chemistry–a review. *Molecules*, *24*(21), 1–33. https://doi.org/10.3390/molecules24213978

Lemaoui, T., Benguerba, Y., Darwish, A. S., Hatab, F. A., Warrag, S. E. E., Kroon, M. C., & Alnashef, I. M. (2021). Simultaneous dearomatization, desulfurization, and denitrogenation of diesel fuels using acidic deep eutectic solvents as extractive agents: A parametric study. *Separation and Purification Technology*, *256*(3), 117861. https://doi.org/10.1016/j.seppur.2020.117861

Lemaoui, T., Darwish, A. S., Hammoudi, N. E. H., Abu Hatab, F., Attoui, A., Alnashef, I. M., & Benguerba, Y. (2020). Prediction of Electrical Conductivity of Deep Eutectic Solvents Using COSMO-RS Sigma Profiles as Molecular Descriptors: A Quantitative Structure–Property Relationship Study. *Industrial & Engineering Chemistry Research*, *59*(29), 13343–13354. https://doi.org/10.1021/acs.iecr.0c02542

Liu, Y., Friesen, J. B., McAlpine, J. B., Lankin, D. C., Chen, S. N., & Pauli, G. F. (2018). Natural Deep Eutectic Solvents: Properties, Applications, and Perspectives. *Journal of Natural Products*, *81*(3), 679–690.
https://doi.org/10.1021/acs.jnatprod.7b00945

Martins, M. A. R., Pinho, S. P., & Coutinho, J. A. P. (2019). Insights into the Nature of Eutectic and Deep Eutectic Mixtures. *Journal of Solution Chemistry*, *48*(7), 962–982.
https://doi.org/10.1007/s10953-018-0793-1

Mbous, Y. P., Hayyan, M., Wong, W. F., Looi, C. Y., & Hashim, M. A. (2017). Unraveling the cytotoxicity and metabolic pathways of binary natural deep eutectic solvent systems. *Scientific Reports*, *7*, 1–14.
https://doi.org/10.1038/srep41257

Mota-Morales, J. D., Sánchez-Leija, R. J., Carranza, A., Pojman, J. A., del Monte, F., & Luna-Bárcenas, G. (2018). Free-radical polymerizations of and in deep eutectic solvents: Green synthesis of functional materials. *Progress in Polymer Science*, *78*, 139–153.
https://doi.org/10.1016/j.progpolymsci.2017.09.005

Pätzold, M., Siebenhaller, S., Kara, S., Liese, A., Syldatk, C., & Holtmann, D. (2019). Deep Eutectic Solvents as Efficient Solvents in Biocatalysis. *Trends in Biotechnology*, *37*(9), 943–959.
https://doi.org/10.1016/j.tibtech.2019.03.007.

Petkovic, M., Seddon, K. R., Rebelo, L. P. N., & Pereira, C. S. (2011). Ionic liquids: A pathway to environmental acceptability. *Chemical Society Reviews*, *40*(3), 1383–1403.
https://doi.org/10.1039/c004968a.

Pollet, P., Davey, E. A., Ureña-Benavides, E. E., Eckert, C. A., & Liotta, C. L. (2014). Solvents for sustainable chemical processes. *Green Chemistry*, *16*(3), 1034–1055.
https://doi.org/10.1039/c3gc42302f.

Roda, A., Matias, A. A., Paiva, A., & Duarte, A. R. C. (2019). Polymer Science and Engineering Using Deep Eutectic Solvents. *Polymers, 11*(5), 912–933.
https://doi.org/10.3390/polym11050912.

Sapir, L., Stanley, C. B., & Harries, D. (2016). Properties of Polyvinylpyrrolidone in a Deep Eutectic Solvent. *Journal of Physical Chemistry A*, *120*(19), 3253–3259.
https://doi.org/10.1021/acs.jpca.5b11927.

Smith, E. L., Abbott, A. P., & Ryder, K. S. (2014). Deep Eutectic Solvents (DESs) and Their Applications. *Chemical Reviews*, *114*(21), 11060–11082.
https://doi.org/10.1021/cr300162p

Stefanovic, R., Webber, G. B., & Page, A. J. (2019). Polymer Solvation in Choline Chloride Deep Eutectic Solvents Modulated by the Hydrogen Bond Donor. *Journal of Molecular Liquids*, *279*, 584-593.
https://doi.org/10.1016/j.molliq.2019.02.004

Van Osch, D. J. G. P., Dietz, C. H. J. T., Warrag, S. E. E., & Kroon, M. C. (2020). The Curious Case of Hydrophobic Deep Eutectic Solvents: A Story on the Discovery, Design, and Applications. *ACS Sustainable Chemistry and Engineering*, *8*(29), 10591–10612.
https://doi.org/10.1021/acssuschemeng.0c00559

Van Osch, D. J. G. P., Zubeir, L. F., Van Den Bruinhorst, A., Rocha, M. A. A., & Kroon, M. C. (2015). Hydrophobic deep eutectic solvents as water-immiscible extractants. *Green Chemistry*, *17*(9), 4518–4521.
https://doi.org/10.1039/c5gc01451d

Vanda, H., Dai, Y., Wilson, E. G., Verpoorte, R., & Choi, Y. H. (2018). Green solvents from ionic liquids and deep eutectic solvents to natural deep eutectic solvents. *Comptes Rendus Chimie*, *21*(6), 628–638.
https://doi.org/10.1016/j.crci.2018.04.002

Warrag, S. E. E., Darwish, A. S., Abuhatab, F. O. S., Adeyemi, I. A., Kroon, M. C., & Alnashef, I. M. (2020). Combined Extractive Dearomatization, Desulfurization, and Denitrogenation of Oil Fuels Using Deep Eutectic Solvents: A Parametric Study. *Industrial and Engineering Chemistry Research*, *59*(25), 11723–11733. https://doi.org/10.1021/acs.iecr.0c01360

Warrag, S. E. E., Darwish, A. S., Adeyemi, I. A., Hadj-Kali, M. K., Kroon, M. C., & Alnashef, I. M. (2020). Extraction of pyridine from n-alkane mixtures using methyltriphenylphosphonium bromide-based deep eutectic solvents as extractive denitrogenation agents. *Fluid Phase Equilibria*, *517*, 112622. https://doi.org/10.1016/j.fluid.2020.112622

Xu, G. C., Ding, J. C., Han, R. Z., Dong, J. J., & Ni, Y. (2016). Enhancing cellulose accessibility of corn stover by deep eutectic solvent pretreatment for butanol fermentation. *Bioresource Technology*, *203*, 364–369. https://doi.org/10.1016/j.biortech.2015.11.002

Zhang, Q., De Oliveira Vigier, K., Royer, S., & Jérôme, F. (2012). Deep eutectic solvents: Syntheses, properties and applications. *Chemical Society Reviews*, *41*(21), 7108–7146. https://doi.org/10.1039/c2cs35178a

Chapter I: Deep Eutectic Solvents

I.1. Introduction

Exposure to organic solvents leads to health hazards including nervous system toxicity, respiratory impairment, reproductive damage, kidney and liver damage, cancer and dermatitis. Nevertheless, they remain widely used due to their importance in almost all chemical processes. Owing to these multiple disadvantages and the serious threat toward environment, several approaches have been considered as replacement to these solvents for use in green technology. These approaches include the use of: *i)* easy recyclable supercritical carbon dioxide ($scCO_2$) or fluorinated solvents, *ii)* solvent free processes, and *iii)* non-volatile systems such as ionic liquids (ILs) and deep eutectic solvents (DESs) (Roda et al., 2019).

In the last approach, non-volatile systems covered first ILs. However, since most of them were found toxic, their synthesis and use became less valued. This disadvantage gave rise to DESs as novel greener analogs (Liu et al., 2019; Vanda et al., 2018). As substitutes to ILs, DESs are much cheaper, non-toxic, most of them are biodegradable and biocompatible. Also, unlike ILs, they need no purification since their individual components are pure, which overpasses waste disposal encountered with ILs after purification (Mokhtary, 2019).

This chapter reports some literature works, including definitions and concepts related to DESs and respective studies to date.

I.2. Fundamentals

Introducing the term "eutectic" dates back to 1884 (Guthrie, 1884). However, the first article on deep eutectic solvents without a metal salt was only published in 2003 (Abbott et al., 2003).

In general, at temperatures lower than 150 °C (often, at room temperature), DESs are at liquid state. DESs exhibit physical properties similar to those of ILs with the difference that they are much cheaper and environmentally friendlier. This introduces DESs as an alternative for both conventional solvents and ILs in many applications (Zhang et al., 2012). Even though DESs are well known as a new class of ILs and both share similar physical characteristics, it is important to notice that they form two different types of solvents due to their different chemical properties (Smith et al., 2014).
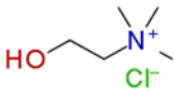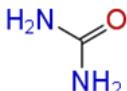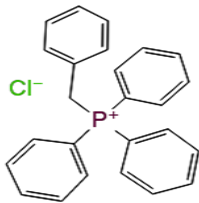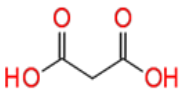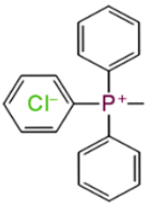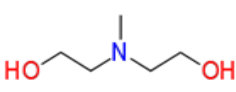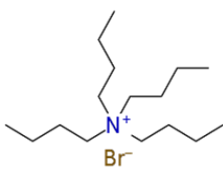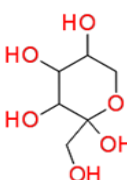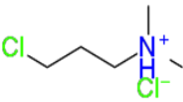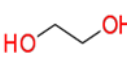
ABBOTT *et al.* defined DESs as being mixtures of quaternary ammonium salts with metal salts producing low lattice energy and freezing point systems (Abbott et al., 2003). Eutectic complexes may also involve halide salts as hydrogen bond acceptors with hydrogen bond donors such as acids, amines and alcohols.

SMITH *et al.* provided a more global definition describing them as eutectic mixtures of LEWIS or BRØNSTED acids and bases containing anionic and/or cationic species (Smith et al., 2014). The authors established a classification regarding the general formula of the DES as seen in Table I.1. Type I DESs also include a large range of metal chloride ionic liquids, such as imidazole chloroaluminates (Wilkes, 2002). Type II and III are formed by a quaternary ammonium salt with either a metal salt hydrate or a hydrogen-bond donor. While type IV is a metal salt-hydrogen bond donor complex (Smith et al., 2014). It is to be noted that the DESs studied in the present work belong to type III of this classification.

Table I.1. General formulae of the DES types (Smith et al., 2014).

Type	Constituents	General formula	Terms
Type I	Metal salt + Organic salt	$Cat^+X^-zMCl_x$	M = Zn, Sn, Fe, Al, Ga, In
Type II	Metal salt hydrate + Organic salt	$Cat^+X^-zMCl_x.yH_2O$	M = Cr, Co, Cu, Ni, Fe
Type III	Hydrogen bond donor + Organic salt	Cat^+X^-zRZ	Z = $CONH_2$, COOH, OH
Type IV	Metal salt + Hydrogen bond donor	MCl_x+RZ	M = Al, Zn & Z = $CONH_2$, OH

DESs are liquid at ambient temperature (Sapir et al., 2016). They form through a non-covalent mechanism involving hydrogen bonding, electrostatic and/or VAN DER WAALS' interactions (Stefanovic et al., 2019; Zdanowicz et al., 2018). Some examples of HBAs and HBDs as DES constituents are shown in Figure I.1.

HBA	HBD

ChCl [a]   Urea

BTPC [b]   MA [c]

MTPC [d]   MDEA [e]

TBAB [f]   D-Fructose

DMAPCHC [g]   EG [h]

[a] : Choline chloride, [b] : Benzyltriphenylphosphonium chloride, [c] : Malonic acid, [d] : Methyltriphenylphosphonium chloride, [e] : N-Methyldiethanol-amine, [f] : Tributylamine bromide, [g] : 3-(Dimethylamino)propyl Chloride Hydrochloride, and [h] : Ethylene Glycol.

Figure I.1. Some examples of HBAs and HBDs forming DESs (Jablonský et al., 2019).

More recently, a class of DESs has been prepared from primary metabolites of plants, which are called natural deep eutectic solvents (NADESs) (Choi et al., 2011). These mixtures intervene in the biosynthesis of water-insoluble molecules within cellular processes (Dai et al., 2013). Since then, they have been extensively used in polymer processes. It is often difficult to distinguish a NADES from a DES, since some of their components are both bio- and petroleum-based (certain acids, alcohols, diols and polyols) (Gómez et al. 2019). Table I.2 lists some NADESs as follows:

Table I.2. Examples of NADESs (Choi et al., 2011).

NADES (HBA : HBD)	Molar Ratio
Choline chloride : Maleic acid	1:1, 2:1, 3:1
Choline chloride : Aconitic acid	1:1
Malic acid : Glucose	1:1
Malic acid : Fructose	1:1
Malic acid : Sucrose	1:1
Citric acid : Trehalose	2:1
Citric acid : Sucrose	1:1
Maleic acid : Glucose	4:1

In polymer technology, GENIES and TSINTAVIS (Genies & Tsintavis, 1985) were the first to prepare electrochemically polyaniline in NH_4F-HF as low melting mixture (LMM) which they compared to aqueous and organic media. They stated that the synthesis involving the LMM gave an almost 100% yield polymer with a better nucleation, adherence and electrochemical properties.

In 1996, DHANALAKSHMI *et al.* prepared semiconducting electroactive films of polyaniline and polypyrrole by electrochemical synthesis in a ternary eutectic mixture. The syntheses gave polymers whose structures were similar to those prepared in aqueous and organic media (Dhanalakshmi et al., 1996).

Upon the knowledge acquired on LMMs and ILs, PÉREZ-GARCÍA *et al.* (Pérez-García et al., 2016) used deep eutectic solvents of choline chloride (ChCl) with either acrylic or methacrylic acid to prepare polyacrylic and polymethacrylic acids via frontal polymerization. Interestingly, the results they reaped showed higher performance of ChCl-based eutectics than both conventional solvents and ionic liquids. This demonstration was auspicious (promising) and opened doors toward the use of DESs in polymer technology (Roda et al., 2019).

Despite their recent birth, harnessing deep eutectic solvents in polymer chemistry is developing at a fast pace in green chemistry (Roda et al., 2019). They are used as solvents (Sapir et al., 2016; Stefanovic et al., 2019), polymer modifiers or plasticizers (Wong et al., 2017), media for electro-polymerization (Hosu et al., 2017; Prathish et al., 2016), functional monomers for extraction and separation in polymer processes (Wang, Li, and Chen 2018; Tang, Zhang, and Row 2015), and in syntheses such as frontal polymerization (Mota-Morales et al., 2018), ring opening polymerization as monomers (Coulembier et al., 2012) and initiators (García-Argüelles et al., 2015), and emulsion polymerization and polycondensation (Carriazo et al., 2012; García-Argüelles et al., 2013).

I.3. Environmental Aspect

Most organic solvents such as chlorofluorocarbons (CFCs) and volatile organic compounds (VOCs) are regarded as toxic and threat for environment and human health. They were banned many decades ago, since CFCs cause ozone depletion and VOCs produce photochemical smog (Blusztajn, 1998; Clark & Tavener, 2007).

ANASTAS and KIRCHHOFF funded acceptance of solvents within green chemistry upon twelve principles. The chemicals to be approved had to fulfill the following acquirements (Anastas & Kirchhoff 2002):

a. Availability: Solvents must be available on a large scale, so that there would be no need to use the conventional chemicals.

b. Price: Novel solvents have to be competitive in terms of price, and costs should ensure sustainability of the chemical process. The probability of choosing the banned solvents must be eliminated.

c. Recyclability: The solvents have to be fully recycled using eco-friendly procedures.

d. Grade: In order to avoid energy-consuming purification, technical grade solvents are preferred. DESs need no purification since their individual components are pure (Mokhtary, 2019).

e. Synthesis: Preparation of the solvents should be through an energy-saving process and the synthesis reaction should be highly atom-efficient.

f. Toxicity: risk for human health and environment safety must be reduced; solvents have to exhibit a negligible toxicity, especially when used for personal and home care products, paints, etc.

g. Biodegradability: Green solvents must not produce toxic metabolites and should be biodegradable.

h. Performance: to be eligible, green solvents should show higher, or at least, similar performances compared to conventional solvents.

i. Stability: During any chemical process, the solvent must be thermally and electrochemically stable.

j. Flammability: Green solvents should be non-flammable to ensure a safe manipulation.

k. Storage: The storage of the solvent should be easy and should fulfil all legislation for an easy transportation.

l. Renewability: Concerning the carbon footprint, the production of green solvents must use renewable raw materials.

Ionic liquids were first reported as alternative to conventional organic solvents till their toxicity and low biodegradability became confirmed and thus contested. Interestingly, the well understanding of their properties, fairly similar to those of deep eutectic solvents, facilitated the tunability of the latter for specific applications (Deetlefs & Seddon, 2010; Ruß & Burkhard, 2012).

On the other hand, the low vapor pressure of DESs decreases considerably their emission to the atmosphere. In the liquid state, most DESs are miscible with water except hydrophobic eutectics (HESs) tailored for specific uses. Their components are non-toxic, natural-based and environmentally benign substances. For instance, ChCl (which is often used in DESs and LMMs) is a biocompatible quaternary ammonium salt known as former vitamin B4, used in animal feed (Frauenkron et al., 2001). It has some important key functions in the human body, such as a precursor for phospholipids and acetylcholine. Urea (which is another important molecule in DESs) is not toxic, since it is produced and used by the body and can be easily excreted in the urine (Leng et al., 2021).

Also, eco-friendly and biodegradable organic compounds, such as carboxylic acids (citric acid, oxalic acid, malonic acid, succinic acid, etc.), amino acids or sugars (glucose, sorbitol, fructose, etc.), can be part of DESs (Abbott et al., 2004; Choi et al., 2011; Francisco et al., 2012).

In addition to the fact that deep eutectic solvents are green products, their use is advantageous since they allow to reduce reagents for reaction (due to the multiple roles they play), replace organic solvents showing improved performance in solvation capacity, improve the yield of reaction reducing by-products, and enable recycling of remnant compounds (Mota-Morales et al., 2011).

In polymer syntheses, DESs play several roles enhancing reaction yields, which avoids chemical disposal and by-products. They may provide monomers through the hydrogen bond donor moiety, while the hydrogen bond acceptor component is either recovered and thus may be used more than once (Mota-Morales et al., 2011), or serves as additive (filler, reinforcing agent, plasticizer, etc.) to the polymer (Roda et al., 2019).

I.4. Properties of Deep Eutectic Solvents

The importance attached to DESs, reflected by the exponentially increasing reported studies, is motivated by their unique characteristics such as negligible toxicity and volatility, biodegradability, biocompatibility, non-flammability, ease of production, and purity (Roda et al., 2019). DESs with unknown properties are difficult to tailor for a specific application. This makes necessary the assessment of the most relevant parameters.

I.4.1. Freezing Point

The main particularity of the eutectic mixtures is their freezing point. The eutectic is acquired at specific molar compositions of hydrogen bond donor and hydrogen bond acceptor. In general, a eutectic mixture is a system that solidifies at very low temperatures (often liquid at room temperature) and at specific compositions, showing a sharp depression of the melting point, as shown in Figure I.2 (Fischer, 2015).
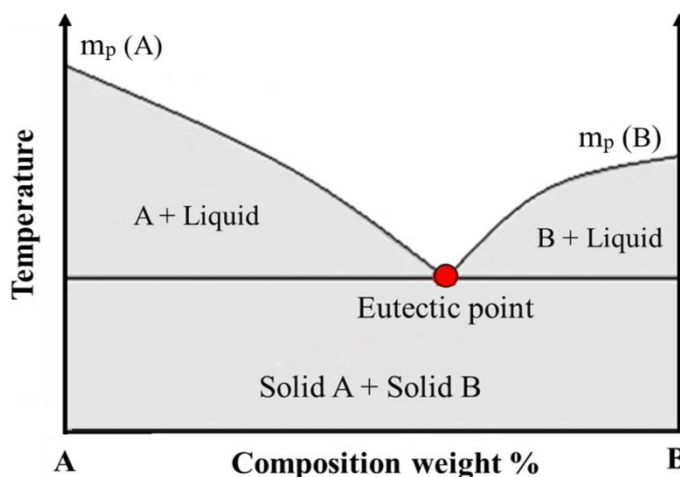
Figure I.2. Phase diagram of a eutectic binary system mixture (Fischer, 2015).

The first study conducted on ChCl/urea mixtures with several molar fractions stated that the eutectic occurs with 1:2 molar ratio for which the freezing point decreases to 12 °C, which is much lower than those of the separate components ($T_{m_{ChCl}}$ = 302 °C and $T_{m_{Urea}}$ = 133 °C). The results reported by the authors are gathered in Figure I.3 (Abbott et al., 2003).
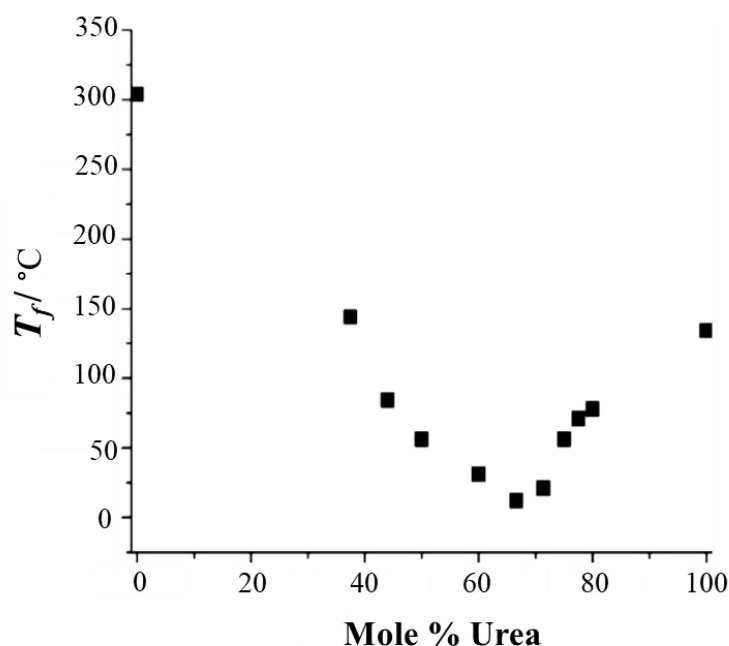
Figure I.3. Freezing point values for different compositions of urea mixed with choline chloride (Abbott et al., 2003).

This decrease observed in the melting point is caused by the hydrogen bonds formed between the HBD molecule and the halide anion of the HBA, responsible of the charge delocalization (Abbott et al., 2003; Rengstl et al., 2014). In other terms, when the hydrogen bond donor interacts with the halide (anion) of the hydrogen-bond acceptor, it exerts an attractive force causing a diminution of the attraction between the anion and cation of the HBA.

I.4.2. Reactivity

As mentioned above, when mixing choline chloride and urea with a molar ratio of 1:2, ABBOTT *et al.* (Abbott et al., 2003) noticed a depression in the melting point of the resulting DES to 12 °C, whereas those of ChCl and urea are 302 and 133 °C, respectively. To provide a plausible explanation, SUN *et al*. (Sun et al., 2013) compared the interaction energies of the cation and anion present in the ChCl salt before and after mixing it with urea. They found that the incorporation of hydrogen bond donor reduces the interaction energy between the cation and anion of the salt and increases the interaction energy between the anion of ChCl and the HBD, which lowers significantly the melting point of the mixture.

Considering the presence of polymers in DES media, interaction energy calculations become more complex. Accordingly, the DES-polymer intermolecular interactions were found to play an important role in the solvation capacity of the DES toward the polymer.

Indeed, in a study carried out by SAPIR *et al.*, 1:2 molar ratio choline chloride:urea DES was compared to water in solvating polyvinylpyrrolidone (PVP). Although both solvents showed good solvating capacity for PVP, FLORY-HUGGINS Solution Theory favored the DES. The interactions within the DES were more comparable to those in DES-polymer than in water-polymer systems (Sapir et al., 2016).

I.4.3. Vapor Pressure

The low volatility is the main property that makes DESs an excellent alternative to organic solvents. The higher the volatility, the more toxic the solvent and more hazardous in handling. This property is expressed in terms of vapor pressure.

I.4.4. Density

Most DESs are denser than water (Khandelwal et al., 2016). Many researchers reported values of DES density ranging between 1.04 and 1.63 g cm^{-3} (Ruß & Burkhard, 2012). In 2012, ZHANG *et al.* reported that two DESs prepared from the same HBA and different HBDs had different densities. According to the authors, this might be due to a different molecular organization of the DESs. Besides, they noticed that these densities were higher than those of pure HBDs. The authors attributed this phenomenon to the hole theory. When a HBA and a HBD are mixed, the average hole radius decreases resulting in an obvious increase in the DES density compared to that of neat HBD (Zhang et al., 2012).

I.4.5. Viscosity

The viscosity has a significant effect on the mass transport phenomena and ionic conductivity of DESs (Aissaoui et al., 2017). In comparison with organic solvents, DESs usually exhibit relatively high viscosities at room temperature (> 100 cP) due to the prevailing hydrogen bond network between the components, which results in a limited mobility of free species (HBA ion) within the DES (Abbott et al., 2004; Fischer, 2015). The large halide ion size, electrostatic or VAN DER WAALS' interactions may also contribute to the high viscosity of DESs (Zhang et al., 2012). Therefore, DESs are used in solutions with water or other solvents for specific needs.

DES viscosity was also reported to depend on the chemical structure of the HBD. For example, di-acid-based DESs are much more viscous than monoacid-based ones. In addition, the presence of one carboxylic or hydroxyl group leads to an increase of the viscosity. Regarding the size of the alkyl chain, the longer the hydrocarbon chain, the higher the viscosity.

As expected, it has also been found that the viscosity of DESs decreases with increasing temperature according to a logarithmic equation based on ARRHENIUS model (Fischer, 2015). The viscosity is the most important parameter considered in selecting DESs for extraction use. Higher extraction yields are achieved by DESs with lower viscosities (Mulia, Fauzia, and Krisanti 2019).

In polymer syntheses, highly viscous DESs are required to ensure high purity and conversion of polymers. DESs with high viscosity are chosen as monomers for polymer synthesis (Mota-Morales et al., 2011). Also, the rate of electro-polymerization which is the synthesis of conductive polymers, was found to depend strongly on the viscosity and conductivity of the DES. In this case, DESs with lower viscosities and higher conductivities are suitable (Fischer, 2015).

I.4.6. Polarity

The polarity is the second parameter considered after the viscosity in determining the extraction capacity of a DES. Both parameters are adjustable depending on the HBD structure. Lower polarities of DESs allow higher yields in extraction process. In a study conducted by MULIA *et al.* on several ChCl:alcohol DESs used as solvents on the extraction of xanthones from the pericarp of *Garcinia mangostana L.*, the authors realized a yield of 3.27 % using ChCl on ethanol mole ratio of 1:1, which is the highest yield to date. Accordingly, the polarity of ChCl:Ethanol DES was the lowest among all (Mulia, Fauzia, and Krisanti 2019).

I.4.7. Conductivity

The conductivity is strongly related to the viscosity (Fischer, 2015), which depends on the composition of the DES. At room temperature, DESs with high viscosity show conductivities lower than 2 mS.cm^{-1} (Zhang et al., 2012).

In polymer synthesis, ZOU and HUANG (Zou & Huang, 2018) prepared anilinium salt:glycol DESs with various ratios in search of the most appropriate medium for polyaniline (PANI) electro-polymerization. The most fitting eutectic was that with the highest conductivity and the lowest viscosity.

In a study conducted by FERNANDES *et al.* (Fernandes et al., 2012) the rates of PANI electro-polymerization in DESs of choline chloride with either ethylene glycol, urea or glycerol were shown to depend strongly on the viscosity and conductivity of the DESs.

I.5. Applications of Deep Eutectic Solvents

The chemical properties of DESs dissimilar to those of ILs, suggest completely different applications (Smith et al., 2014). Many recent works reported the importance of DESs in various applications in green chemistry. Most DESs are excellent solvents for a wide variety of materials including salts, proteins, drugs, amino acids, surfactants, sugars and polysaccharides. Their ability to dissolve CO_2 makes them very attractive for gas purification, catalysis, and chemical fixation of CO_2 (Li et al., 2008; Su et al., 2009). This can be attributed to their strong ability of donating or accepting electrons. DESs can also dissolve various metal oxides extending their use to electrochemical processes. In addition, DESs find an interesting application in the purification of biodiesel (Durand et al., 2013). Some applications of DESs are presented in this section.

I.5.1. Metal processing

The metal processes using DESs include electrochemical deposition, metal extraction, catalyst aldol reactions and synthesis of zeolite analogues (Sapir et al., 2016). In a study on the influence of ChCl-based DESs on the electroactivity of polyaniline-based films, a DES with a dicarboxylic acid (oxalic acid) as HBD was found more efficient as electrolyte than another with a diol (ethylene glycol) in the film longevity and charge storage stability after successive redox cycles. The second DES needed the addition of a protic source (sulfuric acid) to show comparable efficacy (Hillman et al., 2017).

I.5.2. Bioenergy

Several studies reported the use of DESs for the production of glycerol free biodiesel fuel (Shahbaz et al. 2011). Glycerol present in the fuel is responsible of acrolein emission and causes engine corrosion. Acrolein formed when glycerol loses two water molecules, is hazardous for environment and human health. The DESs showed exceptional effectiveness in glycerol separation from the biodiesel, which fulfills international standards (Hayyan et al., 2014).

I.5.3. Polymer technology

Harnessing DESs for polymeric applications is recent, since the first article was published in 2011 (Mota-Morales et al., 2011). The reported studies corresponding to the use of DESs in polymer technology involve synthesis, solubilization, extraction and polymer modification, and more recently DES incorporation in the polymer formulation (Roda et al., 2019).

I.5.3.1. As polymerization media

The first eutectic mixture-assisted polymerization was reported in 1985 (Genies & Tsintavis, 1985). Polyaniline electrochemically synthesized in NH_4F-HF was compared to that prepared in aqueous and organic media. The authors stated that the synthesis involving the eutectic mixture gave an almost 100% yield polymer with a better nucleation, adherence and electrochemical properties.

In 1996, Dhanalakshmi *et al.* (Dhanalakshmi et al., 1996) prepared semiconducting electroactive films of polyaniline and polypyrrole by electropolymerization in acetamide-urea-ammonium nitrate ternary mixture. The structures of the polymers were found similar to those of their analogs prepared in aqueous solutions. Polyaniline films showed higher electroactivity and electrochemical stability compared to polypyrrole in DES and their analogs synthesized in aqueous solutions. The highly conducting polyaniline and polypyrrole have found applications in rechargeable batteries, photovoltaic and electroluminescent devices, microwave absorbers, temperature sensors and capacitors.

I.5.3.2. As solvents

Several investigations reported the high efficacy of DESs in solvating a wide range of products, including insoluble or poorly soluble products in water and conventional solvents. Abbott *et al.* (Abbott et al., 2003) showed an unusual solvation power of the eutectic formed by 1:2 (molar ratio) hydroxyethyl trimethylammonium chloride (choline chloride or ChCl) with urea. This DES has also been used by Sapir *et al.* (Sapir et al., 2016) in a comparative study to water as solvents for poly(vinyl pyrrolidone) (PVP). Although dissolved polymer conformation showed that both were good solvents, the thermodynamic analysis based on Flory-Huggins Solution Theory has proved that the individual intermolecular interactions of PVP were more comparable to those of the DES than water, which favors DES-PVP interactions.

The solvation capacity of a DES also depends on its hydrogen networking. Higher hydrogen bond densities per unit volume increase the DES solvation capacity (Stefanovic et al., 2019).

The type of hydrogen bond donor also influences the solvation quality of a DES for polymers. This has been demonstrated by Chen and his coworkers (Chen et al., 2017) who studied the solvating capacity of 1:2 (molar ratio) ethylammonium bromide (EAB):glycerol and EAB:ethylene glycol toward polyethylene oxide (PEO). The conformation of the

dissolved polymer studied by Small Angle Neutron Scattering showed higher solvation efficacy of ethylene glycol-based DESs for PEO than that of glycerol-based ones.

BAI and *et al.* (Bai, Wei, and Ren 2017) and MAMMILLA *et al.* (Mamilla et al. 2019) stated that the acidity, viscosity and free hydrogen proton content in the DES are the main parameters influencing the polymer extraction efficacy of a DES.

It should be pointed out that DES-polymer systems are more complex than DESs (non-combined to polymers), and must be regarded as reliant on more than one parameter. In a study carried out by STEFANOVIC and co-authors (Stefanovic et al., 2019), the influence of the polymer prone to solvation, the DES hydrogen bond density, and the type of HBD on poly(ethylene oxide) (PEO) solvation conformation in choline chloride-based DESs was investigated. The hydrogen bond donors they chose to compare were urea, ethylene glycol and glycerol. The results revealed that (ChCl:urea) DES formed the strongest and densest hydrogen network, whereas the weakest and less dense network was observed for (ChCl:glycerol). Surprisingly, the PEO-(ChCl:urea) system was found to reinforce the stronger hydrogen bonds, disrupting the weaker ones. This engendered a highly structured solvation environment, where PEO was occluded in a static and coiled conformation. On the other hand, in the ChCl:glycerol weak structure, the polymer took an extended conformation.

DESs have a plasticizing effect on polymers (Wang et al. 2015), decreasing subsequently their glass transition temperature, which also facilitates their processability (Qiao et al., 2012).

I.5.3.3. As catalysts

GARCÍA-ARGÜELLES et al. (García-Argüelles et al., 2015) have experienced the ring-opening polymerization of ε-caprolactone using a eutectic mixture of methane sulfonic acid and the guanidine 1,5,7-triazabicyclo[4.4.0]dec-5-ene as catalyst. They noticed that the eutectics fulfilled remarkably the roles of both solvent and initiator in carrying out the polymerization of ε-caprolactone. The resulting polymers exhibited a high crystallinity (more than 87%) and an excellent capacity to support the growth of murine L929 fibroblasts. We consider that the preparation of biocompatible PCLs at physiological temperatures, and in the absence of reagents other than the monomer and the catalyst, offers an interesting alternative to both self-crosslinked oligomers/macromers of acrylate-based PCL-derivatives and pH/temperature-sensitive PCL copolymers used to date as injectable biomaterials.

I.5.3.4. As functional monomers

a) In electropolymerization: Due to their ionic conductivity, ChCl-based DESs were reported as polymerization media in electrochemical syntheses of conductive polymers such as polyaniline (Fernandes et al., 2012; Zou & Huang, 2018), polymethylene blue (Hosu et al., 2017), and poly(3,4-ethylenedioxythiophene) (Prathish et al., 2014). Furthermore, the use of DESs resulted advantageously in high conversion polymers. As already mentioned above, DESs with higher conductivity and lower viscosity are the most recommended for higher electropolymerization rates (Fischer, 2015).

b) In frontal polymerization: The first DES-assisted frontal polymerization was successfully conducted by MOTA-MORALES *et al.* (Mota-Morales et al., 2011). DESs of choline chloride and acrylic acid or methacrylic acid provided both reaction media and functional monomers via the hydrogen bond donor component (acrylic and methacrylic acids). Introducing DESs allowed to reduce reagents and provided thermal stability to the reaction well known by its exothermic nature, which makes difficult the control of the medium temperature.

c) In emulsion polymerization: Itaconic acid was polymerized by XU et al. (Xu et al., 2016) and filled with silica to prepare composites for solid-phase extraction of trypsin. Itaconic acid monomer was the HBD component of a ChCl-based DES.

d) In polycondensation: Polyester elastomers compose a very important class of polymers used in pharmacology and medicine as drug carriers, for encapsulation and other applications. Due to their elasticity comparable to that of skin tissues, incorporation of antibacterial molecules within the biodegradable polyester crosslinks produces skin wound dressings with exceptional antibacterial activity. These are the characteristics needed in the present study. Indeed, the following sections (chapter III and IV) are dedicated to a detailed study of a biodegradable polyester elastomer-based composite with antibacterial activity and high liquid absorption capacity.

I.6. Conclusion

Although deep eutectic solvents (DESs) represent an excellent alternative to organic solvents, they remain largely unknown to most researchers, especially in polymer technology. Accordingly, this chapter was realized to introduce DESs providing clear definitions,

properties and applications. As novel analogs, DESs are greener, much cheaper, non-volatile, and more interestingly, DESs are capable of dissolving a wider range of products including poorly water-soluble products.

In polymer technology, DESs do not replace only solvents, but catalysts as well. They also may be used as monomers, plasticizers and fillers. In addition to the green aspect, they allow reducing the number of reagents in the process. DES-assisted polymer syntheses reach easily 100% yields with very satisfactory resulting polymers such as good nucleation, adherence and electrochemical properties required for conducting polymers.

Finally, and most importantly, the need for green polymers is opportunely fulfilled by the green media and green monomers contained within DESs.

I.7. References

Abbott, A. P., Boothby, D., Capper, G., Davies, D. L., & Rasheed, R. K. (2004). Deep Eutectic Solvents formed between choline chloride and carboxylic acids: Versatile alternatives to ionic liquids. *Journal of the American Chemical Society, 126*(29), 9142–9147. https://doi.org/10.1021/ja048266j

Abbott, A. P., Capper, G., Davies, D. L., Rasheed, R. K., & Tambyrajah, V. (2003). Novel solvent properties of choline chloride/urea mixtures. *Chemical Communications, 1*, 70–71. https://doi.org/10.1039/b210714g

Aissaoui, T., Benguerba, Y., AlOmar, M. K., & AlNashef, I. M. (2017). Computational investigation of the microstructural characteristics and physical properties of glycerol-based deep eutectic solvents. *Journal of Molecular Modeling*, 23(277), 1-11. https://doi.org/10.1007/s00894-017-3450-5

Blusztajn, J. K. (1998). Choline, a vital amine. *Science*, *281*(5378), 794–795. https://doi.org/10.1126/science.281.5378.794

Carriazo, D., Serrano, M. C., Gutiérrez, M. C., Ferrer, M. L., & del Monte, F. (2012). Deep-eutectic solvents playing multiple roles in the synthesis of polymers and related materials. *Chemical Society Reviews, 41*(14), 4996–5014. https://doi.org/10.1039/c2cs15353j

Chen, Z., McDonald, S., FitzGerald, P., Warr, G. G., & Atkin, R. (2017). Small angle neutron scattering study of the conformation of poly(ethylene oxide) dissolved in deep eutectic solvents. *Journal of Colloid and Interface Science, 506*, 486–492. https://doi.org/10.1016/j.jcis.2017.07.068

Choi, Y. H., van Spronsen, J., Dai, Y., Verberne, M., Hollmann, F., Arends, I. W. C. E., Witkamp, G. J., & Verpoorte, R. (2011). Are natural deep eutectic solvents the missing link in understanding cellular metabolism and physiology? *Plant Physiology, 156*(4), 1701–1705. https://doi.org/10.1104/pp.111.178426

Clark, J. H., & Tavener, S. J. (2007). Alternative solvents: Shades of green. *Organic Process Research and Development, 11*(1), 149–155. https://doi.org/10.1021/op060160g

Coulembier, O., Lemaur, V., Josse, T., Minoia, A., Cornil, J., & Dubois, P. (2012). Synthesis of poly(l-lactide) and gradient copolymers from a l-lactide/trimethylene carbonate eutectic melt. *Chemical Science, 3*(3), 723–726. https://doi.org/10.1039/c2sc00590e

Dai, Y., van Spronsen, J., Witkamp, G. J., Verpoorte, R., & Choi, Y. H. (2013). Natural deep eutectic solvents as new potential media for green technology. *Analytica Chimica Acta, 766*(2010), 61-68.

https://doi.org/10.1016/j.aca.2012.12.019

Deetlefs, M., & Seddon, K. R. (2010). Assessing the greenness of some typical laboratory ionic liquid preparations. *Green Chemistry*, *12*(1), 17–30.
https://doi.org/10.1039/b915049h

Dhanalakshmi, K., Saraswathi, R., & Srinivasan, C. (1996). Synthesis and electrochemical stability of polyaniline and polypyrrole in an ambient temperature acetamide-urea-ammonium nitrate eutectic melt. 82(3), 237–243.
https://doi.org/10.1016/S0379-6779(96)03803-9

Durand, E., Lecomte, J., & Villeneuve, P. (2013). Deep eutectic solvents: Synthesis, application, and focus on lipase-catalyzed reactions. *European Journal of Lipid Science and Technology, 115*(4), 379–385.
https://doi.org/10.1002/ejlt.201200416

Fernandes, P. M. V., Campiña, J. M., Pereira, C. M., & Silva, F. (2012). Electrosynthesis of Polyaniline from Choline-Based Deep Eutectic Solvents: Morphology, Stability and Electrochromism. *Journal of The Electrochemical Society, 159*(9), G97–G105.
https://doi.org/10.1149/2.059209jes

Fischer, V. (2015). Properties and Applications of Deep Eutectic Solvents and Low-Melting Mixtures. PhD Thesis, Universität Regensburg.
https://doi.org/10.5283/epub.31832

Francisco, M., Van Den Bruinhorst, A., & Kroon, M. C. (2012). New natural and renewable low transition temperature mixtures (LTTMs): Screening as solvents for lignocellulosic biomass processing. *Green Chemistry, 14*(8), 2153–2157.
https://doi.org/10.1039/c2gc35660k

Frauenkron, M., Melder, J.-P., Ruider, G., Rossbacher, R., & Höke, H. (2001). Ethanolamines and Propanolamines. *Ullmann's Encyclopedia of Industrial Chemistry*.
https://doi.org/10.1002/14356007.a10_001

García-Argüelles, S., García, C., Serrano, M. C., Gutiérrez, M. C., Ferrer, M. L., & Del Monte, F. (2015). Near-to-eutectic mixtures as bifunctional catalysts in the low-temperature-ring-opening-polymerization of ε-caprolactone. *Green Chemistry, 17*(6), 3632–3643.
https://doi.org/10.1039/c5gc00348b

García-Argüelles, S., Serrano, M. C., Gutiérrez, M. C., Ferrer, M. L., Yuste, L., Rojo, F., & Del Monte, F. (2013). Deep eutectic solvent-assisted synthesis of biodegradable polyesters with antibacterial properties. *Langmuir, 29*(30), 9525–9534.
https://doi.org/10.1021/la401353r

Genies, E. M., & Tsintavis, C. (1985). Redox mechanism and electrochemical behaviour or polyaniline deposits. *Journal of Electroanalytical Chemistry, 195*(1), 109–128.
https://doi.org/10.1016/0022-0728(85)80009-7

Guthrie, F. (1884). On eutexia. *Proceedings of the Physical Society of London, 6*(1), 124–146.
https://doi.org/10.1088/1478-7814/6/1/312

Hayyan, A., Hashim, M. A., Hayyan, M., Mjalli, F. S., & Alnashef, I. M. (2014). A new processing route for cleaner production of biodiesel fuel using a choline chloride based deep eutectic solvent. *Journal of Cleaner Production, 65*, 246–251.
https://doi.org/10.1016/j.jclepro.2013.08.031

Hillman, A. R., Ryder, K. S., Ismail, H. K., Unal, A., & Voorhaar, A. (2017). Fundamental aspects of electrochemically controlled wetting of nanoscale composite materials. *Faraday Discussions, 199*, 75–99.

https://doi.org/10.1039/c7fd00060j

Hosu, O., Bârsan, M. M., Cristea, C., Săndulescu, R., & Brett, C. M. A. (2017). Nanostructured electropolymerized poly(methylene blue) films from deep eutectic solvents. Optimization and characterization. *Electrochimica Acta, 232*, 285–295. https://doi.org/10.1016/j.electacta.2017.02.142

Jablonský, M., Škulcová, A., & Šima, J. (2019). Use of deep eutectic solvents in polymer chemistry–a review. *Molecules, 24*(21), 1–33. https://doi.org/10.3390/molecules24213978

Khandelwal, S., Tailor, Y. K., & Kumar, M. (2016). Deep eutectic solvents (DESs) as eco-friendly and sustainable solvent/catalyst systems in organic transformations. *Journal of Molecular Liquids, 215*, 345–386. https://doi.org/10.1016/j.molliq.2015.12.015

Leng, F., Robeyns, K., & Leyssens, T. (2021). Urea as a Cocrystal Former—Study of 3 Urea Based Pharmaceutical Cocrystals. *Pharmaceutics, 13*(5), 671. https://doi.org/10.3390/pharmaceutics13050671

Li, X., Hou, M., Han, B., Wang, X., & Zou, L. (2008). Solubility of CO_2 in a choline chloride + urea eutectic mixture. *Journal of Chemical and Engineering Data, 53*(2), 548–550. https://doi.org/10.1021/je700638u

Liu, Y., Zhang, H., Yu, H., Guo, S., & Chen, D. (2019). Deep eutectic solvent as a green solvent for enhanced extraction of narirutin, naringin, hesperidin and neohesperidin from Aurantii Fructus. *Phytochemical Analysis, 30*(2), 156–163. https://doi.org/10.1002/pca.2801

Mokhtary, M. (2019). Deep Eutectic Solvents in The Synthesis of Polymers. *Academic Journal of Polymer Science*, 2(3), 555586. https://doi.org/10.19080/ajop.2019.02.555586

Mota-Morales, J. D., Gutiérrez, M. C., Sanchez, I. C., Luna-Bárcenas, G., & Del Monte, F. (2011). Frontal polymerizations carried out in deep-eutectic mixtures providing both the monomers and the polymerization medium. *Chemical Communications, 47*(18), 5328–5330. https://doi.org/10.1039/c1cc10391a

Mota-Morales, J. D., Sánchez-Leija, R. J., Carranza, A., Pojman, J. A., del Monte, F., & Luna-Bárcenas, G. (2018). Free-radical polymerizations of and in deep eutectic solvents: Green synthesis of functional materials. *Progress in Polymer Science, 78*, 139–153. https://doi.org/10.1016/j.progpolymsci.2017.09.005

Pérez-García, M. G., Gutiérrez, M. C., Mota-Morales, J. D., Luna-Bárcenas, G., & Del Monte, F. (2016). Synthesis of Biodegradable Macroporous Poly(l-lactide)/Poly(ϵ-caprolactone) Blend Using Oil-in-Eutectic-Mixture High-Internal-Phase Emulsions as Template. *ACS Applied Materials and Interfaces, 8*(26), 16939–16949. https://doi.org/10.1021/acsami.6b04830

Prathish, K. P., Carvalho, R. C., & Brett, C. M. A. (2014). Highly sensitive poly(3,4-ethylenedioxythiophene) modified electrodes by electropolymerisation in deep eutectic solvents. *Electrochemistry Communications, 44*, 8–11. https://doi.org/10.1016/j.elecom.2014.03.026

Prathish, K. P., Carvalho, R. C., & Brett, C. M. A. (2016). Electrochemical characterisation of poly(3,4-ethylenedioxythiophene) film modified glassy carbon electrodes prepared in deep eutectic solvents for simultaneous sensing of biomarkers. *Electrochimica Acta, 187*, 704–713. https://doi.org/10.1016/j.electacta.2015.11.092

Qiao, Z., Wang, Z., Zhang, C., Yuan, S., Zhu, Y., & Wang, J. (2012). PVAm–PIP/PS composite membrane with high performance for CO_2/N_2 separation. *AIChE Journal, 59*(4), 215–228. https://dôi.org/10.1002/aic

Gómez, A. V., Biswas, A., Tadini, C. C., Furtado, R. F., Alves, C. R. and Cheng, H. N. (2019). Use of Natural Deep Eutectic Solvents for Polymerization and Polymer Reactions. 30(4), 717–726. https://doi.org/10.21577/0103-5053.20190001

Rengstl, D., Fischer, V., & Kunz, W. (2014). Low-melting mixtures based on choline ionic liquids. *Physical Chemistry Chemical Physics, 16*(41), 22815–22822. https://doi.org/10.1039/c4cp02860k

Roda, A., Matias, A. A., Paiva, A., & Duarte, A. R. C. (2019). Polymer science and engineering using deep eutectic solvents. *Polymers, 11*(5), 1–22. https://doi.org/10.3390/polym11050912

Ruß, C., & Burkhard, K. (2012). Low melting mixtures in organic synthesis – an alternative to ionic liquids? J. Green Chemistry, 14(11), 2969-2982. https://doi.org/10.1039/C2GC36005E

Sapir, L., Stanley, C. B., & Harries, D. (2016). Properties of Polyvinylpyrrolidone in a Deep Eutectic Solvent. *Journal of Physical Chemistry A, 120*(19), 3253–3259. https://doi.org/10.1021/acs.jpca.5b11927

Shahbaz, K., Mjalli, F. S., Hashim, M. A., & AlNashef, I. M. (2011). Using deep eutectic solvents based on methyl triphenyl phosphunium bromide for the removal of glycerol from palm-oil-based biodiesel. *Energy and Fuels, 25*(6), 2671–2678. https://doi.org/10.1021/ef2004943

Smith, E. L., Abbott, A. P., & Ryder, K. S. (2014). Deep Eutectic Solvents (DESs) and Their Applications. *Chemical Reviews, 114*(21), 11060–11082. https://doi.org/10.1021/cr300162p

Stefanovic, R., Webber, G. B., & Page, A. J. (2019). Polymer solvation in choline chloride deep eutectic solvents modulated by the hydrogen bond donor. *Journal of Molecular Liquids, 279*, 584–593. https://doi.org/10.1016/j.molliq.2019.02.004

Su, W. C., Wong, D. S. H., & Li, M. H. (2009). Effect of water on solubility of carbon dioxide in (aminomethanamide + 2-hydroxy-N,N,N-trimethylethanaminium chloride). *Journal of Chemical and Engineering Data, 54*(6), 1951–1955. https://doi.org/10.1021/je900078k

Sun, H., Li, Y., Wu, X., & Li, G. (2013). Theoretical study on the structures and properties of mixtures of urea and choline chloride. *Journal of Molecular Modeling, 19*(6), 2433–2441. https://doi.org/10.1007/s00894-013-1791-2

Tang, B., Zhang, H., & Row, K. H. (2015). Application of deep eutectic solvents in the extraction and separation of target compounds from various samples. *Journal of Separation Science, 38*(6), 1053–1064. https://doi.org/10.1002/jssc.201401347

Vanda, H., Dai, Y., Wilson, E. G., Verpoorte, R., & Choi, Y. H. (2018). Green solvents from ionic liquids and deep eutectic solvents to natural deep eutectic solvents. *Comptes Rendus Chimie, 21*(6), 628–638. https://doi.org/10.1016/j.crci.2018.04.002

Wang, R., Li, W., & Chen, Z. (2018). Solid phase microextraction with poly(deep eutectic solvent) monolithic column online coupled to HPLC for determination of non-steroidal anti-inflammatory drugs. *Analytica Chimica Acta, 1018*, 111–118. https://doi.org/10.1016/j.aca.2018.02.024

Wang, S., Peng, X., Zhong, L., Jing, S., Cao, X., Lu, F., & Sun, R. (2015). Choline chloride/urea as an effective plasticizer for production of cellulose films. *Carbohydrate Polymers, 117*, 133–139. https://doi.org/10.1016/j.carbpol.2014.08.113

Wilkes, J. S. (2002). A short history of ionic liquids - From molten salts to neoteric solvents. *Green*

Chemistry, 4(2), 73–80.
https://doi.org/10.1039/b110838g

Wong, C. Y., Wong, W. Y., Loh, K. S., & Mohamad, A. B. (2017). Study of the plasticising effect on polymer and its development in fuel cell application. *Renewable and Sustainable Energy Reviews, 79*, 794–805.
https://doi.org/10.1016/j.rser.2017.05.154

Xu, K., Wang, Y., Li, Y., Lin, Y., Zhang, H., & Zhou, Y. (2016). A novel poly(deep eutectic solvent)-based magnetic silica composite for solid-phase extraction of trypsin. *Analytica Chimica Acta, 946*, 64–72.
https://doi.org/10.1016/j.aca.2016.10.021

Zdanowicz, M., Wilpiszewska, K., & Spychaj, T. (2018). Deep eutectic solvents for polysaccharides processing. A review. *Carbohydrate Polymers, 200*, 361–380.
https://doi.org/10.1016/j.carbpol.2018.07.078

Zhang, Q., De Oliveira Vigier, K., Royer, S., & Jérôme, F. (2012). Deep eutectic solvents: Syntheses, properties and applications. *Chemical Society Reviews, 41*(21), 7108–7146.
https://doi.org/10.1039/c2cs35178a

Zou, F., & Huang, X. (2018). Electropolymerization in proton-functionalized anilinium salts/glycol deep eutectic solvents. *Journal of Materials Science, 53*(11), 8132–8140.
https://doi.org/10.1007/s10853-018-2129-3

Chapter II:
Polycondensation in
Deep Eutectic Solvents

II.1. Introduction

Polyesters possess a large variety of structures and properties depending on the nature of the radical bonded to the ester group. Polyesters are polymers owning numerous and very interesting mechanical properties ranging from extreme hardness to high elasticity that enlarges the range of their applications. Polyester elastomers which are of interest herein, may be tailored based on their components to be biocompatible and biodegradable. Among the most sensitive fields where biodegradable polyester elastomers find an increasing use are pharmacology and medicine (Barrett & Yousaf, 2010). These polymers are harnessed as active principal carriers, materials for drug encapsulation, dressings for wounded skins (Qin et al., 2019), and artificial organs such as heart valves, bladder, muscles and collagen fibers (Leong et al., 2008).

From this knowledge, we would study the synthesis and properties of a benzalkonium salt-filled polyester. The resulting product is expected to be a liquid-absorbent stretchable film with antibacterial activity.

In this framework, the present study pays a particular attention to a poly(diol-citrate) biodegradable elastomer (namely, poly(1,10-decanediol-citrate)) ($PD_{10}CA$) filled with a benzalkonium chloride well known by its highly efficient antibacterial activity, namely dodecyl-dimethylbenzylammonium chloride, abbreviated (DDBAC).

The purpose herein is to combine the respective advantages of each component (i.e., the high flexibility and hydrophilicity of the polymer matrix, and the bactericidal activity of the filler) to tailor a flexible film as food tray coating. In contact with food, the film would slow the decomposition of the latter by hindering the bacterial growth during storage, and absorbing the liquids of packaged product (meat, chicken, fruits…).

This chapter tries to provide a detailed literature about the step process followed to achieve the properties to be fulfilled by $PD_{10}CA$/DDBAC composite required for the purpose cited above. Deep eutectic solvent-assisted polyesterification is also compared to the classical process (without DES) to highlight the advantageous use of DESs in such processes. Components involved in this study are also described in terms of structure, properties, application fields, role and importance attached on respective use of each reagent.

II.2. Polycondensation

Polycondensation occurs in a step reaction mechanism similar to condensation. Condensation links an alcohol molecule with a carboxylic acid to form an ester in a process called esterification, or an amine with a carboxylic acid to form an amide, in an amidation process. In both processes, small molecules are eliminated as by-products such as H_2O, NH_3, MeOH… (Figure II.1).
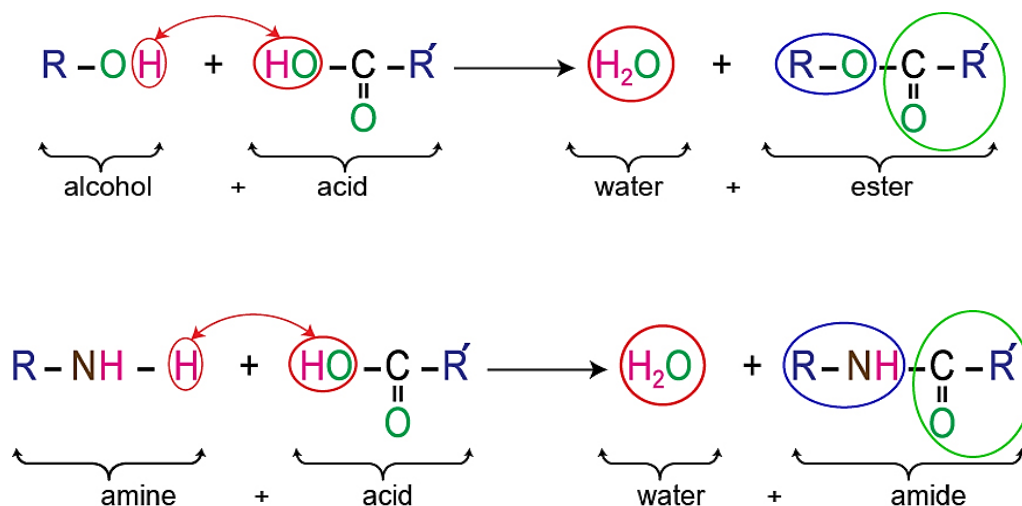
Figure II.1. Mechanisms of condensation reaction (formation of an ester and amide).

Accordingly, polycondensation involves a di- or a polyfunctional carboxylic acid with either a di- or polyfunctional alcohol (mechanism 1 bellow) to produce a polyester (Köpnick et al., 2002), or a diamine to prepare a polyamide (mechanism 2) (Herzog et al., 2013). Polyesterification also occurs by polycondensation of hydroxycarboxylic acids and polymerization of cyclic esters. The reaction being reversible, water molecules must be continuously removed to ensure the polymerization evolution (Köpnick et al., 2002).

Mechanism 1:

n HO-R-OH + n HO$_2$C-R'-CO$_2$H $\longrightarrow$ [O-R-O$_2$C-R'-C(O)]$_n$ + (2n-1) H$_2$O
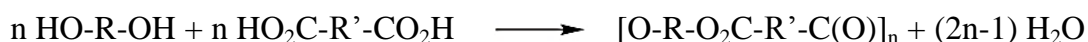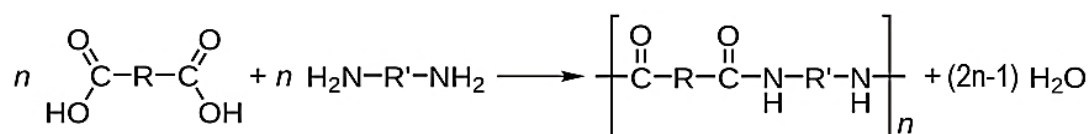
Mechanism 2:

The most typical products resulting from polyesterification and polyamidation processes are polyethylene terephthalate (PET) and Nylon-6,6 respectively. Their representative synthesis mechanisms are illustrated in Figure II.2. Polycondensation is a polymerization where monomers bond through covalent bonds (Zhang et al., 2014).

a) Polyester : Poly(ethyleneterephtalate) PET
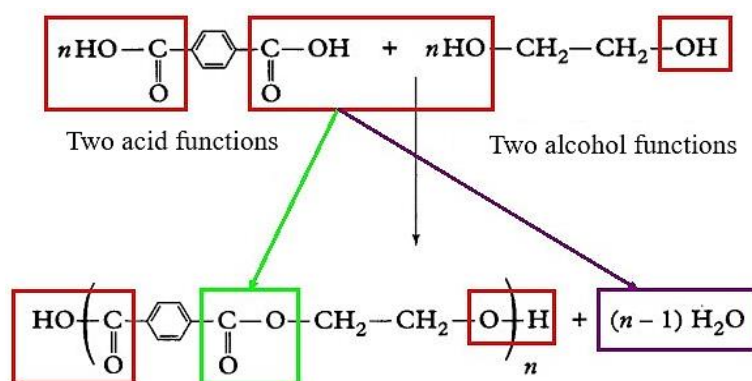
b) Polyamide : Nylon-6,6
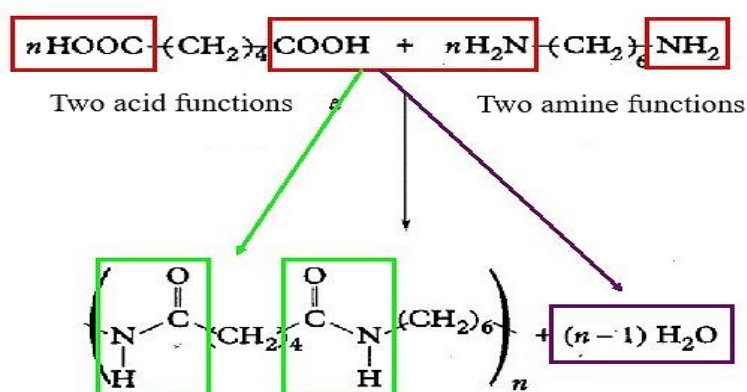
Figure II.2. Reaction mechanisms of polycondensation to produce PET and Nylon-6,6 (Zhang et al., 2014).

At the macroscopic scale, the polymer resulting from polycondensation of bifunctional pairs shows the conformation schematized in Figure II.3 bellow. This scheme describes a linear polyester, but a three-dimensional configuration may be obtained when replacing the diacid by either a triacid, a polyacid or a hydroxycarboxylic acid (Figure II.4) (Yang et al. 2006). The functionality of the polymer formed is the average number of the reacting groups per reacting molecules (Bhat & Kandagor, 2014).
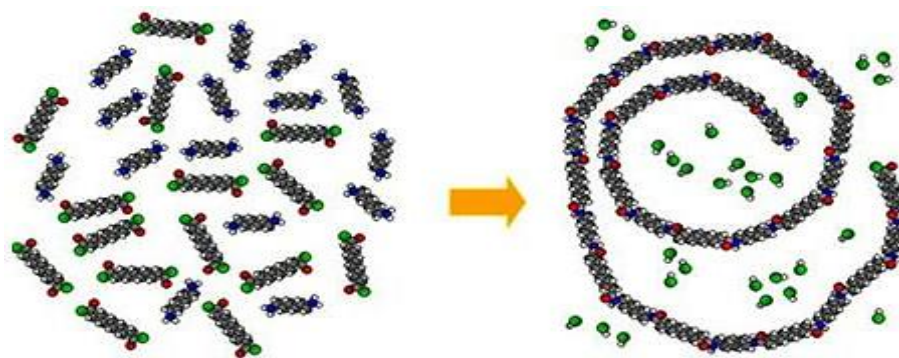
Figure II.3. Scheme of a linear polyester formed by reacting a diol with a diacid (Yang et al. 2006)
(● = C, ● = O, o = H, and ● = OH).
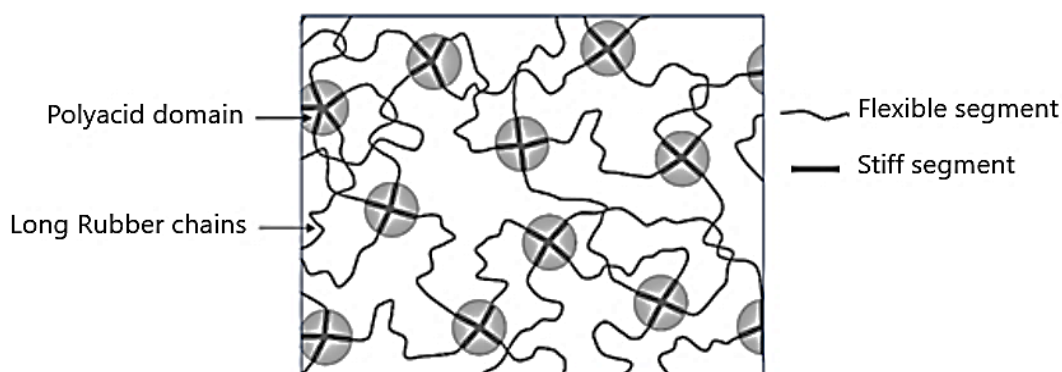
Figure II.4. Crosslinked polyester formed by reacting a diol with a polyacid

II.3. General Properties of Polyesters

Polyesters display an extremely large variety of properties based on the components used, the composition and the synthesis conditions such as temperature and crosslinking time. Regarding the application needed, the main properties conferred to polyester-based materials are linearity, branching and crosslinking degree of the chains, length of linear molecules between crosslinks, flexibility, crystallinity, hydrophilicity, degradability and recyclability (Kong et al., 2014).

II.3.1. Molecular Mass

Linear polyesters show high molecular mass (>10 000) and are categorized as thermoplastic polyesters (Kong et al., 2014). As seen before, these polymers are produced from dicarboxylic acids with diols. Moderately high molecular weight polyesters are those moderately branched. They are prepared from saturated aliphatic or aromatic diacids with di- or triols. They may also be obtained by adding controlled amounts (moderate contents) of polyacids to diols. Finally, low molecular weight polyesters are produced from di-, tri- or polyols with aromatic polyacids, or saturated or unsaturated fatty acids (Duda & Penczek, 2005).

II.3.2. Molecular Mass Distribution

In polyesterification, monomers are not the only reacting molecules. Dimers, oligomers and all molecules, regardless of their length, may polymerize through the terminal hydroxy and carboxy groups in a transesterification. This confers the final product a broad molecular weight distribution (Yang et al. 2006).

The continuous elimination of H_2O molecules during the polymerization reaction propagation also allows the molecules to increase in length, which minimizes the presence of short molecules within the polymer, and consequently narrows the molecular mass distribution (Köpnick et al., 2002).

II.4. Poly (diol-citrates)

Citric acid (CA) with its three carboxylic groups and hydroxy function, is a perfect monomer for the preparation of elastomeric polyesters (Yang et al. 2006). Poly(diol-citrates) are tri-dimensional polyesters prepared based on diols with CA. Referring to Figure II.5, CA (or 2-hydroxypropane-1,2,3-tricarboxylic acid) is a small multi-functionalized molecule that represents the stiff segments of the polymer and thus, the crosslinked network junctions. While the linear diol molecules represent the flexible segment, if they are long enough ($\geq$ C6) to allow chain stretching (Barrett & Yousaf, 2010). The polyesters produced are inexpensive non-toxic biomaterials (Yang et al. 2006).
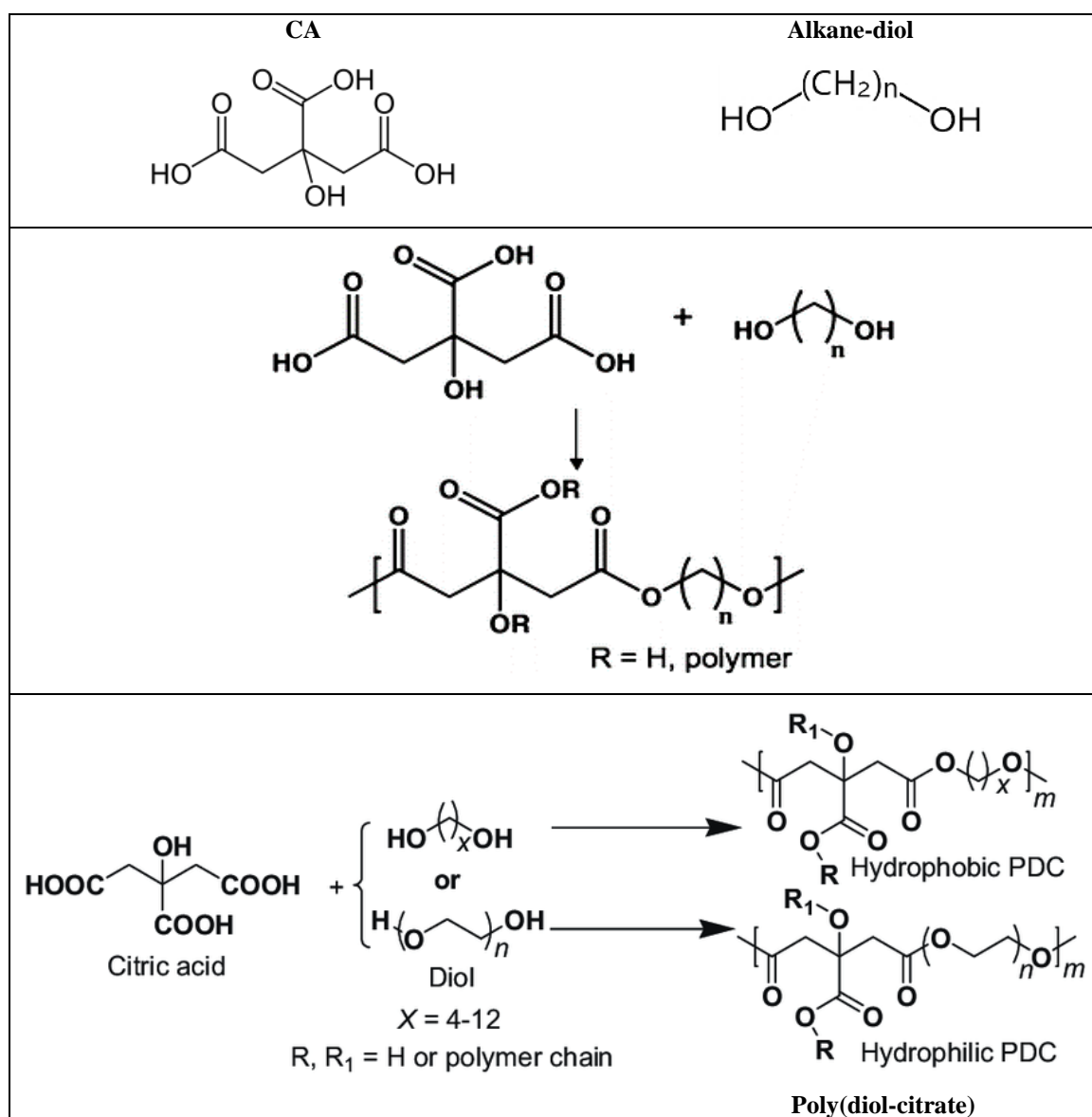
Figure II.5. Structures of monomers and synthesis routes of poly(diol-citrates) (Yang et al. 2006).

The synthesis of poly(diol-citrate) (PDCA) polyesters as biopolymers was patented by YANG *et al.* (Yang et al., 2004). The polycondensation process of CA with aliphatic diols ($C_nH_{2n+2}O_2$, with n = 6 to 12) as described by the authors, is available for the synthesis of biocompatible polyesters whose elastomeric properties are tailored by several parameters such as diol linear chain length, post-polymerization (crosslinking) temperature, and time (Mokhtary, 2019; Yang et al., 2004, 2006).

The synthesis of poly (diol-citrate) polyesters follows two steps:

➢ *Pre-polymerization*: this stage is carried out by mixing equimolar amounts of CA with an aliphatic diol (C_6-C_{12}) in a three-neck round-bottomed flask. The mixture is melted at 160-165 °C under nitrogen flow with a continuous stirring into an oil bath. Then, the temperature is lowered to 140 °C for an hour to obtain the pre-polymer.

➢ *Post-polymerization*: to prepare poly(diol-citrates) with various crosslinking degrees, the post-polymerization is proceeded at various temperatures (37, 60, 80 and 120 °C), for various times (1 day-2 weeks), under vacuum (2 Pa) or no vacuum (Yang, Webb, and Ameer 2004).

The PDCAs are biocompatible, biodegradable and non-toxic elastomers that find multiple applications such as cardiovascular and skin tissue scaffolds. The toxicity of PDCAs has been studied with human aortic smooth muscle cells and human aortic endothelial cells, and were found biocompatible with both. *In vivo* experiments on implanted PDCAs on rats recorded non-inflammatory response (Yang, Webb, and Ameer 2004).

Other applications of PDCAs include gene-delivery systems (Zhang et al., 2009), bio-imaging (Yang et al., 2009), shape-memory polymers for temperature-controlled drug delivery (Concepción et al., 2011), and advanced smart materials for biomedical applications.

II.4.1. Mechanical Behavior

The mechanical properties of PDCAs are tunable by the selected diol, and acid monomer content. Long diol chains confer flexibility, and high CA contents increase the crosslink density and biodegradability (Yang et al. 2006). Low crosslinking degree and relatively high molecular weight of linear chains between crosslinks (long linear chains between crosslinks) are obtained when polyesters are crosslinked at low temperatures. Such properties confer the polyester high elongation and low modulus, which are specific to elastomers (Yang et al., 2004).

Figure II.6 bellow shows that the longer the diol linear chain, the more flexible the polyester. This flexibility is evaluated by the tensile strain magnitude. For instance, a tensile strain equal to 200 % means that under a given tensile stress, the elastomer length reaches two times its initial length without rupture occurring. Besides, higher flexibility of the material needs lower tensile stress to be applied (Y. Wang et al., 2002; Jian Yang et al., 2006).
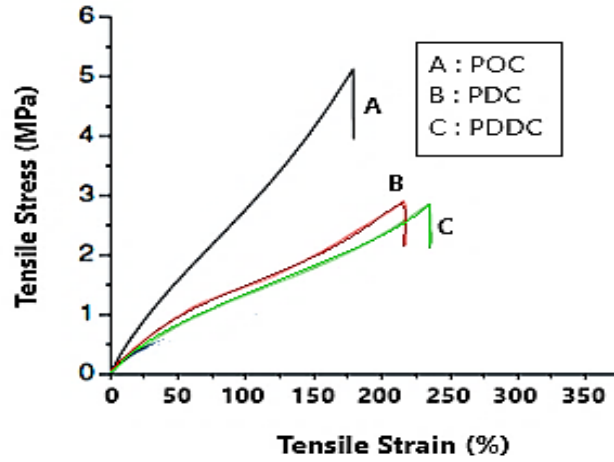
Figure II.6. Mechanical tensile properties of poly(diol-citrates) with different diol linear chains (POC = poly(1,8-octanediol-citrate), PDC = poly(1,10-decanediol-citrate) and PDDC = poly(1,12-dodecanediol-citrate) (Jian Yang et al., 2004).

YOUNG's modulus is calculated from the initial slope. The crosslink density (*n*) is calculated using equation II.1 from the rubber elasticity theory as follows:

$$n = \frac{E_0}{3RT} = \frac{\rho}{M_C} \qquad \text{(II.1)}$$

Where:

n is the number of active network chain segments per unit volume (mol/m^3);

E_0 is YOUNG's modulus (Pa);

R is the universal gas constant (8.3144 J/mol K);

T is the absolute temperature (K);

ρ is the elastomer density (g/m^3);

and M_C is the molecular weight between crosslinks (g/mol) (Wang et al., 2002; Yang et al., 2006).

Mechanical properties of synthesized poly(diol-citrate) polyesters reported values for YOUNG's modulus of 1.60-13.98 MPa, for tensile stress 2.93-11.15 MPa, and rupture strain 117-502 % (Barrett & Yousaf, 2010).

II.4.2. Density

Referring to the results obtained by YANG *et al.*, densities of some poly(diol-citrates) based on linear diols with different chain lengths (1,6-hexanediol, 1,8-octanediol, 1,10-decanediol and 1,12-dodecanediol) were found to decrease with the increasing chain length (Yang et al. 2006) (see Table II.1).

Table II.1. Densities of Poly(1,6-hexanediol citrate) (PHC), Poly(1,8-octanediol citrate) (POC), Poly(1,10-decanediol citrate) (PDC) and Poly(1,12-dodecanediol citrate) (PDDC) (Yang 2006).

Polymer	PHC	POC	PDC	PDDC
Density (g/cm^3)	1.3022 ± 0.0146	1.2429 ± 0.0121	1.1916 ± 0.0094	1.1500 ± 0.0062

II.4.3. Biodegradability

Elastomers and particularly PDCAs are highly amorphous polymers due to crosslinking as well as the long linear chains between the crosslinks. This structure is characterized by the voluminous holes (voids) within the polymer network. This structure confers to the polymer low density so that the material floats. A more interesting property related to the low density is the porosity of the material. This porosity is an important parameter that favors the elastomer for gas and liquid adsorption applications. The degradation of PDCAs depends on the composition and processing. Higher CA monomer contents increase the crosslinking density and accelerates the degradability of the polymer.

The advantageous use of CA as polyfunctional molecule and metabolic product of the body via KREB's cycle, makes unnecessary the use of catalysts and crosslinking agents which confers their polymers a non-controverted biodegradability and biocompatibility (Yang et al. 2006).

II.5. Deep eutectic solvent-assisted polyesterification

Poly(diol-citrates) are biodegradable and biocompatible elastomers very adequate for human tissue engineering. As seen above, the use of CA is highly advantageous since it plays multiple roles including biocompatible monomer, crosslinking agent and polymerization catalyst. The use of DESs as polymerization medium, monomer and/or additive contributes for further biocompatibility and mechanical performance (Serrano et al. 2012). Benzalkonium chloride salts (BACs) have also been chosen as HBAs in the DES and polymer filler for their biocide property. BACs could be simply added to the polyester. However, their incorporation through DES overcomes inherent drawbacks of PDCAs such as short-lasting drug/bactericide delivery.

II.5.1. Benzalkonium chlorides (BACs)

Benzalkonium chlorides (BACs) (Figure II.7) are quaternary ammonium compounds (QACs) that show effective biocide activity against bacteria, fungi and viruses (Mangalappalli-Illathu & Korber, 2006). They have been chosen for the present work due to their high efficacy as disinfectants on some important foodborne pathogens (Fazlara & Ekhtelat, 2012).

n = 8, 10, 12, 14, 16, 18	- Benzalkonium chlorides (BACs), - Alkyl dimethyl benzyl ammonium chlorides, - Alkyl dimethyl (phenylmethyl) quaternary ammonium chlorides, - Ammonium alkyl dimethyl (phenylmethyl) chlorides, - Ammonium alkyl dimethyl benzyl chlorides.
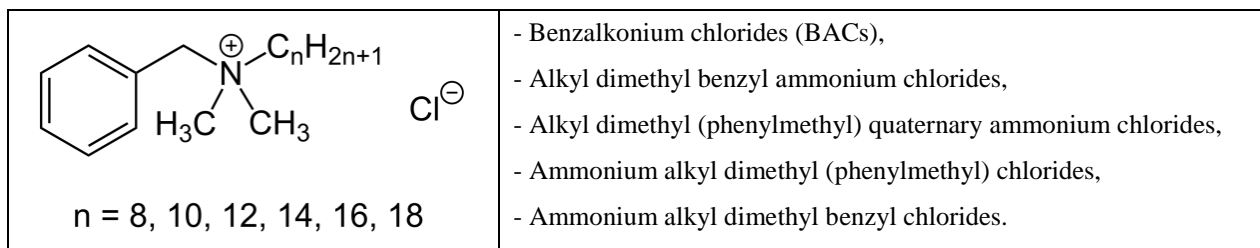
Figure II.7. General structure and different nomenclatures of Benzalkonium chlorides (Merchel & Pereira, 2019).

In 1935, BACs were commercialized as antiseptics, disinfectants and sterilizers for wounded and burned skins for clinical usage. Since then, they have been developed to acquire domestic, agricultural and industrial applications (Merchel & Pereira, 2019). They are present in fabric softeners (Tezel & Pavlostathis, 2012), personal care and cosmetic products including shampoos, conditioners, and body lotions (Choi et al., 2018), ophthalmic solutions and pharmaceutical substances by nasal administration (European Medicines Agency, 2017). BACs are also used for pools, paper products, water tanks, humidifiers, conservation of wood and in food line (Merchel & Pereira, 2019).

For controlled drug release, BACs, zinc oxide (ZnO) nanoparticles, silver-modified fillers, and chlorhexidine were directly mixed with dental resin as bacterial growth inhibitors. Among all, BACs showed better biocompatibility, more efficient antibacterial activity at lower contents, superior mechanical properties, and a more lasting effect expressed by a slower release. In a study conducted by WANG *et al.* in 2017, BACs have been incorporated into the resin through DESs as HBA components to further enhance the above properties, which gave promising results (Wang et al., 2017).

Toxicity of BACs present in food is a quite important criterion to be considered. In other terms, the threshold amount of BACs permissible in food has been determined by the European Food Safety Authority (EFSA) to be 14.4 mg/kg (European Food Safety Authority (EFSA), 2013). In the present study, the BAC-filled poly(diol-citrate) chosen as tray-covering antibacterial film directly contacts the packaged food in which BAC content must not exceed the value cited above.

II.5.2. Synthesis of $PD_{10}CA$-based composite

First, it is important to note that polyesterification occurs not necessarily in the presence of a catalyst since the process may be catalyzed by the constituting hydroxylated acid molecule (CA) (García-Argüelles et al., 2013).

In the present work, the modeling procedure is conducted regarding the mechanism and protocol of synthesis of PDCA-based composite. The description of the protocol adopted by GARCÍA-ARGÜELLES *et al.* is detailed to help modeling program implementing data for accurate results (García-Argüelles et al., 2013).

The DES is first prepared, and then BAC-filled PDCA is synthesized. The DES forms by mixing the diol ($D_{10}DO$) with BAC (DDBAC) in a 3:1 molar ratio and held at 90 °C, under mixing for 24 h till a homogeneous transparent liquid is formed. DES-assisted synthesis of the poly (1,10-decanediol citrate) ($PD_{10}CA$) prepolymer was initiated upon addition of citric acid (1:1 molar ratio with respect to 1,10-decanediol), maintained for 6 h at 90 °C. The polymerization is completed by crosslinking the prepolymer aged at 80 °C for 10 days to obtain the final polymer. During the whole process, the temperature was controlled by using a thermocouple.

Literature also describes the possibility of mixing first the quaternary ammonium salt with the acid molecule to prepare the DES before the alcohol was added in the synthesis protocol of polyesters.

II.5.3. Antibacterial activity and Related Properties of $PD_{10}CA$/DDBAC Composites

Alkyl chain length of BACs varies from C_8 to C_{18}, but only C_{12} and C_{14} derivatives show higher anti-bacterial, antimicrobial and antiviral activity (EU Reference Laboratories for Residues of Pesticides, 2016). Hence, for the upcoming implementation (chapter IV) C_{12} derivative is considered.

For controlled drug release, BACs, zinc oxide (ZnO) nanoparticles, silver-modified fillers, and chlorhexidine were directly mixed with an active dental polymer-based composite (also known as dental resin) as bacterial growth inhibitor. Although showing better biocompatibility, antibacterial activity at lower contents, and mechanical properties, BACs could show superior properties if mixing technique is considered (Wang et al., 2017).

Since they are quaternary ammonium salts, BACs may advantageously be utilized as HBA components for III-type DESs. In 2017, BACs have been incorporated through DESs as HBA components into dental composite (Wang et al., 2017). BACs are also used for food line and domestic cleaning.

In dentistry, damaged teeth are restored using dental resin, which is quickly surrounded by bacteria causing secondary caries. Removing and replacing the resin becomes necessary, but also provokes tissue loss. Several bactericide agents were added to polymers or dental composites to overcome this drawback. Benzalkonium chloride was a more promising filler compared to the rest of candidates such as zinc oxide (ZnO) nanoparticles, which showed a short-term effect, silver-modified fillers, that provided required antibacterial efficacy only at high contents, and chlorhexidine which alters significantly the mechanical strength of the composite (Wang et al., 2017). Accordingly, the present work aims to enhance the conservation of food, particularly meat by the use of bacterial growth inhibitor as a filler for polyester-based film for trays. BACs being perfect candidates for this purpose.

Rate of bactericide release is another parameter to be considered. Fast releasing of chlorhexidine by the dental composite has been noticed to achieve 50% of the initial content within only 14 days (Leung et al., 2005). However, resin loaded with BAC powder showed an antibacterial activity up to 260 days, and with 50% aqueous BAC solution the efficacy lasted 30 days (Othman et al., 2002).

It is to be noticed that high bactericide contents within the resin and fast release decrease considerably the mechanical properties of the composite when the total amount of BAC is consumed creating voids in the structure resulting in porous resin easily degradable (Wang et al., 2017). Also, when benzalkonium chlorides are directly incorporated into the dental resin, the mechanical performance of the composite is altered (Weng et al., 2011). This led the researchers to incorporate BACs into the resin through DESs, which showed bactericide effectiveness and maintained largely the mechanical performances of the composite.

II.5.3.1. Mechanical Properties

Studies using DESs for the synthesis of polyester-based composites where the quaternary ammonium or phosphonium salt was kept within the polymer crosslinks for its antimicrobial effect, noticed that the presence of the HBA slowed the elastomer crosslinking (decreasing the crosslinking degree), generating higher molecular weight of linear chains

between crosslinks (García-Argüelles et al., 2013; Serrano et al., 2012). This was explained by GARCÍA-ARGÜELLES (García-Argüelles et al., 2013) by the important volume created (needed) by the salt bulk molecule to position itself between the crosslinks. The authors also noticed that the salt molecules with higher steric hindrance caused lower crosslinking, thus longer linear molecule chains (Figure II.8). Accordingly, polyesters with lower crosslink density degrade faster.

a) Polyester synthesized by conventional polycondensation	**b)** Polyester/HBA system prepared by DES-assisted polycondensation
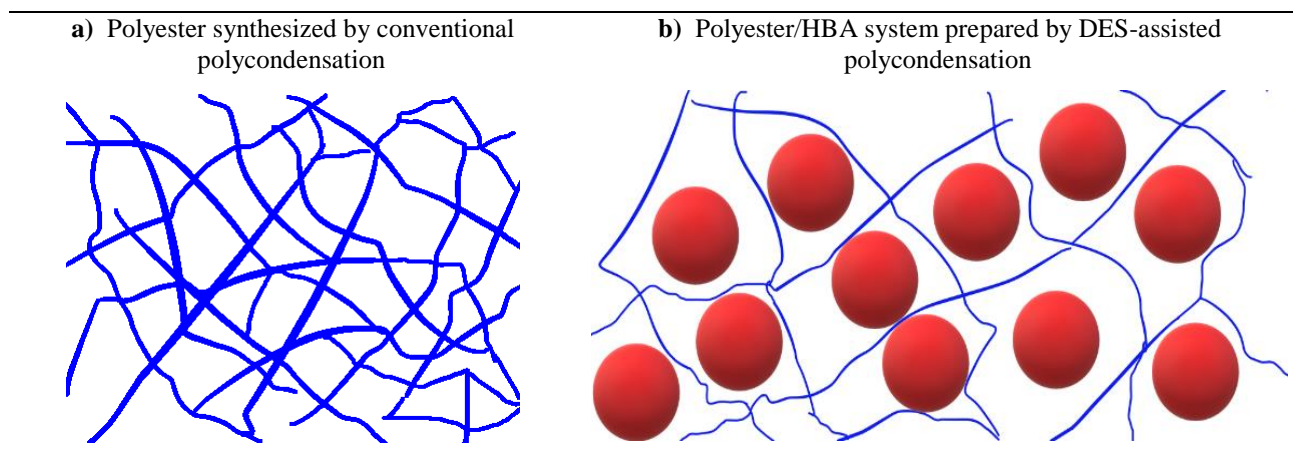
Figure II.8. Effect of steric hindrance by HBA component on the molecular weight of the linear chains between crosslinks of the polyester.

Literature reports that high loading of PDCAs with BACs impacts negatively the mechanical performance of the composite (Muñoz-Bonilla & Fernández-García, 2012; Othman et al., 2002). OTHMAN et al. (Othman et al., 2002) reported that directly incorporating antibacterial agents including BACs into polymers reduces the mechanical strength of the composites. The rapid release of the BACs leads to porous structures within the composite, accelerating the polymer degradation (Wang et al. 2019). This is avoided when the BACs are incorporated in the polymer through DES.

For the specific use as food tray coating, the film to be synthesized must foremost show effective antibacterial activity. Several techniques were developed regarding this requirement including the incorporation of either quaternary nitrogen atoms within the polymer chain, or bactericidal molecules through chemical modification or blending (Muñoz-Bonilla & Fernández-García, 2012).

II.6. Conclusion

Although the use of DESs in polymer processes is recent, their development increases exponentially due to the multiple and important roles they assume. This chapter dealt with those roles played by DESs in polymer technology and specifically in the synthesis of biodegradable polyester elastomer-based composites. Polycondensation process was detailed without and with DESs. Type III deep eutectic solvents in the classification of SMITH (Smith et al., 2014) were chosen. These DESs consist of a quaternary ammonium salt as hydrogen bond acceptor, and a diol as hydrogen bond donor. The contribution of the DES as monomer through the HBD moiety, and as filler through the HBA one were described in detail.

Then, more specifically, the chapter describes benzalkonium/polydiol-citrate biodegradable composites presenting a high liquid absorbing capacity and an interesting antibacterial activity. This suggests their application as stretchable films for trays demonstrating their capacity to ensure a long conservation of food.

II.7. References

Barrett, D. G., & Yousaf, M. N. (2010). Thermosets synthesized by thermal polyesterification for tissue engineering applications. *Soft Matter*, *6*(20), 5026–5036. https://doi.org/10.1039/c0sm00476f

Bhat, G., & Kandagor, V. (2014). Synthetic polymer fibers and their processing requirements. In Advances in Filament Yarn Spinning of Textiles and Polymers. *Woodhead Publishing Limited*. 3-30. https://doi.org/10.1533/9780857099174.1.3

Choi, S. M., Roh, T. H., Lim, D. S., Kacew, S., Kim, H. S., & Lee, B-M. (2018). Risk assessment of benzalkonium chloride in cosmetic products. *J. Toxicol. Environ. Health B. 21*(1), 8–23. https://doi.org/10.1080/10937404.2017.1408552

Duda, A., & Penczek, S. (2005). Mechanisms of Aliphatic Polyester Formation. In Doi, Y., Steinbüchel, A. Eds. *Biopolymers Online*. Weinheim, Germany: Wiley-VCH Verlag GmbH & Co. KGaA. 371–83. https://doi.org/10.1002/3527600035.bpol3b12

EU Reference Laboratories for Residues of Pesticides. (2016). *Analysis of Quaternary Ammonium Compounds (QACs) in Fruits and Vegetables using QuEChERS and LC-MS/MS. 5*, 1–6. http://www.eurl-pesticides.eu/userfiles/file/EurlSRM/EurlSRM_meth_QAC_ShortMethod.pdf

European Food Safety Authority (EFSA). (2013). Evaluation of monitoring data on residues of didecyldimethylammonium chloride (DDAC) and benzalkonium chloride (BAC). *EFSA Supporting Publications*, *10*(9), 1–24. https://doi.org/10.2903/sp.efsa.2013.en-483

European Medicines Agency. (2017). Questions and answers on benzalkonium chloride used as an excipient in medicinal products for human use. Ema/Chmp/704195/2013, 44(828), 1–10. https://www.ema.europa.eu/en/propylene-glycol-esters

Fazlara, A., & Ekhtelat, M. (2012). The disinfectant sffects of benzalkonium chloride on some important foodborne pathogens. *American-Eurassian J. Agric. & Environ. Sci.*, *12*(1), 23–29. https://www.researchgate.net/publication/283600271

García-Argüelles, S., Serrano, M. C., Gutiérrez, M. C., Ferrer, M. L., Yuste, L., Rojo, F., & Del Monte, F. (2013). Deep eutectic solvent-assisted synthesis of biodegradable polyesters with antibacterial properties. *Langmuir*, *29*(30), 9525–9534. https://doi.org/10.1021/la401353r

Herzog, B., Kohan, M. I., Mestemacher, S. A., Pagilagan, R. U., & Redmond, K. (2013). *Polyamides. Ullmann's Encyclopedia of Industrial Chemistry. Weinheim*. 1–36. https://doi.org/10.1002/14356007.a21_179.pub3

Kong, X., Qi, H., & Curtis, J. M. (2014). Synthesis and characterization of high-molecular weight aliphatic polyesters from monomers derived from renewable resources. *Journal of Applied Polymer Science*, *131*(15), 4–10. https://doi.org/10.1002/app.40579

Köpnick, H., Schmidt, M., Brügging, W., Rüter, J., & Kaminsky, W. (2002). Polyesters. *Ullmann's Encyclopedia of Industrial Chemistry. Weinheim. Wiley-VCH*, *28*, 623–649. https://doi.org/10.1002/14356007.a21_227

Leong, K. F., Chua, C. K., Sudarmadji, N., & Yeong, W. Y. (2008). Engineering functionally graded tissue engineering scaffolds. *Journal of the Mechanical Behavior of Biomedical Materials*, *1*(2), 140–152.
https://doi.org/10.1016/j.jmbbm.2007.11.002

Leung, D., Spratt, D. A., Pratten, J., Gulabivala, K., Mordan, N. J., & Young, A. M. (2005). Chlorhexidine-releasing methacrylate dental composite materials. *Biomaterials*, *26*(34), 7145–7153.
https://doi.org/10.1016/j.biomaterials.2005.05.014

Mangalappalli-Illathu, A.K., & Korber, D.R. (2006). Adaptive resistance and differential protein expression of Salmonella enterica serovar enteritidis biofilms exposed to benzalkonium chloride. *Antimicrobial Agents and Chemotherapy*, *50*(11), 3588–3596.
https://doi.org/10.1128/AAC.00573-06

Merchel Piovesan Pereira, B., & Tagkopoulos, I. (2019). Benzalkonium chlorides: Uses, regulatory status, and microbial resistance. *Appl. Environ. Microbiol*. *85*(13), 1-26.
https//doi.org/10.1128/aem.00377-19

Mokhtary, M. (2019). Deep Eutectic Solvents in The Synthesis of Polymers. *Academic Journal of Polymer Science*, *2*(3), 55-59.
https://doi.org/10.19080/ajop.2019.02.555586

Muñoz-Bonilla, A., & Fernández-García, M. (2012). Polymeric materials with antimicrobial activity. *Progress in Polymer Science*, *37*(2), 281–339.
https://doi.org/10.1016/j.progpolymsci.2011.08.005

Othman, H. F., Wu, C. D., Evans, C. A., Drummond, J. L., & Matasa, C. G. (2002). Evaluation of antimicrobial properties of orthodontic composite resins combined with benzalkonium chloride. *American Journal of Orthodontics and Dentofacial Orthopedics*, *122*(3), 288–294.
https://doi.org/10.1067/mod.2002.123947

Qin, H., Owyeung, R. E., Sonkusale, S. R., & Panzer, M. J. (2019). Highly stretchable and nonvolatile gelatin-supported deep eutectic solvent gel electrolyte-based ionic skins for strain and pressure sensing. *Journal of Materials Chemistry C*, *7*(3), 601–608.
https://doi.org/10.1039/c8tc05918g

Serrano, M. C., Gutiérrez, M. C., Jiménez, R., Ferrer, M. L., & Del Monte, F. (2012). Synthesis of novel lidocaine-releasing poly(diol-co-citrate) elastomers by using deep eutectic solvents. *Chemical Communications*, *48*(4), 579–581.
https://doi.org/10.1039/c1cc15284j

Smith, E. L., Abbott, A. P., & Ryder, K. S. (2014). Deep Eutectic Solvents (DESs) and Their Applications. *Chemical Reviews*, *114*(21), 11060–11082.
https://doi.org/10.1021/cr300162p

Tezel, U., & Pavlostathis, S. G. (2012). Role of Quaternary Ammonium Compounds on Antimicrobial Resistance in the Environment. In Antimicrobial Resistance in the Environment. Ed. Keen, P. L. & Montforts, M. H. M. M. John Wiley & Sons, Inc. 349–387. ISBN: 978-0-470-90542-5

Wang, J., Dong, X., Yu, Q., Baker, S. N., Li, H., Larm, N. E., Baker, G. A., Chen, L., Tan, J., & Chen, M. (2017). Incorporation of antibacterial agent derived deep eutectic solvent into an active dental composite. *Dental Materials*, *33*(12), 1445–1455.
https://doi.org/10.1016/j.dental.2017.09.014

Wang, J., Xue, J., Dong, X., Yu, Q., Baker, S. N., Wang, M., Huang, H. (2019). Antimicrobial properties of benzalkonium chloride derived polymerizable deep eutectic solvent. *Int. J. Pharm.* 575, 1-9.
https://doi.org/10.1016/j.ijpharm.2019.119005.

Wang, Y., Ameer, G. A., Sheppard, B. J., & Langer, R. (2002). A tough biodegradable elastomer. *Nature Biotechnology*, *20*(6), 602–606.
https://doi.org/10.1038/nbt0602-602

Weng, Y., Guo, X., Chong, V. J., Howard, L., Gregory, R. L., & Xie, D. (2011). Synthesis and evaluation of a novel antibacterial dental resin composite with quaternary ammonium salts. *Journal of Biomedical Science and Engineering*, *04*(03), 147–157.
https://doi.org/10.4236/jbise.2011.43021

Yang, J., Zhang, Y., Gautam, S., Liu, L., Dey, J., Chen, W., Mason, R. P., Serrano, C. A., Schug, K. A., & Tang, L. (2009). Correction for Yang et al., Development of aliphatic biodegradable photoluminescent polymers. *Proceedings of the National Academy of Sciences of the United States of America*, *106*(28), 11818.
https://doi.org/10.1073/pnas.0906359106

Yang, J., Webb, A. R., & Ameer, G. A. (2004). Novel Citric Acid-Based Biodegradable Elastomers for Tissue Engineering. *Advanced Materials*, *16*(6), 511–516.
https://doi.org/10.1002/adma.200306264

Yang, Jian, Webb, A. R., Pickerill, S. J., Hageman, G., & Ameer, G. A. (2006). Synthesis and evaluation of poly(diol citrate) biodegradable elastomers. *Biomaterials*, *27*(9), 1889–1898.
https://doi.org/10.1016/j.biomaterials.2005.05.106

Zhang, D., Kandagor, V., Bhat, G., Devaux, E., Hagewood, J., Rawal, A., Mukhopadhyay, S., Kuo, C. J., Lan, W. L., Mukhopadhyay, S., Ni, Q. Q., Jin, X. D., Xia, H., Liu, F., Oxenham, W., Ozipek, B., Karakas, H., Imura, Y., Jaffe, M., & Hogan, R. M. C. (2014). Synthetic polymer fibers and their processing requirements. In Advances in Filament Yarn Spinning of Textiles and Polymers; In *Advances in Filament Yarn Spinning of Textiles and Polymers*.
https://doi.org/10.1016/b978-0-85709-499-5.50014-3

Zhang, X. Q., Tang, H., Hoshi, R., De Laporte, L., Qiu, H., Xu, X., Shea, L. D., & Ameer, G. A. (2009). Sustained transgene expression via citric acid-based polyester elastomers. *Biomaterials*, *30*(13), 2632–2641.
https://doi.org/10.1016/j.biomaterials.2009.01.021

Chapter III: Theory and methods

III.1. Introduction

All developing scientific and industrial activities rely on computing techniques as secure, economic and fast procedure through its non-controversy and accuracy. In chemistry, molecular modeling is also a clean method that reduces the use and disposal of expensive, hazardous, non-biodegradable and toxic chemicals. Computational techniques have become more than useful tools in understanding chemical processes. Their most advantageous aspect lies in the determining implements they provide in confirming or refuting experimental findings.

During the last few years, molecular modeling has developed exponentially in several application branches, namely electronic structure of atoms, molecules and organometallic complexes, and the evaluation of their spectroscopic and magnetic properties. Molecular modeling methods offer an alternative in studying chemical systems with an extreme accuracy that is rarely realizable by experiments, besides the ease and zero-risk during proceeding.

In polymer science, modeling means are still under study due to more complex calculations required regarding the size of macromolecules. This makes software programs dedicated to polymer modeling few in number.

This chapter introduces the molecular modeling principle through the quantum methods, equations and approximations that enabled simulation of electronic behavior within atoms, small molecules and macromolecules.

The COnductor-like Screening MOdel for Real Solvents (COSMO-RS) program was described since it has been used in predicting thermodynamic properties of mixtures such as solubility and partial vapor pressure, through quantum mechanical calculations on molecules forming these mixtures (Klamt, 2005).

Herein, theories and methods used for molecules, mixtures and polymer under study are viewed.

III.2. Molecular modeling

Molecular modeling is the term used for methods that simulate the behavior of a particle system. The size of the system studied can range from a diatomic molecule to macromolecules of several hundred thousand of atoms.

Molecular modeling provides a description of the electronic behavior within atoms and molecules with the aim to explain the reactivity modes, understand the processes involving short and long molecules, and locate the active sites in the inter- and intramolecular competitive reactivities.

Such a study imposes determining an expression of the interaction energy between the atoms in the molecular system depending on their relative positions. In this purpose, molecular modeling methods are developed upon two essential approaches to quantify this interaction energy which are Quantum Mechanics and Molecular Mechanics (Bouchareb, 2011). Drawing the most stable conformation of a molecule consists in determining the minimum value of the interaction energy corresponding to the global minimum energy (Boyd, 1983).

III.2.1. Quantum methods (QM)

Quantum mechanics is the extension of the theory of quanta, resulting from the work of PLANCK, their interpretation by EINSTEIN and their application to atomic theory by BOHR and SOMMERFELD. It describes the quantification of certain empirics such as energy and angular momentum and emphasizes PAULI exclusion principle. The new design of particles resulting from the wave-particle duality, explained in the work of BROGLIE in 1923 leads to wave mechanics.

The Quantum Mechanics methods (QMM), which use the distribution of electrons in orbitals around the molecule, involve often long calculation times which limits their use to small molecules or require the use of many approximations. They are particularly suitable for calculating electrostatic charges and potentials, for approaching reaction mechanisms or for polarizability. The main objective of QM is to determine energy and electronic distribution (Bouchareb, 2011).

Quantum chemistry (QC) defines molecular structure as a nucleus around which electrons rotate, which are described by their probability of presence at a point and represented by orbitals (Boyd, 1983).

III.2.1.1. Fundamentals on Quantum Chemistry

a. SCHRÖDINGER'S equation

The quantum chemistry equations are based on solving SCHRÖDINGER'S equation, which is written for stationary states (Schrödinger, 1926):

$$\Psi H = \Psi E \tag{III.1}$$

Ψ: is wave function of the molecule.

E: Eigen value of H

The total Hamiltonian H of a molecule comprising N_e electrons with $\vec{r_1}$ coordinates, mass m_e and charge e, and N_N nuclei with coordinates $\overrightarrow{R_N}$ and atomic number Z_N and mass m_N, is defined by the sum of five terms (kinetics of electrons, kinetics of nuclei, repulsion between electrons, repulsion between nuclei and the term of electron-nucleus attraction).

$$H = -\frac{\hbar^2}{2m_e} \sum_{i=1}^{N_e} \Delta_i^2 - \frac{\hbar^2}{2} \sum_{K}^{N_N} \frac{\Delta_N^2}{m_N} + \sum_{N'>N}^{N} \sum_{N'} \frac{Z_K Z_{N'} e^2}{\|\overrightarrow{R_N} - \overrightarrow{R_{N'}}\|} + \sum_{i=1}^{N_e} \sum_{N=1}^{N_N} \frac{Z_N e^2}{\|\overrightarrow{R_N} - \vec{r_1}\|}$$
$$+ \sum_{i=1}^{N_e} \sum_{j<i} \frac{e^2}{\|\vec{r_1} - \vec{r_j}\|} \tag{III.2}$$

Where $\hbar$ is PLANK's constant with $\hbar = \frac{h}{2\pi}$; Δ_i^2 is the Laplacian of electron i

The first two terms of the equation are kinetic energy operators of electrons T_e and nuclei T_n; the other terms are Coulomb interaction terms for each pair of charged particles: nucleus-nucleus repulsion term V_{nn} , electron-nucleus attraction term V_{en} and electron-electron repulsion term V_{ee}.

$$H = T_e + T_n + V_{nn} + V_{en} + V_{ee} \tag{III.3}$$

b. BORN-OPPENHEIMER'S approximation

The nucleus consists of protons and neutrons (the mass of the proton is close to that of the neutron), the mass of the proton is 1836 times greater than that of the electron. Consequently, in a first approximation the kinetic energy of the nuclei can be neglected in

front of that of the electrons. It is called adiabatic approximation of BORN OPPENHEIMER. In this case, the wave function may be expressed as follows: (Martin 2005).

$$\Psi_n(\{\vec{r_l}\}, \{\overrightarrow{R_N}\}) = \Phi_{\overrightarrow{R_N}}(\{\vec{r_l}\}, X\{\overrightarrow{R_N}\}) \tag{III.4}$$

Where $\Psi_n(\{\vec{r_l}\})$ and $X\{\overrightarrow{R_N}\})$ are respectively the electronic wave function and the wave function of the frozen nuclei.

Replacing H in equation (III.1) by the value in equation (III.2), leads to the following expression:

$$\left\{ -\frac{\hbar^2}{2m_e} \sum_{i=1}^{N_e} \nabla_i^2 + \sum_{i=1}^{N_e} \sum_{j<i} \frac{e^2}{\|\vec{r_i}-\vec{r_j}\|} + \sum_{N'>N}^{N} \sum_{N'} \frac{Z_K Z_{N'} e^2}{\|\overrightarrow{R_N}-\overrightarrow{R_{N'}}\|} - \sum_{i=1}^{N_e} \sum_{N=1}^{N_N} \frac{Z_N e^2}{\|\overrightarrow{R_N}-\vec{r_i}\|} \right\} \Phi_{\overrightarrow{R_N}}$$
$$(\{\vec{r_l}\} = E_{el}(\overrightarrow{R_N}) \; \Phi_{\overrightarrow{R_N}}(\{\vec{r_l}\}) \tag{III.5}$$

Function $\Phi_{\overrightarrow{R_N}}(\{\vec{r_l}\})$ is a proper function of the Hamiltonian with an own value E_{el} $(\overrightarrow{R_N})$ for positions (R_N) of the frozen nuclei. BORN and OPPENHEIMER demonstrated that the nuclei movement is governed by the following equation:

$$\left[-\frac{\hbar^2}{2} \sum_K^{N_N} \frac{\nabla^2}{m_N} + E_{el}(\overrightarrow{R_N})X(\{\overrightarrow{R_N}\}) = E_{nucl}X(\{\overrightarrow{R_N}\}) \right] \tag{III.6}$$

Where $E_{el}(\overrightarrow{R_N})$ is the electronic energy, and E_{nucl} is the nuclei energy.

However, to describe numerically the wave function, two points of M^N order are needed (where M is the number of decompositions of space, and N is the number of electrons). Thus, the direct description for such a wave function is practically impossible, except by some static methods (quantum Monte Carlo methods).

c. Linear Combinations of Atomic Orbitals (LCAO) approximation

The analytical determination of orbitals is generally impossible. We then apply the principle of variations to search for approximate orbitals whose mathematical form is easily manipulated. The most widely used approximation is to consider that molecular orbitals can be closely approximated by Linear Combinations of Atomic Orbitals of the atoms constituting the molecule. It bears the name CLOA in French and LCAO in English. This is obviously an approximation, but calculations show that it is reasonable and provides qualitatively correct results (Volatron, 1993).

A molecular orbital (OM) ϕ_i is written as the sum of atomic orbitals (AO) weighted by numerical coefficients:

$$\phi_i = \sum_p C_{pi} X_p \tag{III.7}$$

Where X_p are the atomic orbitals of the two atoms and C_{pi} are LCAO coefficients, so that the electronic energy calculated is the less possible.

III.2.1.2. HARTREE-FOCK approximation

BORN-OPPENHEIMER approximation shows that the wave function of electrons must satisfy the stationary equation of SCHRÖDINGER (Born and Oppenheimer 1927) (equation III.1). By replacing the Hamiltonian by its expression, the relation (III.1) becomes:

$$\left[\sum_i - \frac{\hbar^2}{2m_e} \nabla_i + \frac{1}{2} \sum_{i \neq j} U_{ij} + \sum_{i,\alpha} U_{i\alpha} \right] \Psi = E\Psi \tag{III.8}$$

This last equation can be solved for a single particle. Interactions not existing between electrons ($U_{i\alpha}=0$), we can decompose, under these conditions, equation (II.8) into a system of several equations. However, a mathematical way must be found which allows for electronic interactions to be considered while keeping the electron system independent. For this purpose, HARTREE introduced an external field in which each electron can move independently of the others. Thus, the Hamiltonian can be put in the following form:

$$H = \sum_{i=1}^{n} H_i \tag{III.2}$$

Where the Hamiltonian corresponding to the electron (i) is:

$$H_i = - \frac{\hbar^2}{2m_e} \Delta_i + V(r_i) + \Omega_i(r_i) \tag{III.3}$$

$\Omega_i(r_i)$ represents the potential energy of an electron (i) subjected to the action of the mean field produced by all the other electrons and $V(r\_i)$ represents the potential energy of this electron in the mean field produced by all the nuclei. the Hamiltonian no longer contains dulls representing the interaction energies of the electrons, the shape of the total wave function is the product of the wave functions of each of the electrons. Therefore, the energy is the sum of the energies of all the electrons:

$$\Psi(r_1, r_2, r_3 \ldots, r_N) = \prod_i^n \Psi_i r_i \tag{III.4}$$

$$E = \sum_i^n E_i \tag{III.5}$$

III.2.1.3. Semi-empirical methods

A semi-empirical method is a method in which part of the calculations necessary for HARTREE-FOCK calculations is replaced by parameters adjusted to experimental values (the Hamiltonian is always parameterized by comparison with reference compounds). In general, all these methods are very precise for given families of products close to those used for parameterization. The semi-empirical methods only consider the electrons of the valence shell; the electrons of the inner layers are included in the nuclear core.

- NDDO method (Neglect of Diatomic Differential Overlap): proposed by POPLE in 1965. All bi-center bi-electronic integrals are retained.

- MNDO method (Modified Neglect of Diatomic Differential Overlap): proposed by DEWAR in 1977.

- Method AM1 (Austin Model 1): proposed by DEWAR in 1985. It corrects the term heart-heart repulsion.

- PM3 method (Parametric Method 3): proposed by STEWART in 1989. It uses an automatic parameterization procedure during calculations.

II.2.1.4. Density Functional Theory (DFT)

The theory of the electronic density functional was developed in two stages, in 1964 and in 1965, by HOHENBERG, KOHN and SHAM (Hohenberg and Kohn 1964; Kohn and Sham 1965). It consists in the reduction of the problem with several bodies in a problem with only one body in an effective field taking into consideration all the interactions in the system.

The fundamental idea is that the exact properties of the ground state of a system formed of nuclei and electrons are functional (function of a function) of the electron density alone. The DFT is based on the following two theorems (Hohenberg and Kohn 1964; Kohn and Sham 1965):

⬥ There is an exact correspondence between the electron density and the external potential of a given physical system; the external potential is determined by a single density up to a constant. The ground state energy of a multi-electron system in an external potential V_{ext} may be written as follows:

$$E[\rho(r)] = \int V_{ext}(r)\, \rho(r)dr + F(\rho(r)) \tag{III.6}$$

(r) is the electronic density; a universal function of ρ that contains the kinetic and Coulomb contribution to the energy that depends not on the system. A unique relation exists within a constant between $V_{ext}(r)$ and (r). (r) is a universal functional in the sense that it does not depend on the external potential which acts on the system.

The term $\int (r)\rho(r)dr$ represents the nuclei-electron interaction.

⊕ The electron density which minimizes the energy of the system is the exact density of the ground state (demonstrated by the variational principle). It therefore remains $F(\rho(r))$ to be determined with:

$$F[\rho(r)]=T[\rho(r)]+ V_{ee}\ [\rho(r)] \tag{III.7}$$

As the expressions of T and V_{ee} are unknown for interacting electron system, KOHN and SHAM suggested the following separations (Kohn and Sham 1965):

$$T[\rho(r)]=T_s\ [\rho(r)]+(T[\rho(r)]- T_s\ [\rho(r)]) \tag{III.8}$$

T_s Kinetic energy of an electron gas without interactions and of the same electron density as the real system, which can be calculated by introducing an orbital description.

$$T_s\ [\rho(r)]= \sum_i f_i \int \phi_i \left(\tfrac{1}{2}\nabla^2\right) \phi_i(r)dr \tag{III.9}$$

f_i : Number of orbital occupations, where $(r)=\sum_i f_i \int |\phi_i|^2$

On the other hand,

$$V_{ee}\ [\rho(r)]= E_H\ [\rho(r)]+(V_{ee}\ [\rho(r)]- E_H\ [\rho(r)]) \tag{III.10}$$

E_H ; HARTREE's energy which represents the COULOMB's interaction energy of a classical charge distribution (which does not take into consideration the discrete distribution of electrons). It is written:

$$E_H\ [\rho(r)]= \tfrac{1}{2} \int \frac{\rho(r)\rho(r\prime)}{|r-r\prime|} dr \tag{III.11}$$

Finally, $[(r)]$ separates in three parts:

$$F[\rho(r)]= T_s\ [\rho(r)]+ E_H\ [\rho(r)]+ E_{xc}[\rho(r)] \tag{III.19}$$

Where:

$$E_{xc}[\rho(r)]=\{ V_{ee}[\rho(r)]-[\rho(r)]\}+(T[\rho(r)]- T_s[\rho(r)]) \tag{III.12}$$

E_{xc} is the exchange-correlation energy not considered in T_S and E_H, which represents the only unknown of our problem. This term is not easy to calculate, but it has the advantage of being much smaller than the other terms. However, several approximations and parameterizations are proposed. SCHRÖDINGER's equation to be solved then becomes:

$$\left(-\frac{1}{2}\nabla^2 + V_{eff}(r)\right)\phi_i(r) = \varepsilon_i\phi_i(r) \tag{III.13}$$

With $V_{eff}(r) = V_H[(r)] + E_{ext}[\rho(r)] + V_{xc}[\rho(r)]$

$$\rho(r) = \sum_{i=1}^{N} f_i |\phi_i(r)|^2 \tag{III.14}$$

Where: ϕ_i are states for a single particle;

$V_H[\rho(r)] = \frac{1}{2}\int\frac{\rho(r\prime)}{|r-r\prime|}dr\prime$; represents HARTREE's potential;

$V_{xc} = \frac{\partial E_{xc}[\rho(r)]}{\partial\rho(r)}$ is the exchange-correlation unknown potential.

III.2.2. Molecular Mechanics (MM)

The expression "Molecular Mechanics" (MM) currently designates a method of calculation which allows, a priori, to obtain results of molecular geometries and energies based on classical mechanics. MM appeared in 1930 (Andrews, 1930), but developed from the 1960s, when computers were more accessible and more efficient. MM is based on BORN-OPPENHEIMER's approximation which suggests that electrons are much faster than nuclei.

MM is a non-quantum method, but it has an interest for large systems; as in the case of biological systems that cannot be approached with quantum methods. In these methods, a potential energy function is associated with each degree of freedom of the molecule: elongation of bonds, variation of valence angles, dihedral (rotation around a bond). These functions are empirical. Optimization of all parameters by energy minimization provides the equilibrium geometry of the various conformers and their relative energies. For molecules with a large number of conformers, there are automatic procedures for finding local energy minima (simulated annealing) (Bouchareb, 2011).

MM resembles "rod and ball" models. An MM calculation results in an arrangement of the nuclei such that the sum of all the energy contributions is minimized; its results mainly concern the geometry and energy of the system. The guiding idea of this method is to establish, by the choice of the energy functions and the parameters they contain, a mathematical model, the "force field", which represents as well as possible the variations of the potential energy, with molecular geometry (Bouchareb, 2011).

The purpose of MM is to calculate the potential energy of a molecule (or a system of molecules) based on the coordinates of atoms:

$$E_p = f(\vec{r_1}, \vec{r_2}, \vec{r_n})$$ (III.15)

Where $\vec{r_1}$ represents the vector of the atom 1 position; Molecular mechanics uses the following approximations:

- Each atom constitutes a particle.
- The atom is considered a rigid sphere-like having given radius and charge.
- Energies are calculated using derivative formulae of classical mechanics.

III.2.2.1. Force field (FF)

A force field is the mathematical model representing the potential energy of a molecule in molecular mechanics. The force field actually averages the electronic interactions between atoms (Allinger, 1976). It allows access to the energetic hypersurface of a molecule by establishing a link between the structural deformations of the system and its potential energy. It designates both the mathematical equation (function of potential energy) and the parameters that compose it (Allinger, 1977).

The potential energy function defines empirical energy, the total energy being broken down into a sum of additive terms each representing interatomic interactions. It is expressed as a sum of contributions from several types of interaction (Bouchareb, 2011). It can be broken down into an intramolecular interaction term and an intermolecular interaction term.

Intramolecular interactions only depend on the internal coordinates of molecules, that is to say bonds, valence angles, and torsions. In fact, to refine the expression of the term potential is to make the description of the system more faithful, coupling terms between different atoms have been introduced.

❖   Intramolecular potential may be expressed in general as:

$$V_{\text{intra.}} = \sum_{Bond} V_{\text{elongation}} + \sum_{Angle} V_{\text{curvature}} + \sum_{Diedral\ Angle} V_{\text{torsion}} + \sum V_{\text{crossed}}$$

Intermolecular interactions consider the interactions which do not interact by terms of bond, angle of curvature and angle of torsion. Non-binding potential is expressed in two terms: VAN DER WAALS' term and an electrostatic energy term. Thus:

$$V_{\text{inter}} = \sum V_{\text{Van der Waals}} + \sum V_{\text{electrostatic}}$$

The expression "force field" covers all the functions as well as the parameters associated with the different types of atoms they contain. The parameters are not force constants and are characteristic of a force field and not of a molecule, so they verify the so-called "transferability" principle on which the interest of this method is based. The goal is to build a mathematical model that describes a set of molecules (Bouchareb, 2011). This mathematical model is set up to represent as accurately as possible variations in potential energy with molecular geometry.

a. Elongation energy

The bonds between atoms in a molecular structure often tend to elongate or contract (Figure III.1).
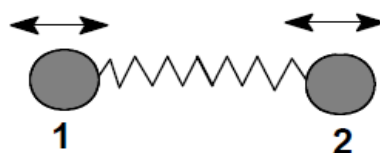
Figure III.1. Elongation between two atoms.

This deformation is governed in first approximation by HOOKE's of spring elongation. We can thus associate an energy of elongation of the form:

$$E(L) = 1/2[K_1 \ (L - L_0)^2]$$
(III.16)

Where K_1 is the elongation constant or HOOKE's constant;

L_0 is the reference bond length;

L is the bond length in the model.

b. Bending energy

The fluctuation of the atoms around their equilibrium position generates a deformation of the valence angles (Figure III.2).
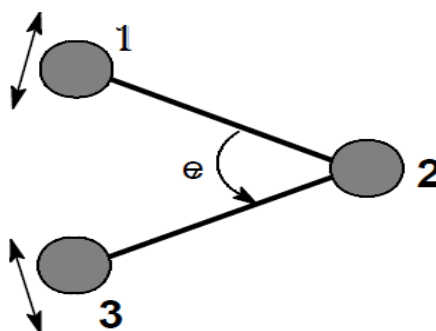
Figure III.2. Valence angle deformation.

This phenomenon is governed by a bending energy which can be expressed in the same forms as above, namely, to put it simply:

$$E(\theta) = 1/2[K_f(\theta - \theta_0)^2] \qquad \text{(III.17)}$$

Where K_f : Bending constant;

θ_0: Reference valence angle;

θ: Valence angle in the molecule;

the couple { K_f, θ_0 } represents here also un sub-ensemble of the force field.

c. Torsional energy

It concerns the dihedral angle formed by atoms 1-2-3-4. In particular, it accounts for the 3D structure of the molecule (Figure III.3).
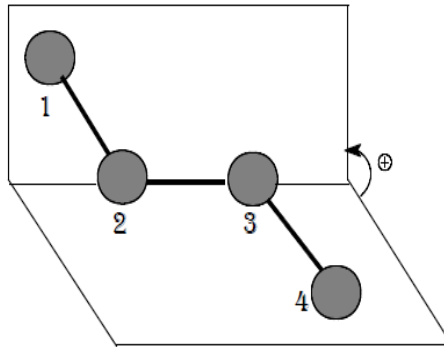
Figure III.3. Dihedral angle formed by atoms 1-2-3-4.

The evaluation of this energy E (ϕ) is done by a function developed in FOURIER's series. The dihedral angle (ϕ) defines the torsion around link 2-3.

$$E(\phi) = 1/2 \, [V_1(1+\cos \phi) + V_2 \, (1 - \cos 2 \phi) + V_3 \, (1+\cos 3 \phi)] \qquad \text{(III.18)}$$

V_1, V_2, V_3 are the constants of the torsional energy potential.

d. Addition of cross terms

All of the energy terms listed so far represent simple movements of atoms in the molecule. To take into account the effects of couplings between two non-independent movements, it is customary to add one or more additional interaction terms (Lipkowitz 1995). The most commonly formulated are: The elongation-flexion term E (L, θ) (Figure III.4) which is expressed by:

$$E(L, \theta) = K_{1f} \, (L - L_0)(\theta - \theta_0) \qquad \text{(III.19)}$$
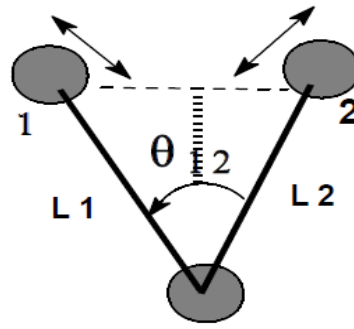
Figure III.4. Elongation-flexion coupling.

And the term flexion-torsion $E(\phi, \theta)$ is expressed as follows:

$$E(\phi,\theta) = K_{ft} (\theta - \theta_0)(\phi - \phi_0) \tag{III.20}$$

e.   VAN DER WAALS' energy

This energy involves atoms that are not linked to each other and not linked to a common atom (Meyer and Forrest, 1981). It consists of two parts, one repellent and the other attractive, and can be expressed by the following equation:

$$E(vdw) = \varepsilon^*[- C_1(r^*/r)^6 + C_2 \exp(-C_3 (r/r^*))] \tag{III.29}$$

ε^*: energy parameter that characterizes the depth of the potential well at the distance;

r^*: sum of VdW radii of interacting atoms;

r: interatomic distance

and C_1, C_2, C_3: constants of the force field.

This energy can therefore be represented as a function of the interatomic distance "r" as follows (Figure III.5):
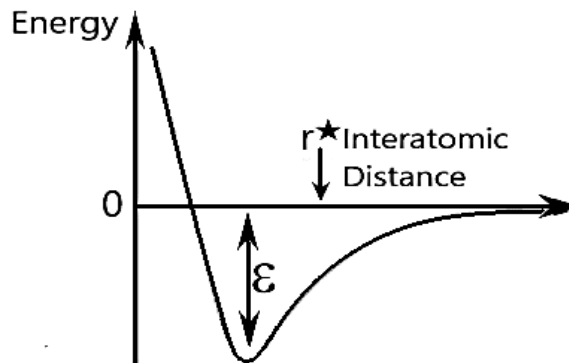
Figure III.5. VAN DER WAALS' energy curve.

f. *Electrostatic energy*

The electrostatic interactions can, in certain cases, take on a considerable importance, in particular in the case of molecules having two or more atoms (Figure III.6).
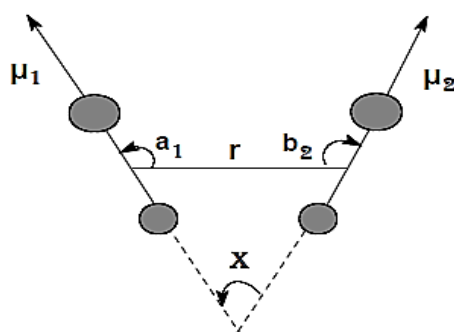
Figure III.6. Electrostatic interactions between two atoms.

MEYER et al (Meyer and Forrest, 1981) proposed to introduce an electrostatic term even for hydrocarbons. It can be expressed from the atomic charges or the dipole moments of each bond.

❖ In the first case:

$$E(e) = \sum q_1 q_2 \ / D. \ d_{12} \tag{III.21}$$

D: local dielectric constant of the medium; $q_1 q_2$ atomic partial charges of atoms 1,2; d_{12} interatomic distance.

❖ In the second case:

$$E(e) = \ \mu_1 \mu_2 \ (\cos X - 3\cos a_1 \ .\cos b_2) \ / \ D. \ r_{12}{}^3 \tag{III.22}$$

r: distance between the middles of the two bonds;

μ_1 , μ_2 : represent respectively the dipolar moments of the two bonds;

X: angle between the two moment vectors;

a_1, b_2: angles formed respectively between μ_1 and r, and μ_2 and r.

III.2.2.2. *Parameterization*

It is important to note that force fields are a purely empirical approach. They are parameterized so that all the different contributions can reproduce a series of experimental results. A field must therefore always be considered as an indivisible entity and it is excluded to combine the terms and / or parameters of two fields in the hope of obtaining a better set (Brooks et al., 1983).

In addition, the parameterization often aims so that the force field can realistically deal with a particular category of compounds. We can thus find fields intended more especially for the modeling of small organic molecules and macromolecules (Roterman et al., 1989), nucleotides (Momany and Ronte, 1992) or even organometallic complexes (Roterman et al., 1989). It is therefore first important to check if the chosen field is suitable for the system to be studied.

III.2.2.3. Different force Fields in molecular mechanics

Different force fields are proposed in the literature, they are distinguished from each other by the terms in the development of the energy expression of the molecule. Each has a specific field of application, so the choice of a force field depends on the properties and application of the system to be studied.

a.   MM2/MM3/MM4

MM2 is the first force field developed by TRISTRAM and VERGOTEN (Tristram and Vergoten, 1996). It was originally designed for simple molecules (alkanes, alkenes, non-conjugated alkynes, amines, etc.), but its improved versions MM3 (1989) and MM4 (1996) allow it to process increasingly complex organic molecules.

b. Optimized Potentials for Liquid Simulations (OPLS)

The Optimized Potentials for Liquid Simulations (OPLS) program, as its name suggests, has been designed in 1988 by JORGENSEN and RIVES (Jorgensen and Rives, 1988) to optimize the potential that enables the description of solvation properties. In our study, the solvation characteristics of the DES studied toward the acid are needed and their calculation is required.

c. Universal Force Field (UFF)

RAPPÉ and coworkers (Rappé et al., 1992) designed a Universal Force Field (UFF) capable of simulating molecules containing any combination of atoms in the periodic table.

III.3. Properties Implemented by Conductor-like Screening Model for Real Solvents (COSMO-RS) model

The three-dimensional structures of the individual molecules DDBAC, $D_{10}DO$, CA, and $PD_{10}CA$ were first constructed utilizing the Materials Studio^{TM} software by importing the "Standard Database Format" (SDF) file of each molecule.

As for the DDBAC:$D_{10}DO$ (1:3) mixture, DESs have previously been modeled through three main methods, which are the electroneutral method, the metafile method, and the molecular pair method. Here, we utilized the third method "molecular pair", which is a robust method that is capable of accurately capturing the correct three-dimensional geometry between the HBA and the HBD. The method also enables identifying how the HBA and the HBD are physically bonded together, and how the HES interacts with a certain substance as a whole.

After the structures are loaded into the Materials Studio^{TM} software, the geometries were optimized at the Density Functional Theory (DFT) level using "Perdew-Burke-Ernzerhof" (PBE) as the generalized gradient approximation, "Becke, 3-parameter, Lee–Yang–Parr" (B3LYP) as the exchange-correlation potential, and "double numerical polarization" (DNP) as the numerical basis set for determining the total energy of the system and solving the Self-Consistent Field (SCF). The SCF margin was fixed to 1×10^{-6} HARTREE with 500 cycles (Alareeqi et al., 2021).

III.3.1. Surface Charge Densities (SCD)

The quantum chemical COSMO-RS model is a fast and insightful method for modeling the interactions of molecules (or a mixture of molecules) that combines statistical thermodynamics and quantum chemistry in order to predict numerous physical, chemical, and thermodynamic properties and behaviors of classical organic solvents, and ILs from a molecular perspective (Klamt, 2005).

Also, despite their recent discovery, these models have also been utilized extensively for modeling DESs and their interactions with other types of molecules (classical organic solvents and ILs) (Warrag et al., 2020). A complete summary of details on the quantum chemical modeling and the molecular modeling of DESs in general is reported in the literature (Alkhatib et al., 2020).

In order to determine the surface charge densities (SCDs) of the molecules, the geometrically optimized structures from Materials Studio^{TM} were exported as "COSMO" files and then imported into the COSMO-RS software "COSMO*ThermX*". COSMO-RS calculations were then done on the imported surfaces where the surface is considered as a sum of i segment areas (a_i), with each segment having a screening charge density of (σ_i). Based on the polarities of the surfaces (a_i), (σ_i) is calculated, and a colored virtual conductor cloud forms around the molecules on the basis of the calculated (σ_i). For instance, Figure III.7 illustrates an example of the surface charge density distribution of $D_{10}DO$ showing its HBA, HBD, and neutral regions. The red color is assigned to the HBA region, the blue to HBD, and the green to the non-polar area.

HBA Region
"negative charges"

Non-Polar Region
"neutral charges"

HBD Region
"positive charges"
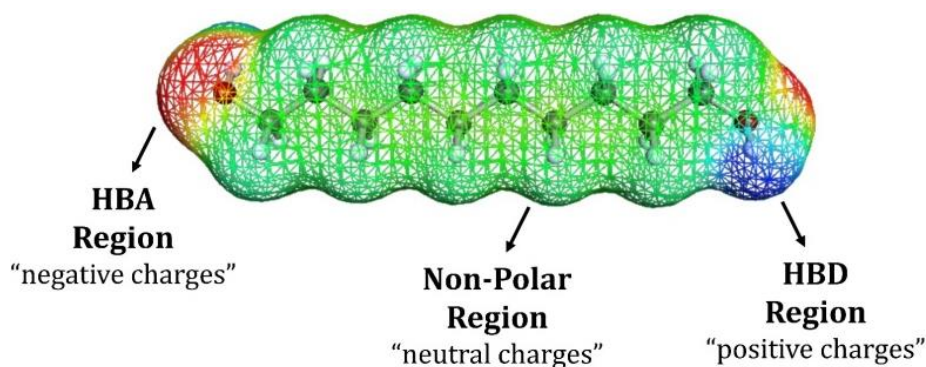
Figure III.7. Surface charge density distribution and its meaning shown for 1,10-decanediol ($D_{10}DO$) as an example.

III.3.2. Sigma-Profiles and Sigma-Potentials

The molecular polarity, which is a polarization charge density of a molecule, allows to determine the ability of a molecule to interact in the presence of another molecule (Fischer, 2015). This is available for the HBA and HBD molecules when mixed to form a eutectic solvent. It is possible to describe and schematize the screening charge or polarization charge density (σ) by means of COSMO-RS, which is a quantum chemical model with statistical thermodynamics (Klamt, 1995).

HIZADDIN *et al.* defined the σ-profile as being a distribution function giving the relative surface value with polarity σ in the molecule (Hizaddin et al., 2016).

For basic quantum chemical COSMO calculations, the molecule is supposed to be surrounded by a discrete surface embedded in a virtual conductor. Each surface segment has a characteristic area and a screening charge density noted (SCD). COSMO*therm* proceeds to the compound information reading from the COSMO files and transforms the screening charge surface into σ-profile which is a probability histogram $P(\sigma)$, by applying a local averaging algorithm over i segment areas a_i (Hammoudi et al., 2020). After determining the σ-profile of each molecule, the σ-profile of a mixture based on these molecules is calculated as follows (Hizaddin et al., 2016; Warrag et al., 2020):

$$P(\sigma) = \sum_i x_i \, P^{x^i}(\sigma) \tag{III.23}$$

where x_i is the molar fraction of i;

P^{x^i} is the σ-profile of i,

and i represents a specific component in the mixture.

Afterwards, the σ-potentials, $\mu(\sigma)$ of the molecules are calculated based on their previously calculated σ-profiles utilizing KLAMT's equation as follows (Klamt, 1995; Warrag et al., 2020):

$$\mu(\sigma) = -RTIn\left(\int d\sigma' P(\sigma) \cdot e^{\left(-\frac{1}{2}\alpha'^{(\sigma+\sigma')^2} - \frac{\mu'(\sigma')}{RT} \right)} \right) \tag{III.243}$$

Where:

α' is a general interaction fitting parameter to describe the energy of the geometrically optimized structure of the molecule;

and $\mu(\sigma)$ is the chemical potential.
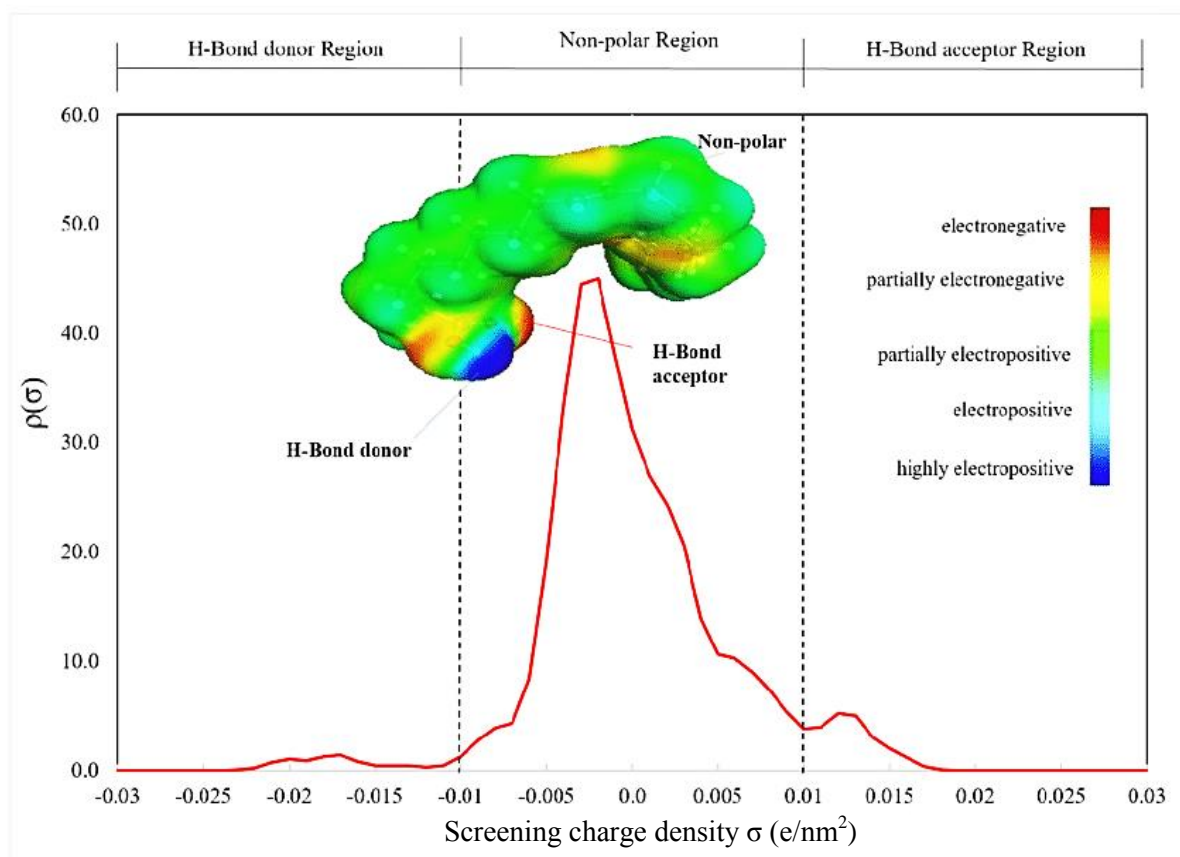
Figure III.8: Representative schemes of surface charge densities and σ-profile of a molecule (Abbott et al., 2003)

For mixtures, molecular interactions are considered by COSMO-RS as local pair interactions of segments within molecular COSMO-surfaces (Durand et al., 2013).

Negative sigma-profiles correspond to positive polarities, while positive p_S values correspond to negative polarities. Also, narrow peaks indicate low polarities, while broad peaks indicate high polarities (Aissaoui et al., 2017). The sigma profile for each DES is divided into three regions: the HBD region, the nonpolar region, and the HBA region. The three regions are separated by the threshold value for hydrogen bonding $\sigma_{hb} = \pm 0.0084$ e Å^{-2}. Peaks at $\sigma < -\sigma_{hb}$ prove the presence of compounds exhibiting affinity towards hydrogen bond donors, whereas peaks at $\sigma > +\sigma_{hb}$ are specific to compounds exhibiting affinity towards hydrogen bond acceptors.

III.3.3. Density

The density of DESs is higher than that of water (Khandelwal et al., 2015). The density values reported in the literature vary from 1.04 to 1.63 g cm^{-3} (Hizaddin et al., 2016; Ruß and Burkhard, 2012). In a study conducted by ZHANG *et al.*, the results attested that DESs based on the same HBA show densities that vary depending on the HBD moiety (Zhang et al., 2012). According to the authors, this might be due to a different molecular organization of the DESs. Besides, they noticed that these densities were higher than those of pure HBDs. The authors attributed this phenomenon to the hole theory. When a HBA and a HBD are mixed, the average hole radius decreases resulting in an obvious increase in the DES density compared to that of neat HBD (Zhang et al., 2012).

RACKETT's equation (Rackett, 1970) was not the only mathematical form to calculate density. SPENCER and DANNER used all the available methods predicting densities and finally concluded that the more accurate estimation was the equation they modified for saturated liquids as a function of temperature (Spencer and Danner, 1972) as a function of temperature:

$$V_S = V' Z_{RA}^{(1-T/T_C)^{2/7}} \tag{III.25}$$

Where V_S is saturated molar volume of liquid at reduced temperature,

V' is a characteristic volume usually close to the critical volume;

and Z_{RA} is RACKETT's compressibility factor.

$$V_S = \left(\frac{RT_C}{P_C}\right) Z_{RA}^{(1+(1-T/T_C))^{2/7}} \tag{III.26}$$

where P_c and T_c are the critical pressure and critical temperature, respectively.

III.3.4. Viscosity

The viscosity has a significant effect on the mass transport phenomena and ionic conductivity of DESs (Aissaoui et al., 2017). DESs usually exhibit high viscosities at room temperature due to the prevailing hydrogen bond network between the components, which results in a limited mobility of free species within the DES (Durand et al., 2013). The large ion size, electrostatic or VAN DER WAALS' interactions may also contribute to the high viscosity of DESs (Zhang et al., 2012). Therefore, DESs are usually used in solutions with water or other solvents for specific needs.

The viscosity of the DES was reported to depend on the chemical structure of the HBD (Durand et al., 2013). For example, di-acid-based DESs are much more viscous than those based on monoacids. In addition, the presence of one extra carboxylic or hydroxyl group leads to an increase in the viscosity. It was reported that the longer the alkyl chain on the HBA or HBD, the higher the viscosity (Tomé et al., 2018). As expected, it was also found that the viscosity of DESs decreases with increasing the temperature according to a logarithmic equation based on ARRHENIUS' model (Fischer, 2015).

In this work GRUNBERG-NISSAN's equation was used to calculate the viscosity of the liquid mixture using the following mixing rule (Fischer, 2015):

$$\ln \eta_{lmix} = \sum_{i=1}^{N} x_i \ln \eta_{li}$$ (III.27)

Where η_{lmix} is the viscosity of the liquid mixture, η_{li} is the viscosity of the pure component i, and x_i is the mole fraction of component i in the mixture. η_{li} was computed using COSMO*thermX* software and then, the GRUNBERG-NISSAN's equation was used to calculate the viscosity of the mixture. It should be noted that computational estimation of viscosity becomes less reliable for DESs with long hydrocarbon chains (Aissaoui et al., 2017).

III.3.5. Vapor Pressure

The low volatility is the main property that makes DESs the best alternative to organic solvents. The higher the volatility, the more toxic the solvent and hazardous in handling. The volatility is expressed in terms of vapor pressure.

Two possibilities are available in calculating the vapor pressure, expressed in bar units. The first possibility experimental vapor pressures of individual pure compounds as input data for the calculation. This method may provide further accuracy to the calculated vapor pressures in mixtures. The second method, which has been used in our study consists in using the difference of the free energies between the chemical potential of the gas phase, assuming perfect gas with a reference state pressure of 1 bar, and the chemical potential of the liquid phase according to equation III.28:

$$p_i = exp(\mu_i^{pure} - \mu_i^{gas})/RT$$ (III.28)

Vapor pressures of some DESs calculated at 25.15 °C by SHAHBAZ *et al.* (Shahbaz et al., 2016), were found between 0.02 x 10-3 and 3.4 x 10-3 mbar. These values are negligible and thus, indicative of extremely low volatility.

III.3.6. Activity Coefficient at Infinite Dilution

The activity coefficient γ_i of compound i depends on the molar fraction of this compound in the mixture. The activity coefficient at infinite dilution (γ_i^∞) is a crucial parameter in assessing solvent-solute systems that provides information about the solvent affinity for the solute. Using the previously calculated chemical potentials of the molecules $\mu(\sigma)$, the activity coefficient can be calculated as follows (Diedenhofen et al., 2003):

$$\gamma_i^\infty = exp\left(\frac{\mu_i^{DES} - \mu_i}{RT}\right) \tag{III.29}$$

Where:

μ_i^{DES} is potential of the solute in the DES;

μ_i is the potential of the pure solute;

R is the gas constant with a value of 8.3145 J·mol^{-1}·K^{-1};

and i denotes a particular component, which in our case is the solute in the DES.

III.3.7. Interaction Energies and Reactivity

As seen in chapter I, the melting point of a DES is much lower than those of its pure constituents (HBA and HBD) (Abbott et al., 2003). The explanation provided by SUN *et al.*, attributed the phenomenon to the fact that the already existing interaction energies between the halide moiety (anionic fraction) and the ammonium (cation) within the salt, are weakened when the HBD molecule is introduced to form the eutectic solvent (Sun et al., 2013). Indeed, due to its higher electro-positivity, the HBD molecule attracts strongly the halide of the salt to allow formation of the DES. A strong intensity interaction establishes between the HBD and the HBA anion, which reduces the interaction between the cation and anion of the HBA. This lowers significantly the melting point of the mixture as schematized in Figure III.9 as follows.
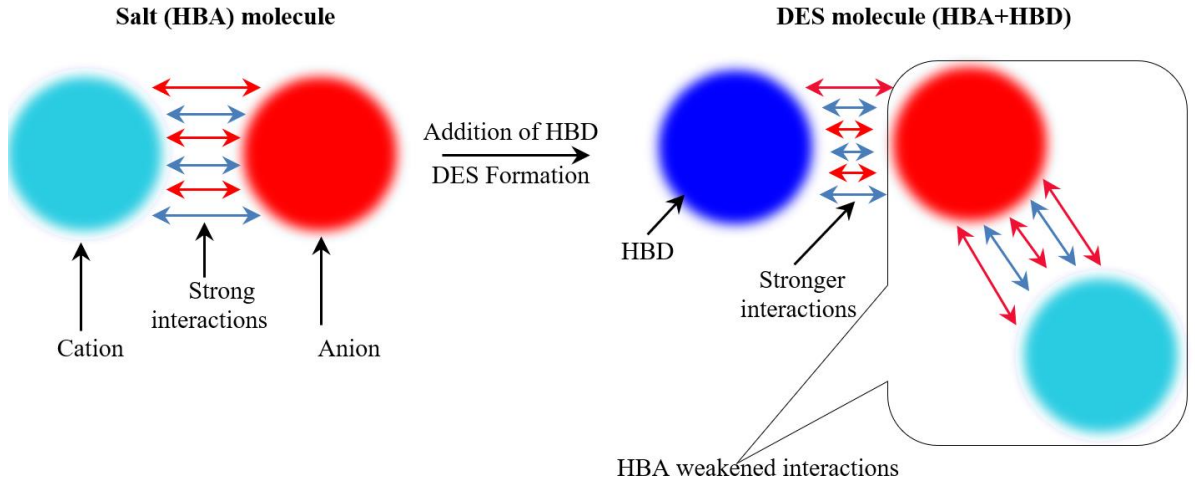
Figure III.9. Influence of HBD on the HBA cation and anion interaction energy during the formation of the DES.

Within a deep eutectic solvent, the interactions between the HBA and HBD are week. The energies of these interactions as estimated by the following equations and calculated using the COSMO*ThermX* software, include the electrostatic–misfit energy (E_{MF}), the hydrogen bonding energy (E_{HB}) and VAN DER WAALS' energy (E_{VdW}). The total interaction energy of the mixture (E_{mix}) is given by the summation of the three energies (Warrag et al., 2020).

$$E_{mix} = E_{MF} + E_{HB} + E_{VdW} \tag{III.30}$$

With:

$$E_{MF}(\sigma, \sigma') = a_{eff} \; {\alpha'}/{2} \, (\sigma + \sigma')^2 \tag{III.31}$$

$$E_{HB} = a_{eff} \; c_{HB} \; min(0; \; min\,(0, \sigma_{donor} + \sigma_{HB}) \; max(0; \sigma_{acceptor} - \sigma_{HB})) \tag{III.30}$$

$$E_{VdW} = a_{eff}(\tau_{VdW} + \tau'_{VdW}) \tag{III.31}$$

where σ and σ′ are the surface charge densities;

a_{eff} is the effective contact area between two surface segments;

α′ is an interaction parameter;

c_{HB} is the hydrogen–bond strength;

σ_{HB} is the threshold for hydrogen–bonding;

τ_{VdW} and τ'_{VdW} are adjustable VAN DER WAALS' interaction parameters.

Furthermore, two quantities, derived from density functional theory are used to characterize any chemical system: the electronic chemical potential *"µ"* and the chemical hardness *"η"* (Pearson, 1992).

DESs result from hard interactions between HBAs and HBDs and thus, own high cohesion energies, unlike substances resulting from covalent bonding. The hardness of DESs is a parameter that corresponds to its resistance to charge transfer, calculated from the molecular frontier energies. The terms assigned to frontier orbitals are the Higher Occupied Molecular Orbital and Lower Unoccupied Molecular Orbital, noted "HOMO-LUMO" (Durand et al., 2013).

HOMO and LUMO are essential in determining the amount of energy necessary to electron exchange in a molecule. HOMO is associated with the tendency of a species to donate electrons, while LUMO is associated with the tendency to receive electrons. Molecules with a large HOMO-LUMO energy gap are hard molecules, which means highly stable and not likely to charge transfer because they resist changes in their electron number and distribution. This stability results in preventing crystallization of DESs at room temperature. Softness (S) is defined as the reciprocal of the hardness (Hammond et al., 2016).

DFT calculations with the DMol3 module were further carried out to evaluate the chemical reactivity using the Higher Occupied Molecular Orbital energy (E_{HOMO}) and the Lower Unoccupied Molecular Orbital energy (E_{LUMO}), which are crucial parameters in assessing the amount of energy required for an electron exchange to occur within a molecule (Aissaoui et al., 2017). The HOMO energy is related to the ability of a molecule to donate a pair of electrons, while the LUMO energy is related to the ability of a molecule to accept a pair of electrons. These energies can then be utilized to calculate several characteristic quantum chemical parameters such as: the energy band gap (ΔE_{gap}), the chemical hardness (η), the electronic chemical potential (μ_x), and the electrophilicity index (ω), which can be calculated as follows (Hizaddin et al., 2016):

$$\Delta E_{gap} = E_{LUMO} - E_{HOMO} \tag{III.34}$$

$$\eta = \frac{E_{LUMO} - E_{HOMO}}{2} \tag{III.35}$$

$$\mu_x = \frac{E_{LUMO} + E_{HOMO}}{2} \tag{III.36}$$

$$\omega = \frac{\mu^2}{2\eta} \tag{III.37}$$

III.3.8. Blend Binding Energy Distributions

In addition to the COSMO*ThermX* calculations, further calculations using DFT with the DMol3 module were conducted to assess the blend binding energy (E_{blend}). The E_{blend} is a crucial parameter in determining the suitability of a polymer-additive combination by evaluating the change in free energy between the mixture energy and the sum of free energies of the pure constituents. The parameter can be calculated as follows (Abdoune et al., 2019):

$$E_{blend} = \frac{1}{2} Z(E_{bs} + E_{sb} - E_{bb} - E_{ss})$$
(III.38)

Where Z represents the coordination number;

E_{ij} is the binding energy between constituents i and j;

the subscript b represents the continuous base phase (polymer matrix);

and the subscript s represents the discontinuous screen phase (additive).

The blend energy also enables calculating FLORY-HUGGINS' interaction parameter (χ). The quantum chemical χ parameter describes the mutual interactions between the $PD_{10}CA$ and DDBAC compounds of the composite, and can be calculated as follows (Abdoune et al., 2019):

$$\chi = \frac{E_{blend}}{RT}$$
(III.32)

Where R is the gas constant with a value of 8.3145 $J \cdot mol^{-1} \cdot K^{-1}$;

and T is the temperature in Kelvins, which was set to 298.15 K.

III.3.9. Fukui Function Indices

Using the DMol3 module, the Fukui function, $f(r)$, at a certain site k of the molecule can be calculated as a Maxwell relation defined as the derivative of electronic density of a molecule, $\rho(r)$, with respect to the number of electrons *(N)* at constant electronic potential, $V(r)$, which is mathematically expressed as follows (Geerlings et al. 2003):

$$f(r) = \left(\frac{\partial \rho(r)}{\partial N}\right)_{V(r)} \tag{III.40}$$

Utilizing a finite difference approximation on the Fukui function, $f(r)$, two Fukui expressions for cationic and anionic atoms can be obtained as follows (Delley 2006):

$$f^+(r) = \left(\frac{\partial \rho(r)}{\partial N}\right)^+_{V(r)} = \rho_{N+1}(r) - \rho_N(r) \tag{III.41}$$

$$f^-(r) = \left(\frac{\partial \rho(r)}{\partial N}\right)^-_{V(r)} = \rho_N(r) - \rho_{N-1}(r) \tag{III.42}$$

Where $f^+(r)$ and $f^-(r)$ are the Fukui functions for cationic and anionic atoms, respectively, and $\rho_{N+1}(r)$, $\rho_N(r)$, *and* $\rho_{N-1}(r)$ are the electronic density values at distance (r) in the system consisting of $(N + 1)$, (N), and $(N - 1)$ electrons, respectively.

III.3.10. Solubility

The solubility is an important parameter to determine or predict in a mixture. It measures the ability of a solvent to dissolve a certain amount of solute (Maleki, 2017). It is expressed in unit g/L solution if mass fraction is considered in parameterization, or mol/L solution if molar fraction is considered.

The solubility of compound i in a solvent is predicted by COSMO-RS based on the intermediate results from Quantum Mechanical (QM) calculations already performed on each molecule taken individually.

To enable calculation of the solubility of solid compounds, ΔH_m, T_m and optionally ΔC_p are inserted as input data in the COSMO-RS program. This method is not valid in case of a solubility of a liquid in a solvent. FLORY-HUGGINS' model is also used to deduce solubility of a polymer in a solvent.

In polymer synthesis, the solubility of the monomer in the solvent is one of the critical key parameters that determines the feasibility of the process. Based on its fundamental importance, the solubility of CA in the HES, which is based on a solid-liquid equilibrium (SLE) calculation, was determined using the COSMO*ThermX* software at 25.15 °C and atmospheric pressure. The high solubility is presumably a result of the high hydrogen bonding energy.

III.4. Conclusion

This chapter introduced molecular modeling descriptors of the electronic behavior of atoms and molecules to explain their reactivities, understand the folding processes of molecules of various sizes, and explain the reasons of favoring a specific route between competitive possibilities in terms of interactive sites.

Interaction energy of atoms in a molecular system is expressed based on their relative positions by quantitative empirics. Molecular modeling methods are used to evaluate the interaction energy defined above by means of two approaches namely, Quantum Mechanics and Molecular Mechanics.

The methods of quantum mechanics use the distribution of electrons in orbitals around the molecule and require the use of approximations suitable for calculating electrostatic charges and potentials, for approaching reaction mechanisms or for polarizability. The main objective of quantum mechanics is to determine energy and electronic distribution.

The three-dimensional structures of the individual molecules DDBAC, $D_{10}DO$, CA, and $PD_{10}CA$ may be constructed utilizing the Materials Studio^{TM} software. The HES may be modeled through a method capable of accurately capturing the correct three-dimensional geometry between the HBA and the HBD. The method also enables identifying how the HBA and the HBD are physically bonded together, and how the HES interacts with a substance.

After the geometries are loaded into the Materials Studio^{TM} software, the geometries may be optimized at the DFT level using B3LYP "Becke, 3-parameter, Lee–Yang–Parr", and DNP "double numerical polarization" as the numerical basis set for determining the total energy of the system.

The quantum chemical COSMO-RS "Conductor-like Screening Model for Real Solvents" method serves to model the interactions and behaviors of molecules and mixtures that predict numerous physical, chemical, and thermodynamic properties such as the surface charge densities (SCDs) of the molecules, showing the HBA, HBD, and neutral regions. The DMol3 module allows to calculate Fukui functions for cationic and anionic atoms.

III.5. References

Abbott, A. P., Capper, G., Davies, D. L., Rasheed, R. K., & Tambyrajah, V. (2003). Novel solvent properties of choline chloride/urea mixtures. *Chemical Communications*, *1*, 70–71. https://doi.org/10.1039/b210714g

Abdoune, Y., Benguerba, Y., Benabid, S., Khither, H., Sobhi, W. and Djafer Benachour. (2019). Numerical Investigation of Polyethylene Glycol Polymer (PEG) and Dithymoquinone (DTQ) Interaction Using Molecular Modeling. *Journal of Molecular Liquids,* 276, 134–40. https://doi.org/10.1016/j.molliq.2018.11.105.

Aissaoui, T., AlNashef, I M., Qureshi, U. A., and Benguerba, Y. (2017). Potential Applications of Deep Eutectic Solvents in Natural Gas Sweetening for CO_2 Capture. *Reviews in Chemical Engineering*, *33*(6): 523–50. https://doi.org/10.1515/revce-2016-0013.

Alareeqi, S., Bahamon, D., Nogueira, R. P. and Vega, L. F. (2021). Understanding the Relationship between the Structural Properties of Three Corrosion Inhibitors and Their Surface Protectiveness Ability in Different Environments. *Applied Surface Science* 542(148600), 1-38. https://doi.org/10.1016/j.apsusc.2020.148600.

Alkhatib, I. I., Bahamon, D., Llovell, F., Abu-Zahra, M. R.M. and Vega, L. F. (2020). Perspectives and Guidelines on Thermodynamic Modelling of Deep Eutectic Solvents. *Journal of Molecular Liquids 298*, 112183. https://doi.org/10.1016/j.molliq.2019.112183.

Allinger, N. L. (1976). Calculation of Molecular Structure and Energy by Force-Field Methods. *Advances in Physical Organic Chemistry, 13*(C), 1–82. https://doi.org/10.1016/S0065-3160(08)60212-9.

Allinger, N. L. (1977). Conformational analysis. 130. MM2. A Hydrocarbon Force Field Utilizing VI and V2 Torsional Terms. *J. Am. Chem. Soc.* 99(25), 8127–8134. http://dx.doi.org/10.1021/ja00467a001

Andrews, B. Y., Donald H. (1930). Quantum Mechanics in Drug Design: Methods and Applications Issue published: July 1, 1983. Drug Information Journal, 17 (3), 121-131 https://doi.org/10.1177/009286158301700301

Benabid, S., Streit, A. F.M., Benguerba, Y., Dotto, G. L., Erto, A. and Barbara Ernst. (2019). Molecular Modeling of Anionic and Cationic Dyes Adsorption on Sludge Derived Activated Carbon. *Journal of Molecular Liquids, 289*, 111119. https://doi.org/10.1016/j.molliq.2019.111119.

Benguerba, Y., AlNashef, I. M., Erto, A., Balsamo, M., and Ernst. B. (2019). A Quantitative Prediction of the Viscosity of Amine Based DESs Using σ-Profile Molecular Descriptors. *Journal of Molecular Structure 1184*, 357–363. https://doi.org/10.1016/j.molstruc.2019.02.052.

Born, M., and Oppenheimer. R. (1927). Zur Quantentheorie Der Molekeln. *Annalen Der Physik, 389* (20), 457–484. https://doi.org/10.1002/andp.19273892002.

Bouchareb, F. (2011). Contribution à l'étude de la Stabilité des Complexes de « Métaux-Pyrazoles »

Par Modélisation Moléculaire., Thèse université Abou-Bakr Belkaid, Tlemcen.
https://www.theses-algerie.com/7692526795605443/

Boyd, D. B. (1983). Quantum Mechanics in Drug Design: Methods and Applications. *Therapeutic Innovation & Regulatory Science 17*(3), 121–131.
https://doi.org/10.1177/009286158301700301.

Delley, B. (2006). The conductor–like screening model for polymers and surfaces. *Mol. Simul.* 32, 117–123.
https://doi.org/10.1080/08927020600589684

Diedenhofen, Michael, Frank Eckert, Andreas Klamt, Cosmologic Gmbh, Co Kg, Burscheider Strasse, and D- Leverkusen. 2003. "Prediction of Infinite Dilution Activity Coefficients of Organic Compounds in Ionic Liquids Using COSMO-RS. *J. Chem. Eng. Data* 48(3), 475–479.
https://doi.org/10.1021/je025626e

Durand, E., Lecomte, J. and Villeneuve. P. (2013). Deep Eutectic Solvents: Synthesis, Application, and Focus on Lipase-Catalyzed Reactions. *European Journal of Lipid Science and Technology 115* (4), 379–85.
https://doi.org/10.1002/ejlt.201200416.

Fischer, V. (2015). Properties and Applications of Deep Eutectic Solvents and Low-Melting Mixtures. PhD Thesis, Universität Regensburg.
https://doi.org/10.5283/epub.31832

Geerlings, P., De Proft, F., Langenaeker, W. (2003). Conceptual density theory, *Chem. Rev*. 103, 1793–1873.

https://doi.org/10.1021/cr990029p

Hammoudi, N. H., Benguerba, Y., Attoui, A., Hognon, C., Lemaoui, T., Sobhi, W., Benaicha, M., Badawi, M. and Monari, A. (2020). *In Silico* Drug Discovery of IKK-β Inhibitors from 2-Amino-3-Cyano-4-Alkyl-6-(2-Hydroxyphenyl) Pyridine Derivatives Based on QSAR, Docking, Molecular Dynamics and Drug-Likeness Evaluation Studies. *Journal of Biomolecular Structure and Dynamics.* 1–17.
https://doi.org/10.1080/07391102.2020.1819878.

Hizaddin, H. F., Hadj-Kali, M. K., Ramalingam, A., and Hashim, M. A. (2016). Extractive Denitrogenation of Diesel Fuel Using Ammonium- and Phosphonium-Based Deep Eutectic Solvents. *Journal of Chemical Thermodynamics 95*, 164–173.
https://doi.org/10.1016/j.jct.2015.12.009.

Hohenberg, P., and Kohn, W. (1964). Inhomogeneous Electron Gas. *J., Phys. Rev. 136* (3), 864.
https://doi.org/10.1103/PhysRev.136.B864

Jorgensen, W.L., and Rives, J. T. (1988). The OPLS Potential Functions for Proteins. Energy Minimizations for Crystals of Cyclic Peptides and Crambin. *Am. Chem. Soc. 110*, 1657.
https://doi.org/10.1021/ja00214a001

Khandelwal, S.; Taylor, Y. K.; Kumar, M. (2015). Deep Eutectic Solvents (DESs) as Eco-Friendly and Sustainable Solvent/Catalyst Systems in Organic Transformations." *J. Mol. Liq. 215*, 345–386.
https://doi.org/10.1016/j.molliq.2015.12.015

Klamt, A. (1995). Conductor-like Screening Model for Real Solvents: A New Approach to the Quantitative Calculation of Solvation Phenomena. *Journal of Physical Chemistry 99* (7), 2224–2235.
https://doi.org/10.1021/j100007a062.

Klamt, A. (2005). COSMO-RS From Quantum Chemistry to Fluid Phase Thermodynamics and Drug

Design, *Elsevier. Amsterdam.* ISBN 0-444-51994-7.
https://doi.org/10.1021/je0602317

Kohn, W., Sham, L. (1965). Self-Consistent Equations Including Exchange and Correlation Effects. *J., Phys. Rev. 140* (5), 1133.
https://doi.org/10.1103/PhysRev.140.A1133

Lemaoui, T., Darwish, A. S., Attoui, A., Abu Hatab, F., Hammoudi, N. H., Benguerba, Y., Vega, L. F. and AlNashef, I. M. (2020). Predicting the Density and Viscosity of Hydrophobic Eutectic Solvents : Towards the Development of Sustainable Solvents. 15–17.
https://doi.org/10.1039/d0gc03077e.

Lemaoui, T., Hammoudi, N. H., AlNashef, I. M., Balsamo, M., Erto, A., Ernst, B. and Benguerba, Y. (2020). Quantitative Structure Properties Relationship for Deep Eutectic Solvents Using σ-Profile as Molecular Descriptors. *Journal of Molecular Liquids 309*, 113165.
https://doi.org/10.1016/j.molliq.2020.113165.

Lipkowitz, K. B. (1995). Pitfalls to Avoid. *J. Chem. Educ.,* Mm, 1070–1075.
https://doi.org/10.1021/ed072p1070

Maleki, A., Kettiger, H., Schoubben, A., Jessica, M., Ambrogi, V., Hamidi, M., (2017). PT US CR, *Journal of Controlled Release.*
https://doi.org/10.1016/j.jconrel.2017.07.047.

Martin, R. (2005). Electronic Structure : Basic Theory and Practical Methods , Martin, R. M., Cambridge University Press, 2004 . *Physics 27*(1997), 2005.
https://doi.org/10.1017/CBO9780511805769

Meyer, A.Y., and Forrest, R.F. (1981). Electrostatic Term Even for Hydrocarbons. *Journal of American Chemical Society, 103*, 4664.

Rackett, H. G. (1970). Equation of State for Saturated Liquids. *Journal of Chemical and Engineering Data 15* (4), 514–517.
https://doi.org/10.1021/je60047a012.

Rappé, A. K., Casewit, C. J., Kolwell, K. S. and Skiff, W. M. (1992). UFF, a Full Periodic Table Force Field for Molecular Mechanics and Molecular Dynamics Simulations. *J. Am. Chem. Soc. 2*, 10024–10035.
https://doi.org/10.1021/ja00051a040

Ruß, C., and Burkhard, K. (2012). Low melting mixtures in organic synthesis – an alternative to ionic liquids? *J. Green Chemistry, 14*, 2969.
https://doi.org/10.1039/b000000x

Schrödinger, E. (1926). Quantisierung Als Eigenwert Problem. *Phys. Leipzig, 79*, 361–376.
https://doi.org/10.1002/andp.19263840404

Shahbaz, K., Mjalli, F. S., Vakili-Nezhaad, G., AlNashef, I. M., Asadov, A. and Farid. M. M. (2016). Thermogravimetric Measurement of Deep Eutectic Solvents Vapor Pressure. *Journal of Molecular Liquids 222*, 61–66.
https://doi.org/10.1016/j.molliq.2016.06.106.

Spencer, C. F., and Danner, R. P. (1972). Improved Equation for Prediction of Saturated Liquid Density. *Journal of Chemical and Engineering Data 17*(2), 236–241.
https://doi.org/10.1021/je60053a012.

Sun, H., Li, Y., Wu, X. and Li, G. (2013). Theoretical Study on the Structures and Properties of Mixtures of Urea and Choline Chloride. *Journal of Molecular Modeling 19*(6), 2433–2441.

https://doi.org/10.1007/s00894-013-1791-2.

Tomé, L. I.N., Baião, V., da Silva, W. and Brett, C. M. A. (2018). Deep Eutectic Solvents for the Production and Application of New Materials. *Applied Materials Today 10*, 30–50. https://doi.org/10.1016/j.apmt.2017.11.005.

Tristram, F., Durier, V. and Vergoten, G. (1996). The Structures and Vibrational Frequencies of a Series of Aliphatic Alcohols as Obtained Using the Spectroscopic Potential SPASIBA. *Journal of Molecular Structure, 378*(3), 249–256. https://doi.org/10.1016/0022-2860(95)09183-1.

Volatron, Y. J. 1993. An Introduction to Molecular Orbitals. 1st edition. *Oxford University Press*. ISBN 9780195069181

Warrag, S. E. E., Darwish, A. S., Idowu, A., Adeyemi, M., Hadj-Kali, K., Kroon, M. C. and AlNashef, I. M. (2020). Extraction of Pyridine from N-Alkane Mixtures Using Methyltriphenylphosphonium Bromide-Based Deep Eutectic Solvents as Extractive Denitrogenation Agents. *Fluid Phase Equilibria 517*, 112622. https://doi.org/10.1016/j.fluid.2020.112622.

Zhang, Q., De Oliveira Vigier, K., Royer, S. and Jérôme. F. (2012). Deep Eutectic Solvents: Syntheses, Properties and Applications. *Chemical Society Reviews 41*(21), 7108–7146. https://doi.org/10.1039/c2cs35178a.

Chapter IV: Results and discussion

IV.1. Introduction

The use of DESs being recent in polymer technology, it was necessary to perform a theoretical study on a series of DESs to gain knowledge on this new class of green solvents before commencing modeling polymer synthesis and composite preparation using a DES as reaction medium, monomer and filler in part two of the chapter.

In a first step, binary deep eutectic solvents (DESs) are computationally *(in-silico)* designed by combining three quaternary ammonium salts, namely tetramethylammonium chloride (TMAC), choline chlorine (ChCl) and betaine (Bet.) as HBAs with sorbitol (Sor.), glycerol (Gly.), urea (Ur), ethylene glycol (EG), glucose (Glu.), acetic acid (AA), caffeic acid (Caf. A) and 1,2-butanediol (1,2-But.) as (HBDs). The chosen components are among the most that were reported in the literature. Preparation of DESs with high stability relies on the interaction mechanisms between the HBAs and HBDs within the DES. In the present work, interaction energies are calculated by means of COnductor-like Screening MOdel for Real Solvents (COSMO-RS) theory, which is also used to calculate σ–profiles and σ–potentials. The charge density, Fukui indices, reactivity and combination mechanisms are predicted using Dmol3 module (Materials Studio) for each component and the resulting DESs. COSMO*thermX* functions are utilized to calculate the physicochemical properties of the designed DESs. Comparison of the calculated properties is expected to provide satisfactory information about the stability and performance of the chosen deep eutectic solvents. Most of the DESs studied here have been experimentally investigated and results are reported by the literature. The present chapter being a computational investigation, is expected to provide theoretical results that match mostly with the results found in the literature.

In the second part of this chapter, we suggest utilizing a benzalkonium chloride-based hydrophobic eutectic solvent (HES) as reaction medium, monomer and filler for the synthesis of a poly(diol citrate) (PDCA). Spotting the light on the molecular-level interactions and mechanisms, a theoretical computational study is conducted to evaluate the feasibility of the process by exploiting a combination of geometrical optimizations, COSMO-RS quantum chemical calculations, density functional theory (DFT) calculations, reactivity calculations, and a blend compatibility study. The studied HES is comprised of dodecyldimethylbenzyl ammonium chloride (DDBAC) as HBA and 1,10-decanediol ($D_{10}DO$) as the diol HBD at a 1:3 M ratio. The results to be obtained, are expected to demonstrate that DDBAC-based HESs can be considered as potential solvents for antimicrobial PDCA composites. Additionally, the modeling framework reported in this work can be utilized for screening new types of DESs

promoting an efficient design approach of new PDCA composites with tailored properties based on the choice of the DES.

IV.2. Physicochemical properties of selected ammonium salt-based DESs
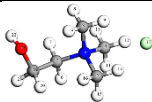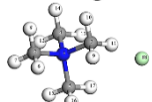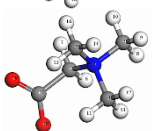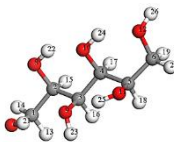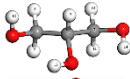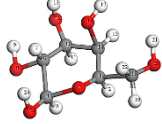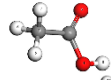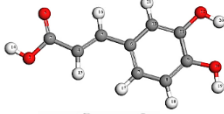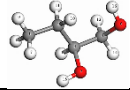
IV.2.1. Computational details

Unlike conventional solvents, the physicochemical and thermodynamic properties of DESs are scarce and not easy to predict. Experimental methods alone cannot be relied on in designing and selecting appropriate DESs for specific processes. Thus, COSMO-RS (thermodynamic model based on quantum chemical calculations) was utilized as an advantageous tool for fast, accurate and reliable tool for modelling and predicting the properties of the chosen DESs.

COSMO-RS theory involves interacting molecular surfaces computed by means of quantum chemical methods (QCM). COSMO-RS associates an electrostatic theory of descriptors of locally interacting molecular surfaces with a statistical thermodynamics approach. COSMO-RS theory considers a liquid as an ensemble of molecules closely packed and ideally partitioned. Statistical averaging thermodynamic properties of compounds within the ensemble of interacting surface pieces. COSMO*therm* being a program based on COSMO-RS, is utilized to compute thermophysical data of liquids. All current parameterization sets of versions C30_1501 include the Quantitative Structure Property Relationships (QSPR) parameters for prediction at room temperature (Klamt et al., 2010). The calculated parameters include HBA type (cation substructure, alkyl chain length, choice of anion), HBD type, HBA: HBD molar ratio, electronic and molecular structure, and physicochemical properties. The computational procedure is adequate for choosing the appropriate component pairing for forming DESs and predicting their behavior.

Table IV.1 bellow lists the components used as HBAs and HBDs in this work with their melting points before mixing. The molar surfaces and volumes were computed using COSMO-RS.

Table IV.1. Structure, melting point, molar volume and molar surface of HBAs and HBDs of DESs.

Nomenclature	Formula	Chemical Structure	T_M (°C)	Volume (Å³)	Surface (Å²)	[Ref.]
Hydrogen bond acceptors (HBAs)						
ChCl	$C_5H_{14}ClNO$		302	1171.116	647.237	(Aissaoui et al., 2017)
TMAC	$C_4H_{12}NCl$		425	976.468	557.425	(Li et al., 2018)
Bet	$C_5H_{11}NO_2$		293	958.912	534.842	(Lide, 2007)
Hydrogen bond donors (HBDs)						
Sor	$C_6H_{14}O_6$		88–102	1266.759	690.046	
Gly	$C_3H_8O_3$		18	718.048	444.912	(Zhang et al., 2012)
Ur	CH_4N_2O		132.7-135	468.193	318.474	
EG	$C_2H_6O_2$		-12.9	525.036	348.271	
Glu	$C_6H_{12}O_6$		146	DG: 1239.154 G: 1212.646	661.405 650.169	(Lide, 2007)
AA	CH_3COOH		16.6	486.501	327.194	
Caf. A	$C_9H_8O_4$		212	1305.753	726.206	(Zhang et al., 2012)
1,2-but	$C_4H_{10}O_2$		-50	777.963	472.196	(Lide, 2007)

Key: ⬤ Carbon   🟢 Chlorine   🔴 Oxygen   🔵 Nitrogen   ⚪ Hydrogen

While Table IV.2 shows the possible combinations obtained from a series of HBAs and HBDs chosen with the corresponding molar ratios and DES melting points. It is worth noting that melting points of DESs are lower than those of pure components (Table IV.1).

Table IV.2. HBA, HBD, molar ratios and freezing temperatures of the corresponding DESs.

DES	HBA	HBD	Molar ratio	T_f [°C]	[Ref.]
DES1		Sor	1 : 1	23	(García et al., 2015)
DES2		Gly	1 : 2	-40	(Klamt et al., 2010)
DES3		Ur	1 : 2	12	(Li et al., 2016)
DES4	ChCl	EG	1 : 2	-66	(Zhang et al., 2012)
DES5		Glu	1 : 1	-	(Klamt et al., 2010)
DES6		AA	1 : 2	-	(Li et al., 2016)
DES7		Caf.A	1 : 0.5	67 ± 3	(Tang et al., 2015)
DES8		1,2-but	1 : 2		(Durand et al., 2013)
DES9		Sor	1 : 0.5	-	(Hizaddin, 2016)
DES10		Gly	1 : 2	-	(Hizaddin, 2016)
DES11		Ur	1 : 2	-	(Li et al., 2016)
DES12	TMAC	EG	1 : 2	-	(Hizaddin, 2016)
DES13		Glu	1 : 1	-	
DES14		AA	1 : 2	L. R. T.	(Li et al., 2016)
DES15		Caf. A	1 : (0.5, 1, 1.5, 2)*	-	
DES16		1,2-but	1 : (1, 2, 3, 4)*	-	
DES17		Sor	3 : 1	-	(Dai et al., 2013)
DES18		Gly	1 : 2	-	(Li & Row, 2017)
DES19		Ur	1 : 2	-	(Li et al., 2016)
DES20	Bet.	EG	1 : 1	-	
DES21		Glu	1 : 2	-	
DES22		AA	1 : 2	L. R. T.	(Li & Row, 2017)
DES23		Caf. A	1 : (0.5, 1, 1.5, 2)*	-	
DES24		1,2-but	1 : (1, 2, 3, 4)*	-	

L. R. T.: Liquid at room temperature, *: Experienced Molar ratios gave liquid mixtures (in our lab)

Some DESs that are listed in Table IV.2 were not reported in the literature, e.g. TMAC/Caf.A (DES15), TMAC/1,2-But (DES16), Bet/CA (DES23), Bet/1,2-But (DES24). The properties of these DESs were computed (*in silico*).

The interaction study between the HBAs and HBDs was carried out using the COSMO-RS theory. The two main steps required to perform COSMO-RS calculations can be summarized as follows:

1) Geometry optimization of each species involved in forming the DES using Dmol3 module (Delley, 2000) from the modeling package Materials Studio 2017™ developed by Accelrys Incorporation (Cambridge, UK) (Pirhadi et al., 2016) using B3LYP functional and DNP basis set (4.4 basis file). COSMO files were then produced for each HBD and HBA to be used in the second step. In addition, Fukui indices were calculated;

2) Preparation of DESs by means of COSMO*thermX* software by importing the COSMO files obtained after geometry optimization. The "mixture" function was used for a combination of an HBD with an HBA to obtain the desired DES. COSMO*thermX* functions were then used to calculate the physicochemical properties such as density, activity coefficient and vapor pressure of the obtained DESs. COSMO*thermX* was also used to calculate σ–profiles (polarities), σ–potentials (affinities) and interaction energies (Eckert and Klamt, 2002).

IV.2.2. Results and discussion

IV.2.2.1. Sigma-profiles and sigma-potentials

HIZADDIN *et al.* (Hizaddin, 2016) defined the σ-profile as being a distribution function giving the relative surface value with polarity in the molecule.

For basically quantum chemical COSMO calculations, the molecule is supposed to be surrounded by a discrete surface embedded in a virtual conductor. Each surface segment has a characteristic area and a screening charge density (SCD) noted (σ). COSMO*therm* uses the compound information from COSMO files and transforms the screening charge surface into a screening charge distribution. σ-profiles give a detailed and reliable description of the polarity of molecules.

For mixtures, molecular interactions are considered by COSMO-RS as local pair interactions of segments within molecular COSMO-surfaces. Consider a mixture system *S* of X_i compounds with mole fraction x_i. The σ-profile of the system noted p_S, is the weighted sum of the σ-profiles of the components.

Negative sigma-profile values (p_S) correspond to positive polarities, while positive p_S values correspond to negative polarities. Also, narrow peaks indicate low polarities, while broad peaks indicate high polarities (Aissaoui et al., 2017). The sigma profile for each DES is divided into three regions: the HBD region, the nonpolar region, and the HBA region as shown in Figure IV.1 The three regions are separated by the threshold value for hydrogen bonding $\sigma_{hb} = \pm 0.0084$ e Å^{-2}. Peaks at $\sigma < -\sigma_{hb}$ show the presence of compounds with affinity towards hydrogen bond donors, whereas peaks at $\sigma > +\sigma_{hb}$ are specific to compounds exhibiting affinity towards hydrogen bond acceptors.
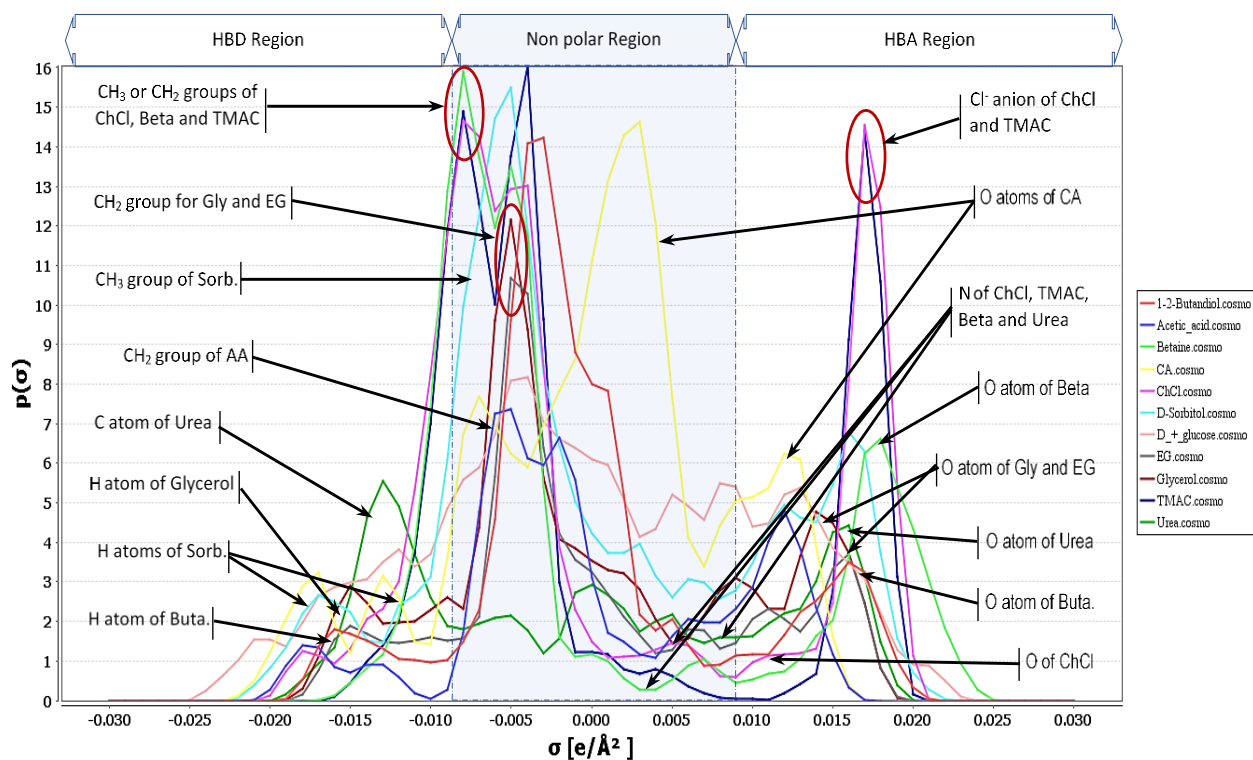
Figure IV.1. Sigma-profiles of HBAs and HBDs constituting the DESs as a function of polarity.

Sigma profile graphs for each species are shown in Figure IV.1. The recorded peaks range between -0.025 and +0.025 e.Å^{-2}, and their interpretation is detailed below :

a. **In HBA region**: Two positive peaks appear at 0.015 to 0.02 e.Å^{-2} for ChCl and TMAC molecules showing the strong electronegativity of Cl$^-$ anion. Two broad peaks located at 0.012-0.018 e.Å^{-2} belong to the oxygen atom of glycerol and ethylene glycol. While a weak oxygen atom peak appears for ChCl. It is clear that for ChCl, the chlorine peak is broader than that of oxygen atom. This is indicative of a higher electronegativity and thus, a higher ability of attracting hydrogen atom from the second component of the DES.

    To confirm this, Figure IV.2 comparatively highlights the most favorable interaction sites by a representation of charge densities for TMAC and betaine compared to that of ChCl. Indeed, this figure shows clearly the high polarity of Cl atom in TMAC, and O atoms in betaine. This polarity, represented by a dark red color, can also be seen for Cl atom in ChCl. However, the oxygen atom charge density shows a very weak polarity in ChCl which is represented by a light red "non-accentuated" COSMO-region surrounding the oxygen atom.
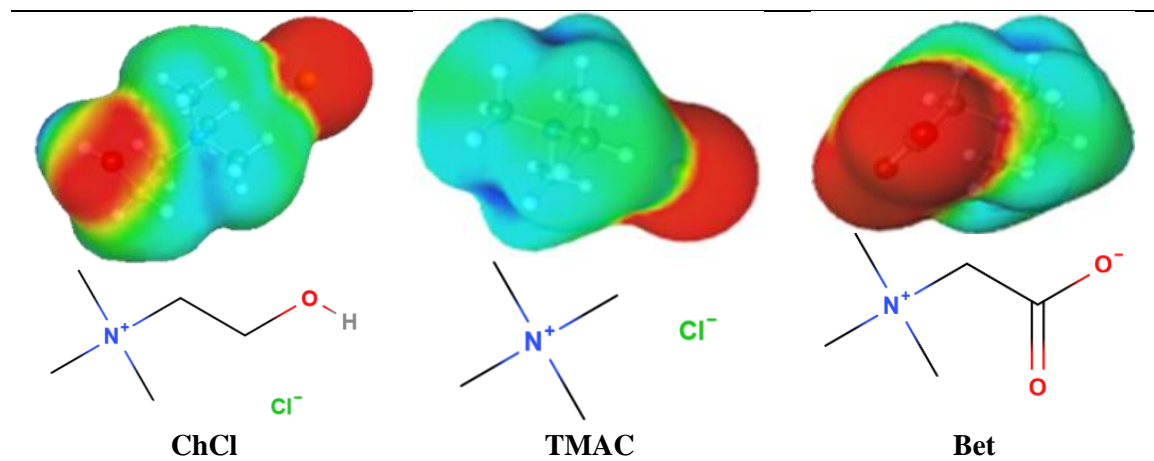
Figure IV.2. Charge densities and chemical structures of ChCl, TMAC and Betaine.

D-sorbitol molecule shows two wide peaks attributed to H- and C-bonded oxygen atom representing the negative polarities of the molecule.

b. **In the non-polar region**: Among all components containing nitrogen atom, only urea molecule reveals a N peak in this region. Also, peaks specific to CH_3 and CH_2 groups of ChCl, TMAC and betaine are observed in the non-polar region. Narrow peaks were recorded at the negative σ value of (-0.004 e.Å^{-2}) for EG and glycerol, indicating the presence of CH_3 group in this region.

c. **In HBD region**: Sorbitol molecule shows two broad peaks attributable to H atoms. The broad peaks noticed at the negative values of σ between -0.01 and - 0.008 e.Å^{-2} indicate the positive charge of H atom in glycerol molecule.

While O atom is present in all components except TMAC, the corresponding peaks are close to the non-polar region within the HBA area. Oxygen peak becomes much closer to the non-polar region in the presence of Cl^- anion such as for ChCl molecule.

The σ-potential is the chemical potential of a surface segment with screening charge density σ characteristic to a given system, which describes the affinity of the solvent for a molecular surface of polarity σ (Hizaddin, 2016).

Figure IV.3 representing sigma-potential curves shows clearly the strong affinity of betaine towards HBDs by the tendency of the corresponding curve to less negative values of chemical potential in the HBD region. Then, comes ChCl in second place followed by TMAC. In the opposite side, the best affinity towards HBAs was for caffeic acid, acetic acid and glucose, respectively. These results show that the preferential HBA:HBD pairing is betaine:caffeic acid.
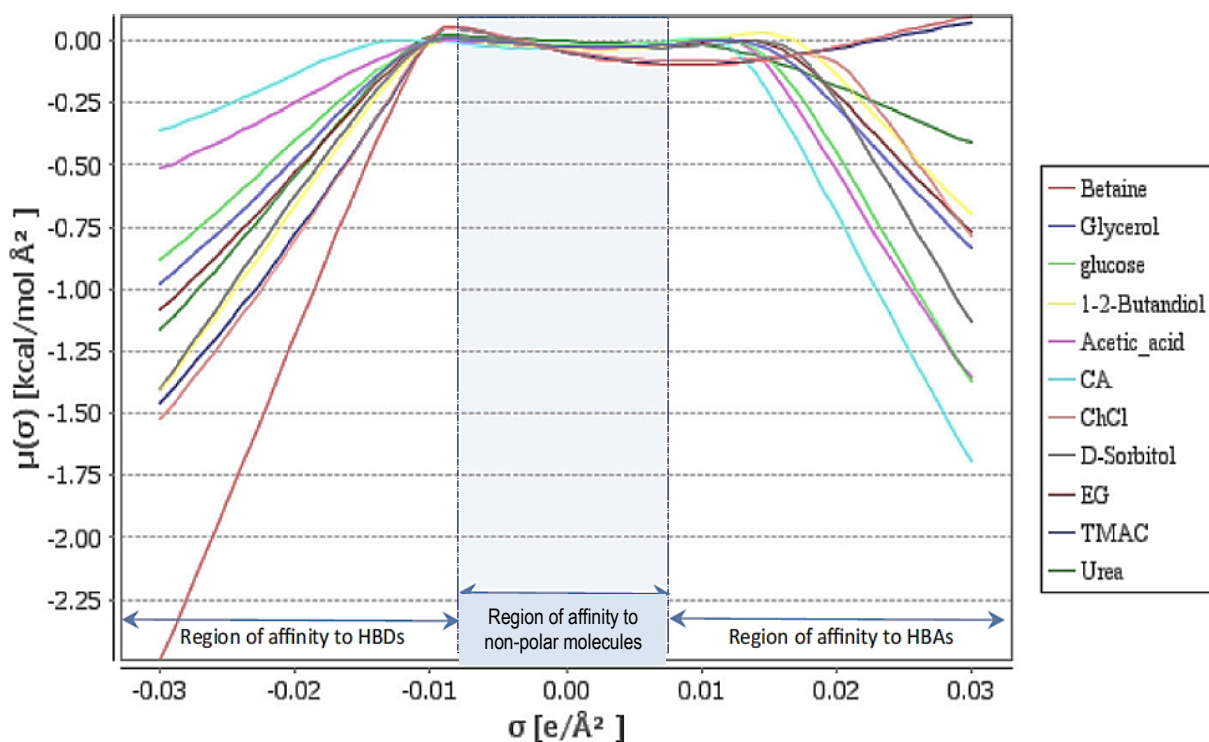
Figure IV.3. Sigma-potentials of HBAs and HBDs composing the DESs as a function of density distribution.

IV.2.2.2. Physicochemical properties

1) Infinite Dilution Activity Coefficient

Activity coefficients of DESs were investigated to gain comprehensive view on defining the most appropriate component to serve as solvent and the one to serve as solute. A reliable quantitative method based on COSMO-RS for solvent screening allows predicting the value of the infinite activity coefficient (γ^{∞}). Prediction of γ^{∞} values can also be used for DES screening and tailoring for different applications (eg. separation processes).

For each DES, activity coefficient at infinite dilution of HBD (γ_A^{∞}) was calculated at room temperature assuming that the HBD is extremely diluted into the HBA (HBD amount infinitely negligible within the DES). Similarly, activity coefficient at infinite dilution of HBA (γ_D^{∞}) was calculated assuming the HBA extremely diluted into the HBD (HBA amount infinitely negligible within the DES). ($\ln \gamma^{\infty}$) for the solutes in the potential solvents are summarized in Table IV.3.

Table IV.3. Values of ($ln\ \gamma_A^\infty$) and ($ln\ \gamma_D^\infty$) for HBAs and HBDs within the studied DESs.

DES	Activity coefficient		DES	Activity coefficient	
	$ln\ \gamma_A^\infty$	$ln\ \gamma_D^\infty$		$ln\ \gamma_A^\infty$	$ln\ \gamma_D^\infty$
DES1	- 5.410	- 3.161	DES13	- 18.894	- 13.045
DES2	- 9.130	- 3.806	DES14	- 24.919	- 5.686
DES3	- 6.911	- 3.297	DES15	- 34.110	- 18.787
DES4	- 6.519	- 2.179	DES16	- 4.325	- 2.416
DES5	- 17.327	- 11.416	DES17	- 12.761	- 10.429
DES6	- 23.185	- 4.815	DES18	- 15.298	- 8.066
DES7	- 32.307	- 16.260	DES19	- 10.701	- 6.154
DES8	- 2.838	- 1.370	DES20	- 12.521	- 5.159
DES9	- 6.549	- 4.271	DES21	- 24.485	- 22.149
DES10	- 11.287	- 4.945	DES22	- 29.810	- 8.614
DES11	- 9.008	- 4.149	DES23	- 38.906	- 26.570
DES12	- 8.401	- 2.995	DES24	- 8.866	- 5.024

In terms of activity coefficient, the most interesting mixtures are those containing Caffeic acid extremely diluted in HBDs in the following decreasing order: Caf.A in bet for DES_{23}, followed by Caf.A in TMAC for DES_{15}, then Caf.A in ChCl for DES_7, where $ln\ \gamma_{Bet}^\infty$ = -38.906, $ln\ \gamma_{TMAC}^\infty$ = -34.110, and $ln\ \gamma_{ChCl}^\infty$ = -32.307, respectively. Then come successively also in decreasing order: Acetic acid extremely diluted in betaine ($ln\ \gamma_{Bet}^\infty$ = -29.810) for DES_{22} > bet into Caf.A ($ln\ \gamma_{CafA}^\infty$ = -26.570) for DES_{23} > AA in TMAC ($ln\ \gamma_{TMAC}^\infty$ = -24.919) for DES_{14} > Glu in bet ($ln\ \gamma_{Bet}^\infty$ = -24.485) for DES_{21} > AA in ChCl ($ln\ \gamma_{ChCl}^\infty$ = -23.185) for DES_6 > Bet in Glu ($ln\ \gamma_{Glu}^\infty$ = -22.149) for DES_{21} > EG in TMAC ($ln\ \gamma_{TMAC}^\infty$ = -18.894) for DES_{13} > Glu in TMAC ($ln\ \gamma_{Caf.A}^\infty$ = -18.787) for DES_{15}.

2) Vapor pressure.

The main particularity of DESs is their low volatility compared to those of organic solvents used in industry. Vapor pressures of the considered DESs were calculated at 25.15 °C and represented in Table IV.4. Shahbaz *et al.* (Kaveh Shahbaz et al., 2016) reported the experimental vapor pressure of selected DESs at different temperatures. The reported values for DES_2 and DES_3 at 70 °C are 0.02 and 3.4 x 10^{-3} mbar, respectively. The large difference between the measured and predicted values was also reported by Aissaoui *et al.* (Aissaoui et al., 2016). It is worth noting that the calculated and measured values of the vapor pressure of DES_2 and DES_3 have the same trend.

Table IV.4. Calculated vapor pressures for the DESs at 25°C.

DES	Vapor Pressure (mbar)	DES	Vapor Pressure (mbar)
DES1	6.424×10^{-13}	DES13	1.636×10^{-10}
DES2	5.662×10^{-4}	DES14	3.370×10^{-1}
DES3	6.765×10^{-6}	DES15	$[1.21 \times 10^{-10} - 1.832 \times 10^{-9}]$
DES4	8.582×10^{-2}	DES16	$[7.668 \times 10^{-4} - 2.020 \times 10^{-3}]$
DES5	3.468×10^{-13}	DES17	6.656×10^{-8}
DES6	4.295×10^{-1}	DES18	2.265×10^{-4}
DES7	4.148×10^{-12}	DES19	1.139×10^{-4}
DES8	1.600×10^{-3}	DES20	8.819×10^{-3}
DES9	3.356×10^{-9}	DES21	6.507×10^{-13}
DES10	4.340×10^{-4}	DES22	10^{-1}
DES11	1.385×10^{-4}	DES23	$[1.072 \times 10^{-10} - 1.237 \times 10^{-8}]$
DES12	6.888×10^{-2}	DES24	$[2.194 \times 10^{-4} - 1.568 \times 10^{-3}]$

The lowest calculated vapor pressure value was for DES_5 (3.468×10^{-13} mbar) making it the least volatile DES. Arranging the DESs according to their vapor pressure in increasing order leads to : $P^V_{DES_5} < P^V_{DES_1} < P^V_{DES_{21}} < P^V_{DES_7} < P^V_{DES_{13}} < P^V_{DES_{15}} < P^V_{DES_9} < P^V_{DES_{23}} < P^V_{DES_{17}} < P^V_{DES_3} < P^V_{DES_{19}} < P^V_{DES_{11}} < P^V_{DES_{18}} < P^V_{DES_{10}} < P^V_{DES_2} < P^V_{DES_{24}} < P^V_{DES_8} < P^V_{DES_{16}} < P^V_{DES_{20}} < P^V_{DES_{12}} < P^V_{DES_4} < P^V_{DES_{22}} < P^V_{DES_{14}} < P^V_{DES_6}$.

Calculations show vapor pressure values ranging between 3.468×10^{-13} mbar, for DES_5, and 0.4295 mbar, for DES_6. Which represents an insignificant volatility of the DESs.

3) Density

The Rackett equation modified by Spencer and Danner was employed with COSMO-RS to predict the density of DESs as described by Shahbaz *et al.* (Shahbaz et al., 2011).

Values of calculated densities using COSMO*therm* are listed in Table IV.5. In agreement with what was mentioned above, the calculated values range between 1.04 (DES_{16}) and 1.433 g cm^{-3} (DES_{21}) making the results reliable.

ZHANG *et al*. reported experimental densities of 1.25 and 1.12 g.cm^{-3} for ChCl:Ur (1:2) and ChCl:EG (1:2), respectively (Zhang et al., 2012). These values are very close to the calculated values of 1.286 and 1.1 g.cm^{-3}, for DES_3 and DES_4, respectively (Table IV.5). For ChCl:Gly (1:2), the calculated density found equal to 1.202 g.cm^{-3} (DES_2), is in agreement with both experimental values reported in the literature of 1.18 g.cm^{-3} (Zhang et al., 2012) and

1.19 g.cm^{-3} (Aissaoui, Benguerba, et al., 2017). It is also considered in good agreement with the calculated value of 1.227 g.cm^{-3} using the COSMO-RS theory and Amsterdam Density Functional (ADF) package (Aissaoui, Benguerba, et al., 2017).

DURAND *et al.* (Durand et al., 2013) reported an experimental value of density for ChCl:Glu (1:1) DES of 1.24 g.cm^{-3}, whereas the predicted value was 1.362 g.cm^{-3}. The difference is slightly higher than for ChCl:Gly, but remains acceptable.

In addition, the calculated value of density for TMAC:Gly (1:2) DES of 1.175 g.cm^{-3} is in good agreement with the experimental value of 1.155 g.cm^{-3} reported by Rodriguez *et al.* (Rodriguez et al., 2016). These examples confirm the reliability of COSMO*therm* for the calculation of the density of DESs.

4) Viscosity

The discrepancies between the experimental and theoretical viscosity values are due to the adoption of the classic GRUNBERG-NISSAN mixture rule (Eq III.36) instead of its modified form that accounts for the binary interaction coefficients. Although the GRUNBERG-NISSAN correlation usually gives poor results for polar mixtures (Marczak et al., 2012), it was used here for its simplicity (Table IV.5).

Table IV.5. Predicted densities and viscosities of DESs.

DES	Density (g/cm^3)	Viscosity (cP)	DES	Density (g/cm^3)	Viscosity (cP)
DES1	1.264	1.288×10^5	DES13	1.322	4.962×10^5
DES2	1.202	3.952×10^3	DES14	1.073	2.057×10^1
DES3	1.286	3.877×10^3	DES15	1.165-1.278	$[7.373 \times 10^2 – 1.423 \times 10^3]$
DES4	1.099	3.870×10^3	DES16	1.040-1.045	$[8.215 \times 10^1 – 9.949 \times 10^1]$
DES5	1.362	5.019×10^5	DES17	1.183	6.157×10^4
DES6	1.100	3.860×10^3	DES18	1.196	1.131×10^2
DES7	1.218	8.427×10^3	DES19	1.279	3.834×10^1
DES8	1.069	3.931×10^3	DES20	1.098	3.758×10^1
DES9	1.166	8.198×10^4	DES21	1.433	6.619×10^5
DES10	1.175	1.124×10^2	DES22	1.093	2.132×10^1
DES11	1.259	3.760×10^1	DES23	1.205-1.298	$7.387 \times 10^2 – 1.424 \times 10^3$
DES12	1.073	3.086×10^1	DES24	1.052-1.075	$8.326 \times 10^1 – 9.993 \times 10^1$

According to Table IV.5, DESs seem to show viscosities of various orders:

i. $\eta_{DES_{21}} > \eta_{DES_5} > \eta_{DES_{13}} > \eta_{DES_1}$ (order of viscosities: 10^5 cP)

ii. $\eta_{DES_9} > \eta_{DES_{17}}$ (order of viscosities: 10^4 cP)

iii. $\eta_{DES_7} > \eta_{DES_2} > \eta_{DES_8} > \eta_{DES_3} > \eta_{DES_4} > \eta_{DES_6} > \eta_{DES_{23}}$ (order of viscosities: 10^3 cP)

iv. $\eta_{DES_{15}} > \eta_{DES_{18}} > \eta_{DES_{10}}$ (order of viscosities: 10^2 cP)

v. $\eta_{DES_{24}} > \eta_{DES_{16}} > \eta_{DES_{19}} > \eta_{DES_{20}} > \eta_{DES_{12}} > \eta_{DES_{14}} > \eta_{DES_{22}}$ (less than 100 cP)

The predicted viscosity for ChCl:Glycerol (1:2) DES of 3952 cP is an order of magnitude higher than the experimental values of 365.7 cP (Rodriguez et al., 2016), 259 cP (Zhang et al., 2012) and 350 cP (Aissaoui et al., 2017).The predicted viscosity of ChCl:Urea (1:2) DES, 3877 cP, is much higher than the experimental value of 750 cP reported in the literature (Zhang et al., 2012).

The experimental value of 37 cP for ChCl:EG (1:2) reported by ZHANG *et al.* (Zhang et al., 2012) is much lower than the value calculated in this work, 3870 cP. Surprisingly, the experimental viscosity of TMAC: Glycerol (1:2) reported equal to 406.9 cP (Rodriguez et al., 2016), is higher than value found by calculation which is 112.4 cP. Based on the above, more work is needed to understand the reason for the difference between the experimental values and those calculated here using COSMO-RS program.

5) **Reactivity**

HOMO and LUMO are the terms assigned to frontier orbitals (Higher Occupied Molecular Orbital and Lower Unoccupied Molecular Orbital, respectively), and essential in determining the amount of energy necessary to electron exchange in a molecule. HOMO is associated with the tendency of a species to donate electron while LUMO is associated with the tendency to receive electron. Molecules with a large HOMO-LUMO energy gap are hard molecules, which means highly stable and not likely to charge transfer because they resist changes in their electron number and distribution. This stability results in preventing crystallization of DESs at room temperature (Hammond et al., 2016). Softness (*S*) is defined as the reciprocal of the hardness (Table IV.6).

Table IV.6. Energies of Highest Occupied Molecular Orbital (E_{HOMO}) and Lowest Unoccupied Molecular Orbital (E_{LUMO}), Hardness (η), Electronic chemical potential (μ) and electrophilicity index (η) for HBAs and HBDs expressed in eV.

Comp	HBAs			HBDs							
	ChCl	**TMAC**	**Bet**	**Sorb**	**Gly**	**Ur**	**EG**	**Glu**	**AA**	**CA**	**1,2-But**
E_{HOMO}	-6.18	-6.23	-6.32	-7.35	-7.4	-7.19	-7.38	-7.32	-7.71	-5.92	-7.46
E_{LUMO}	1.32	1.48	0.65	1.04	1.63	1.31	1.78	1.06	0.07	-1.89	1.71
η	3.75	3.86	3.49	4.19	4.51	4.25	4.58	4.19	3.89	2.02	4.59
μ	-2.43	-2.37	-2.83	-3.16	-2.89	-2.94	-2.80	-3.13	-3.82	-3.90	-2.87
ω	0.79	0.73	1.15	1.19	0.92	1.02	0.85	1.17	1.87	3.78	0.90

Hardness, as well as electronic chemical potential and related electrophilicity, are crucial in pairing the appropriate HBA/HBD systems. In the analysis of the chemical reactivity of a molecule, electrophilicity is generally used as a structural depictor. A molecule with low chemical potential is a good electrophile, while a hard molecule has a low electron acceptability. Consequently, a measure of molecular electrophilicity depends on both the chemical potential and the chemical hardness. In addition, the higher the electrophilicity (thus lower "μ" and "η"), the higher the ability of the molecule to attract electrons.

In terms of increasing electrophilicity (Table IV.6), results give the following order:

➢ HBDs: $\omega_{EG} < \omega_{1,2-Buta} < \omega_{Gly} < \omega_{Urea} < \omega_{Glu} < \omega_{Sorb} < \omega_{AA} < \omega_{CA}$

➢ HBAs: $\omega_{TMAC} < \omega_{ChCl} < \omega_{Betaine}$

These results show that betaine is the strongest electron acceptor and CA is the strongest electron donor (possessing the lowest ionization potential, $I_p = -E_{HOMO}$ and thus the higher HBD (ω), which indicates that Betaine/CA is the most energetically stable DES.

For each component, Fukui indices (according to MULLIKEN) listed in Table IV.7, show the atoms presenting the prevailing polarities (f^+ for anion attractive atoms, and f^- for cation attractive atoms). These dominant polarities make the corresponding atoms the favorable sites to either hydrogen, electrostatic or VAN DER WAALS' bonding with each other (HBAs with HBDs).

Table IV.7. Fukui indices (MULLIKEN) for HBAs and HBDs.

Comp	Molecule	Fukui Indices	
		f^+	f^-
HBAs	ChCl	H22 → 0.411	Cl17 → 0.748
		H7 → 0.177	
	TMAC	H6 → 0.156	Cl18 → 0.727
		H7 → 0.155	
	Bet	C17 → 0.177	O18 → 0.380
		O19 → 0.160	O19 → 0.373
HBDs	Sor	H23 → 0.416	O8 → 0.194
		H16 → 0.176	O9 → 0.105
	Gly	H12 → 0.458	O4 → 0.216
		H13 → 0.332	O5 → 0.176
	Ur	C1 → 0.282	O2 → 0.445
			N3 → 0.123
	EG	H10 → 0.636	O3 → 0.308
		H9 → 0.283	O4 → 0.201
	Glu	H17 → 0.232	O20 → 0.095
		H21 → 0.207	H19 → 0.089
	AA	C2 → 0.310	O3 → 0.487
			O4 → 0.131
	Caf. A	C5 → 0.132	O10 → 0.900
		O3 → 0.190	C9 → 0.086
	1,2-But	H15 → 0.380	O5 → 0.293
		H16 → 0.255	O6 → 0.202

From these values, it can be observed that:

✓ Chlorine atoms of ChCl and TMAC are more electronegative than oxygen atoms of betaine

✓ Within caffeic acid molecule, oxygen atom exhibits the highest electronegativity, followed by C, which also presents a polarity in the molecule.

✓ H10 atom of EG presents the higher positive polarity among all HBDs then H12 of glycerol, followed by H23 atom of sorbitol.

✓ 1,2-Butanediol followed by acetic acid present H atoms with moderate electro-positivity

✓ Caffeic acid exhibits the weakest polarity among the HBDs. Which is expressed by the lowest $f+$ value. Followed by urea and then glucose showing slightly higher values.

As mentioned above, COSMO-RS is a two-step approach proceeding by COSMO (as an extension of the Continuum Solvation Model (CSM) of quantum mechanics) calculation of molecules using Density Functional Theory (DFT), and statistical thermodynamics (as an extension to Real Solvents (RS) part) of the molecular interactions. COSMO-RS computes the interaction energy of interacting components in terms of polarization charge densities, σ and σ' (Hizaddin, 2016). Interaction energies including the electrostatic-misfit energy E_{MF}, hydrogen-bond energy E_{HB}, VAN DER WAALS' energy E_{VdW}, and (DES) mixture energies are calculated using equations I.1-I.4 (see chapter I).

Table IV.8 summarizes the values of the interaction energies contributing in maintaining the stability of the DESs. Regardless of the sign, the higher the value, the more important the contribution of the energy type. It is clear that hydrogen-bond energy is the most contributing energy for most DESs. Results reported in the literature (Durand et al., 2013; Fischer, 2015) agree with the results of this work, indicating that DESs have specifically a strong and complex hydrogen-bonding network between the DES components. Higher values of mixture energies are indicative of more stable DESs.

Using the calculated E_{mix} values, the stability of DESs in decreasing order is as follows:

$DES_5 > DES_{21} > DES_6 > DES_2 > DES_7 > DES_1 > DES_{23} > DES_4 > DES_8 > DES_3 > DES_{13} > DES_{15} > DES_{18} > DES_{10} > DES_{12} > DES_{19} > DES_{22} > DES_{11} > DES_{24} > DES_{20} > DES_{14} > DES_{16} > DES_9 > DES_{17}$.

Table IV.8. Interaction Misfit, H-Bond and VAN DER WAALS' energies, and mixture energy of considered DESs in Kcal/mol.

DES	E_{MF}	E_{HB}	E_{VdW}	E_{Mix}
DES1	5. 039	- 19.329	- 8.807	- 23.098
DES2	4.303	- 21.636	- 8.750	- 26.083
DES3	4.646	- 16.769	- 8.810	- 20.933
DES4	4.962	- 19.118	- 8.842	- 22.998
DES5	4.054	- 25.663	- 8.719	- 30.327
DES6	4.571	- 22.534	- 8.789	- 26.751
DES7	4.700	- 19.572	- 8.929	- 23.801
DES8	5.110	- 18.794	- 8.887	- 22.572
DES9	6.141	- 7.049	- 7.851	- 8.759
DES10	4.452	- 12.314	- 7.641	- 15.503
DES11	4.845	- 7.992	- 7.686	- 10.833
DES12	5.196	- 9.702	- 7.746	- 12.252
DES13	4.260	- 16.188	- 7.619	- 19.548
DES14	5.829	- 7.985	- 7.863	- 10.019
DES15	3.796	- 15.527	- 7.725	- 19.456
DES16	5.905	- 6.940	- 7.894	- 8.929
DES17	6.435	- 8.266	- 6.868	- 8.699
DES18	4.167	- 16.101	- 6.814	- 18.747
DES19	4.647	- 9.588	- 6.891	- 11.832
DES20	5.899	- 9.086	- 6.870	- 10.057
DES21	2.520	- 23.050	- 8.133	- 28.662
DES22	5.659	- 10.557	- 6.830	- 11.728
DES23	3.509	- 19.728	- 6.861	- 23.080
DES24	5.734	- 9.674	- 6.889	- 10.829

IV.3. Synthesizing Polydecanediol-Citrate Composite Using Benzalkonium Chloride-based Hydrophobic Eutectic Solvent

IV.3.1. Selection Criteria and Synthesis Procedure

We have selected dodecyldimethylbenzyl ammonium chloride (DDBAC) as the salt molecule because it is already commercialized as active bactericide commonly utilized in wounded skins and wastewater treatment. DDBAC is also a common ingredient in various domestic products (Lee et al., 2018). As for the diol monomer, we have selected 1,10-decanediol ($D_{10}DO$) constituent as Garcia-Arguelles *et al.* reported that molecules with higher steric hindrance caused lower crosslinking (García-Argüelles et al., 2013), and thus, since polyesters with lower crosslink density degrade faster, a diol with a longer linear chain was chosen. Another advantage of utilizing DESs in polycondensation is that the presence of a DES has been previously reported to reduce the elastomer crosslinking, generating a higher molecular weight of linear chains between crosslinks (García-Argüelles et al., 2013; Serrano

et al., 2012). This is due to the additional volume created by the salt bulk molecule as a result of its position between the crosslinks. Additionally, it has been previously reported that DESs have a plasticizing effect on polymers (Wang et al., 2015), decreasing their glass transition temperature (Martins et al., 2014) and facilitating their processability (Mano et al., 2015). Introducing DESs in polymerization process also reduces the total number of reagents and provides additional thermal stability to exothermic reactions, making it easier to control the medium temperature (Mota-Morales et al., 2011). The polycondensation reaction of $D_{10}DO$ and CA is illustrated in Figure IV.4 where $D_{10}DO$ represents the $n = 10$ diol.
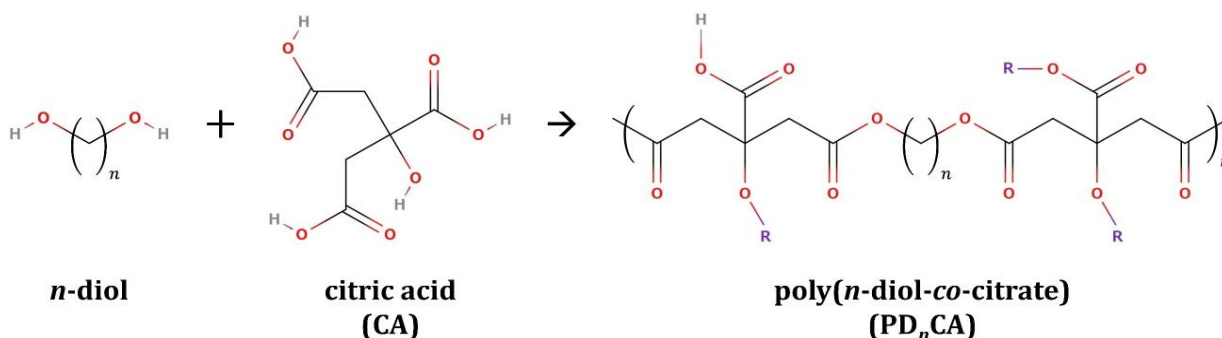
Figure IV.4. Polycondensation synthesis scheme of poly(diol-citrate). R represents hydrogen or a crosslinked polymer chain, i represents the degree of polymerization, and n and represents the diol chain length.

The process of preparing the DDBAC-filled poly(1,10-decanediol-citric acid) ($PD_{10}CA$) occurs through three major steps: *i)* the formation of the HES (polymerization medium, monomer, and filler), *ii)* the pre-polymer preparation (initiation of polymerization step till pre-polymer is formed), and finally, *iii)* crosslinking stage and the composite formation via DDBAC-filled PDCA. The first step consists in mixing DDBAC as HBA and $D_{10}DO$ as HBD at a 1:3 molar ratio by stirring the mixture at a temperature of $90^{o}C$ until a clear homogeneous liquid is obtained (Jablonský et al., 2019). The second step occurs when CA is added to the HES at the same molar ratio regarding $D_{10}DO$ (mixture molar ratio of 1:3:3 for DDBAC, $D_{10}DO$, and CA, respectively) to initiate the polycondensation process. The mixture is then left for crosslinking to occur during 10 days under stirring at about $90\ ^{o}C$. The final product is DDBAC-filled $PD_{10}CA$ elastomer. A summary of the methodology scheme is shown in Figure IV.5.

The resulting elastomer-based composite film can find use in various applications such as food tray coating which is the purpose of the present study. The DDBAC-filled $PD_{10}CA$ film is expected to be used as tray-coating to absorb the liquids of packaged food and inhibit bacterial growth to ensure longer conservation time of meat, and fruits (see Figure IV.6).
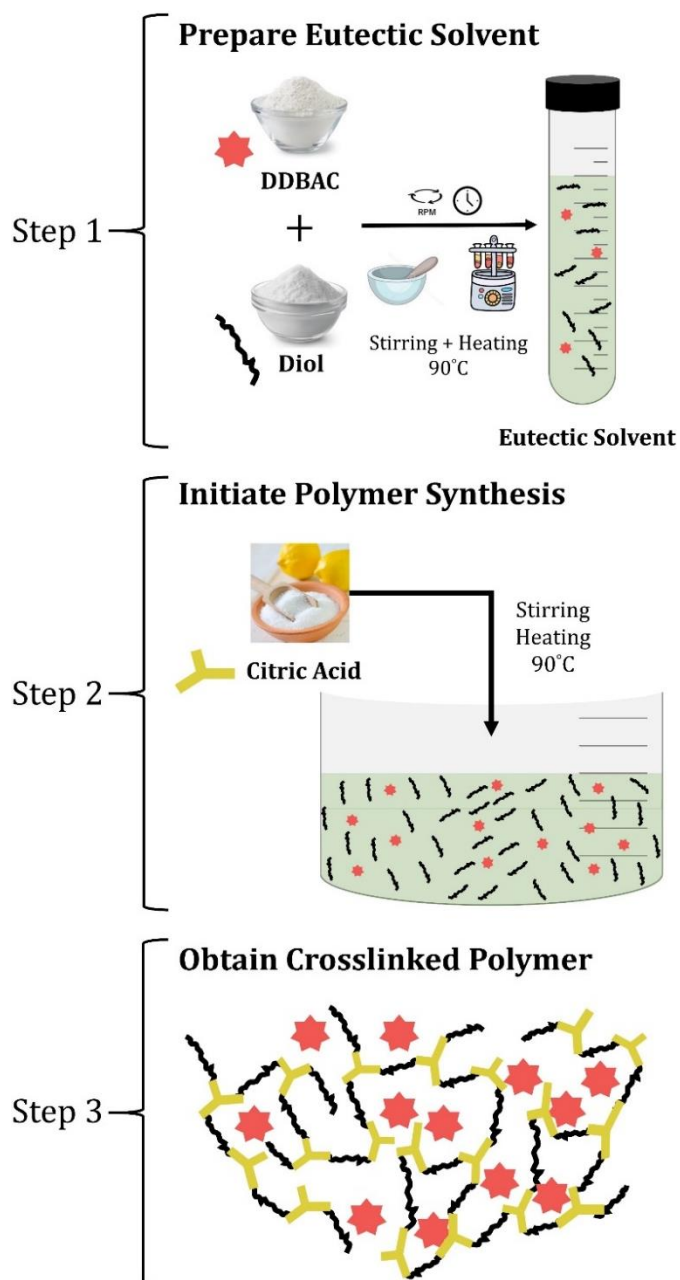
Figure IV.5. Summary of the methodology scheme to synthesize DDBAC-filled poly(1,10-decanediol-*co*-citric acid). (García-Argüelles et al., 2013)
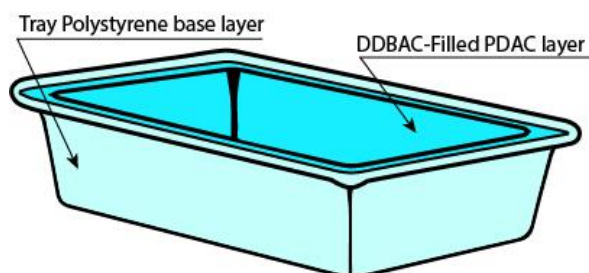
Figure IV.6. Bactericide-filled Polyester layer in the food tray.

IV.3.2. Geometry Optimization and Fukui Function Indices

All the calculations were made through the "DMOL3_PBE_C30_1501.ctd" parameterization file. A visual representation of the optimized geometry of the DDBAC:D_{10}DO (1:3) HES mixture with its hydrogen bonding interactions (dashed black lines) is shown in Figure IV.7, as detected by the software.

Key:
● carbon   ● Hydrogen   ● Oxygen
● nitrogen   ● Chloride   - - - hydrogen bonding
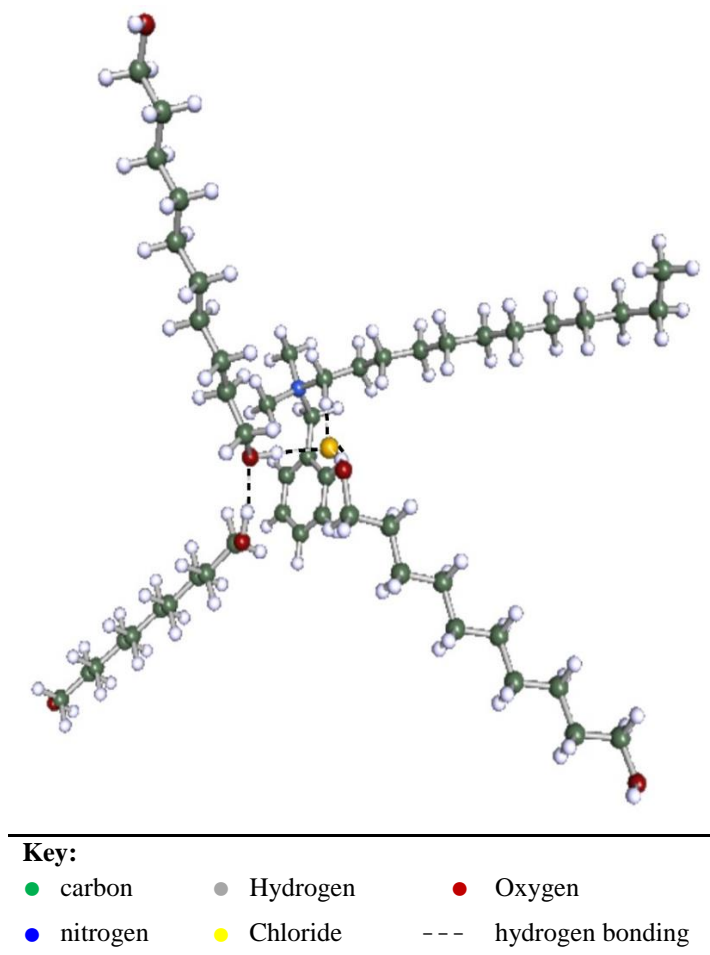
Figure IV.7. Geometrically optimized three dimensional structure of the DDBAC:D_{10}DO (1:3) mixture. The black lines represent the hydrogen bonding interactions detected by the software.

Figure IV.8 bellow, shows the labelled Fukui function indices of each atom in CA, D_{10}DO, DDBAC, and the DDBAC:D_{10}DO (1:3) mixture.

Figure IV.8. Local atomic Fukui function indices of each atom in the modeled molecules.

IV.3.3. Results and Discussion

IV.3.3.1. Surface Charge Densities (SCD) and σ-Profiles

Figure IV.9 bellow shows the SCD distribution of the geometrically optimized molecular structures of DDBAC, $D_{10}DO$, CA, DDBAC:$D_{10}DO$ (1:3) HES mixture, and $PD_{10}CA$ elastomer. The green segments denote the non-polar "neutral" parts of the molecules. The red segments symbolize the negatively charged "hydrogen-accepting" fragments of the molecules. Conversely, the blue segments represent the positively charged "hydrogen-donating" portions.
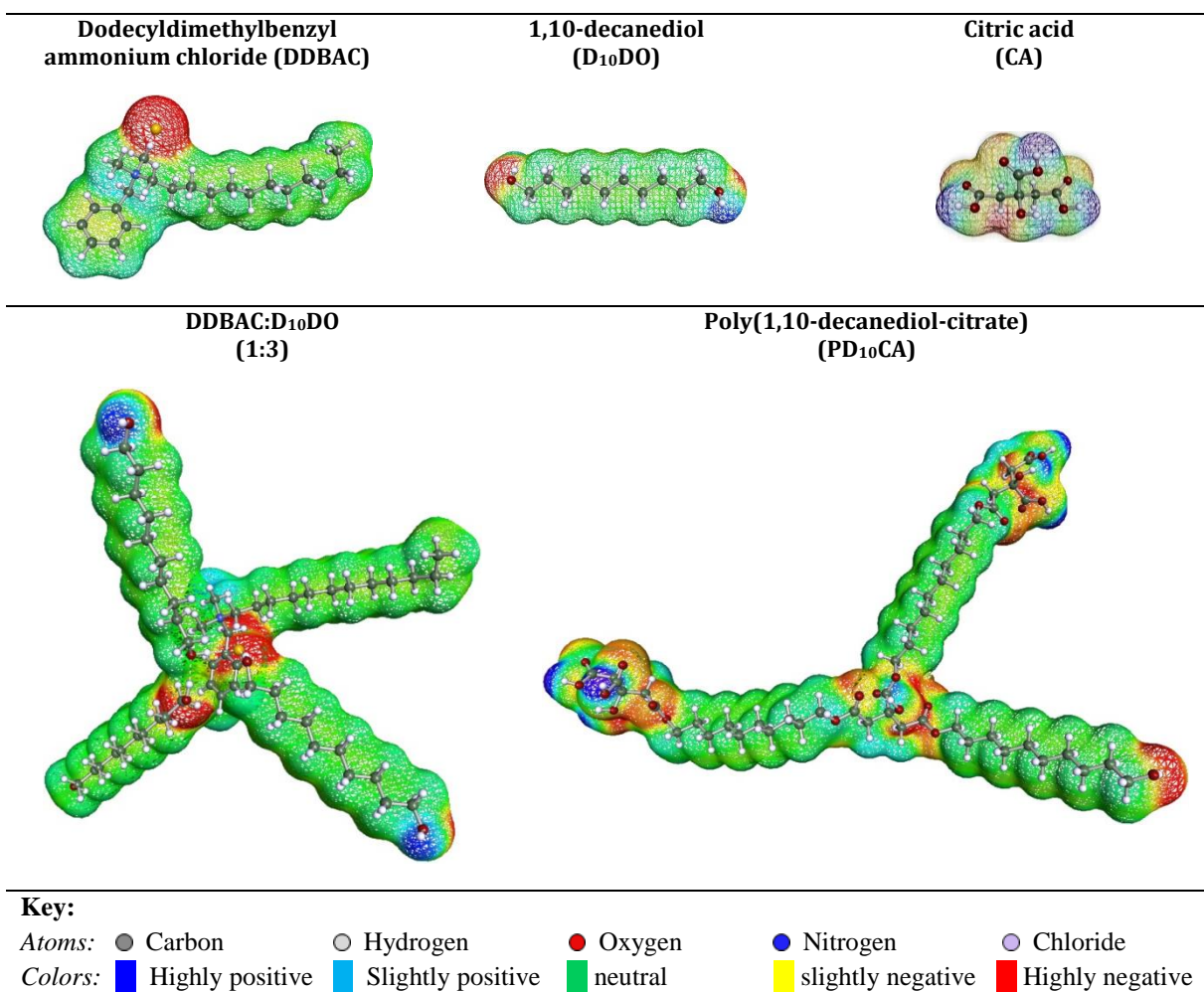
Figure IV.9. Surface charge density distributions of DDBAC, $D_{10}DO$, CA, the DDBAC:$D_{10}DO$ (1:3) HES mixture, and $PD_{10}CA$.

The SCD data were used to determine the σ-*profiles* of each molecule, which helped to obtain the results shown in Figure IV.10. The σ-*profile* of a molecule is a distribution of atomic charges within the molecule, or more appropriately at the surface of the latter that describes the relative probability of a molecular surface segment to have a particular screening charge density noted σ (Adeyemi et al., 2020; Warrag et al., 2018). These profiles also provide the "chemical information" necessary in predicting a possible interaction between two molecules.

The location of each peak in the σ-*profile* provides an indication about its polarity and thus, the tendency to attract or repulse another molecule. In this sense, the σ-*profiles* of the molecules under study show three main regions:

-   *The HBD region:* Negative values of σ ($\sigma < 0$ e·Å^{-2}) denote the positively charged segments of the molecules within the HBD region.
-   *The neutral region:* The σ values around zero charge density ($\sigma \approx 0$ e·Å^{-2}) represent the non-polar segments of the molecules within the neutral region.
-   *The HBA region:* While the positive σ values ($\sigma > 0$ e·Å^{-2}) refer to the negatively charged segments of the molecules within the HBA region.

Such a zonal repartition occurs based on the hydrogen bonding threshold value, which is set at $\sigma_{HB} = \pm 0.008$ e·Å^{-2}. Accordingly, molecules possessing peaks at $\sigma < \sigma_{HB}$ are defined as exhibiting hydrogen bond donating tendencies (HBDs), while molecules possessing peaks at $\sigma > \sigma_{HB}$ are considered owing tendencies as hydrogen bond acceptor molecules (HBAs) (Adeyemi et al., 2020; Warrag et al., 2018).
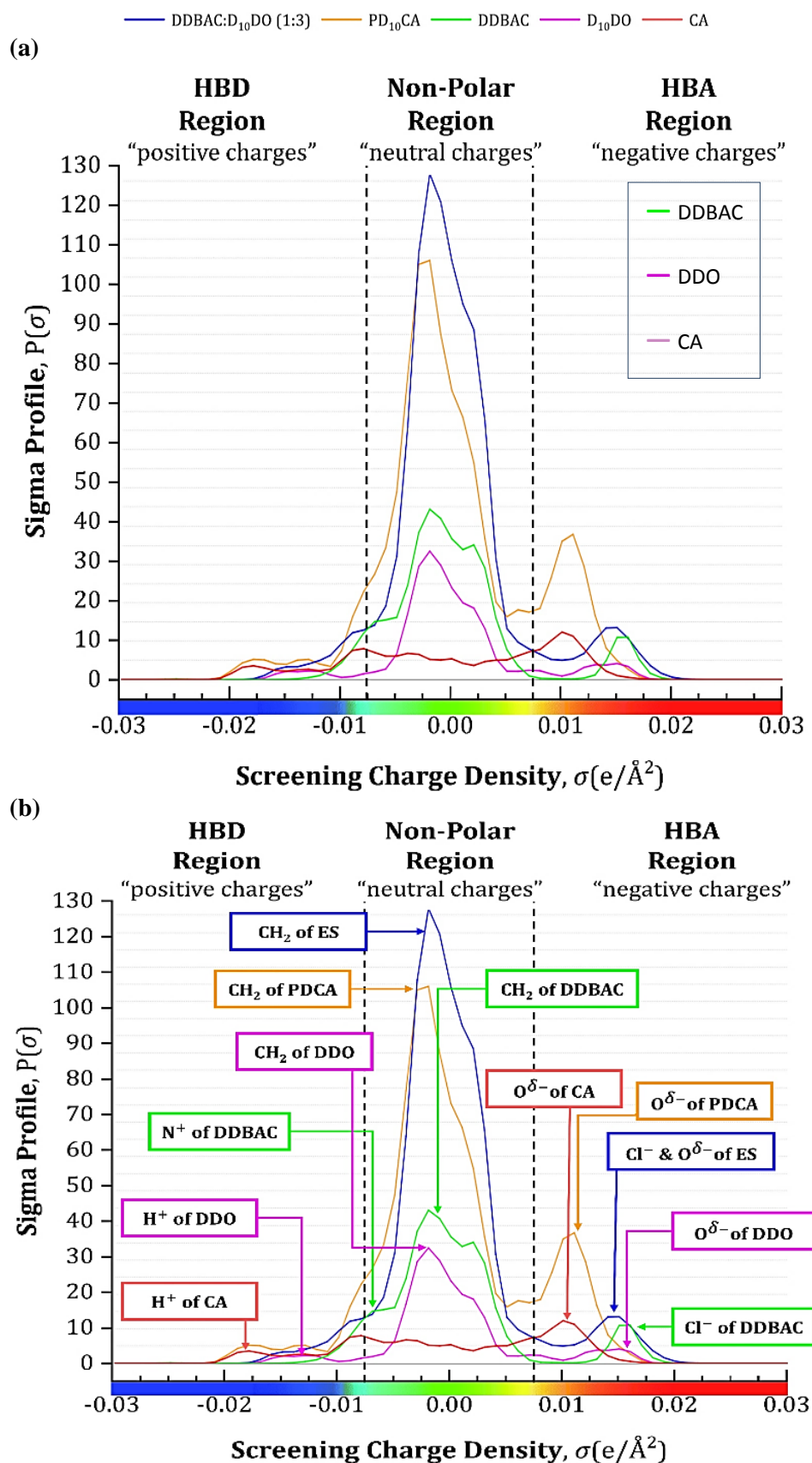
Figure IV.10. (a) σ-*Profile* distributions of DDBAC, D_{10}DO, CA, the DDBAC:D_{10}DO (1:3) HES mixture and PD$_{10}$CA, and (b) the σ-*Profile* with each major peak labeled.

The peaks in Figure IV.10 (a) located within the HBD region ($-0.0200 < \sigma < -0.0080$ e·Å^{-2}) represent H^+ protons in a molecule as seen for CA and D$_{10}$DO. The peaks near the black dashed line within $-0.0080 < \sigma < -0.0050$ e·Å^{-2} denote the N^+, $H^{\delta+}$, and $C^{\delta+}$ atoms in a molecule (*e.g.* DDBAC). The peaks in the neutral region around zero at $-0.0050 < \sigma < +0.0050$ e·Å^{-2} belong to the non-polar $-CH_3, -CH_2,$ and $-CH$ groups in a molecule (DDBAC, D$_{10}$DO). The peaks near the black dashed line at the limit of the neutral region toward the HBA region, within $+0.0050 < \sigma < +0.0080$ e·Å^{-2} refer to the π-bond containing parts of $C = C^{\delta-}$ and $C^{\delta-} = O$ atoms in a molecule (*e.g.* CA). Finally, the peaks in the HBA region ($+0.0080 < \sigma < +0.0200$ e·Å^{-2}) represent the $O^{\delta-}$ and Cl^- atoms in a molecule (*e.g.* DDBAC, D$_{10}$DO, CA). The σ-profiles were reproduced with detailed labels of the atoms and groups responsible for the peaks apparition to allow better understanding of the polarity of the molecules as shown in Figure IV.10 (b). Illustrations from Figure IV.9 and Figure IV.10 are explained in details for each molecule in Table IV.9 bellow:

Table IV.9. Summary of the observations made from the surface charge distributions and the σ-*profiles* of DDBAC, D$_{10}$DO, CA, the DDBAC:D$_{10}$DO (1:3) HES, and PD$_{10}$CA.

Abbreviation	Observations and Tendencies
Components	
DDBAC	The molecule is primarily considered as a HBA. Its high polarity is evident by the deep red segment of the Cl^- atom (≈ 0.0150 e·Å^{-2}). Although the molecule is large, the polarity is concentrated at a single area, which helps predict the molecule interaction tendencies. N^+ atom shows some weak hydrogen donating capacity (light blue segment). However, its peak in the σ-*profile* is not quite within the donating region (nearby the vertical dashed line in the neutral region). The molecule is also mostly green with large peaks in the neutral region corresponding to the high concentration of $-CH_2$ groups. This suggests that the molecule could be considered highly hydrophobic with the only hydrophilic parts being N^+ and Cl^- atoms within the molecule.
D$_{10}$DO	The diol exhibits both HBD and HBA tendencies stemming from H^+ and $O^{\delta-}$ respectively, located at the ends of the molecule, which are represented by the blue ($-0.0170 < \sigma < -0.0100$ e·Å^{-2} peaks) and red segments ($+0.0100 < \sigma < -0.0170$ e·Å^{-2} peaks). As for DDBAC, D$_{10}$DO is mostly non-polar indicating that the molecule is highly hydrophobic, except for the hydrophilic portions due to the presence of H^+ and $O^{\delta-}$ atoms.
CA	This acid also shows both HBD and HBA tendencies stemming from H^+ and $O^{\delta-}$, respectively, that are positioned around the molecule. However, unlike DDBAC and D$_{10}$DO, this molecule is entirely hydrophobic, which is evidenced by the lack of green segments on the molecule, and the small peaks located in the neutral region ($-0.0050 < \sigma < +0.0050$ e·Å^{-2}).

Eutectic Mixture and Polymer

DDBAC:D$_{10}$DO (1:3)

The geometrical optimization of the molecule indicates that the eutectic solvent forms a fairly tetrahedral geometry with the Cl^- atom of the DDBAC molecule being the center and the H^+ donating segments of the D$_{10}$DO molecule are physically bonded with Cl^- atom through hydrogen bonding. Also, by examining the σ-*profile* of the eutectic solvent, it can be observed that the peak contained within the HBA region is quite larger than that of the DDBAC molecule. This is due to the fact that the peak in the HBA region of the HES actually contains two peaks: peak of Cl^- for DDBAC, and that of $O^{\delta-}$ for D$_{10}$DO, leading to a more pronounced amount of accepting segments. It can also be seen from that the eutectic mixture of DDBAC:D$_{10}$DO (1:3) could be considered highly hydrophobic due to the molecule being mostly green with large peaks in the neutral region corresponding to the high concentration of $-CH_2$ groups.

PD$_{10}$CA

As for the HES, the polymer is also considered highly hydrophobic due to the molecule mostly green with large peaks in the neutral region corresponding to the high concentration in $-CH_2$ groups. However, the σ-*profile* of the polymer reveals that the peaks contained within the HBA region are larger than those of DDBAC, D$_{10}$DO, and CA. This is due to the fact that the peaks in the HBA region of the polymer contain a large number of $O^{\delta-}$ atoms that stem from the D$_{10}$DO and citrate groups, which form after the polymerization reaction leading to a very large amount of hydrogen bond accepting segments positioned in the center of the molecule and surrounding the molecule. Some HBD activity in the extremities can be observed from the remaining H^+ parts of the constituent molecules that were not polymerized.

IV.3.3.2. σ-Potentials

Affinities of molecules toward either polar or non-polar species were also determined by means of the corresponding σ-*potential* distributions, as illustrated in Figure IV. The σ-*potential* of a molecule may be defined as the tendency of a surface segment carrying a given polarity σ to be attracted to a particular type of solvent (*i.e.,* HBA, HBD, and non-polar solvents) (Warrag et al., 2020). Examining the σ-*potential* distributions of the components (DDBAC, D$_{10}$DO, and CA) in Figure IV. enables to observe the high affinity of DDBAC toward HBDs, followed by D$_{10}$DO, and lastly CA. Regarding the HBA affinities, CA was observed to exhibit the highest affinity, followed by D$_{10}$DO. DDBAC showed no affinity towards HBAs, and in fact, based on its σ-*potential* distribution, it can be said that the DDBAC molecule would mainly repel HBA solvents due to its very highly electron-withdrawing nature. These distributions confirm that DDBAC and D$_{10}$DO molecules interact with each other through hydrogen bonding networks with DDBAC as the HBA and D$_{10}$DO as the HBD. It can also be observed that DDBAC molecule is more compatible with the CA molecule. Nonetheless, CA is not present during the HES formation step, and thus would not inhibit the interactions between DDBAC and D$_{10}$DO. The affinity between DDBAC and

$D_{10}DO$ is sufficient enough to establish various types of interactions including VAN DER WAALS' interactions, hydrogen bonding, and entropy of mixing.
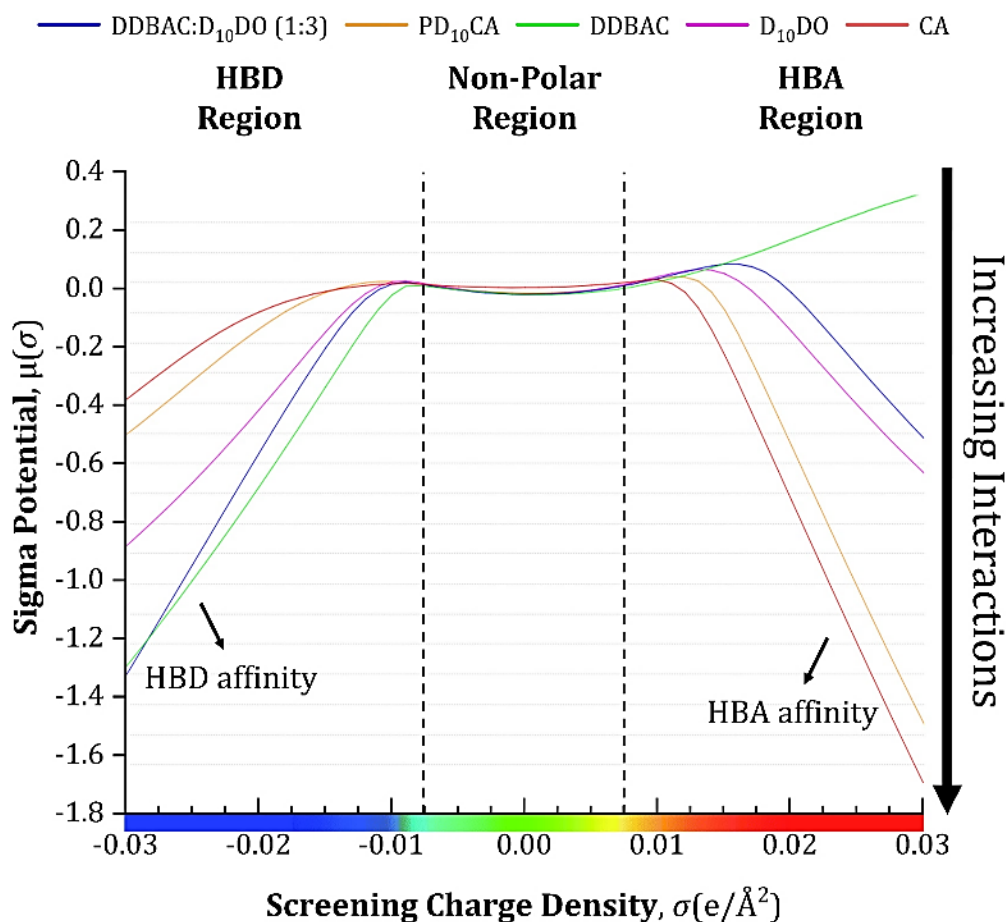
Figure IV.11. σ-*Potential* distributions of DDBAC, $D_{10}DO$, CA, DDBAC:$D_{10}DO$ (1:3) HES, and PD$_{10}$CA.

Results showed that DDBAC:$D_{10}DO$ (1:3) exhibited affinity toward both HBAs and HBDs, with a higher affinity toward HBDs. This finding is of great significance since it demonstrates that the HES may show sufficient interactions with the CA molecule leading to efficient solvation of the CA monomer into the HES. Also, the ternary interactions between the negatively charged DDBAC with both CA and $D_{10}DO$ provide a strong network that helps contain the DDBAC additive within the polymer crosslinks. As for the polymer, it can be seen that the polymer showed a fairly similar behavior to the HES, where it exhibits affinity toward both HBAs and HBDs, with a higher affinity to HBAs.

IV.3.3.3. Fukui Function Indices

The reactivity of a certain molecular site k to a nucleophilic attack (*i.e.,* by anionic species) or an electrophilic attack (*i.e.,* by cationic species) can be determined using the Fukui function (Geerlings et al. 2003). The Fukui function results provide important information about the most appropriate sites for donating electrons (least affected by migration of electrons), or accepting new electrons (most stabilized by addition of electrons). The Fukui results in this work were determined using DFT calculations in the DMol3 module. The comprehensive lists of data for each atom constituting the DDBAC, $D_{10}DO$, HES, and CA molecules are available in Tables A.1 to A.4 of the Appendices. Table IV.10 lists the most significant results obtained from the Fukui function indicating the most suitable sites for nucleophilic and electrophilic attacks. These sites are identifiable by their greatest values of f^- and f^+ corresponding to nucliophiles (anionic atoms) and electrophiles (cationic atoms), respectively. It is worth noting that the location indices of each component listed in Table IV.10 are shown in the chemical structures of Figure IV.

Table IV.10. Most significant Fukui anionic and cationic atoms in CA, DDBAC, $D_{10}DO$, and the HES[a].

	Anionic Atoms, f^- (HOMO)		Cationic Atoms, f^+ (LUMO)	
CA	O(#13)	$\rightarrow 0.209$	C(#6)	$\rightarrow 0.169$
	O(#9)	$\rightarrow 0.202$	O(#9)	$\rightarrow 0.141$
	O(#7)	$\rightarrow 0.100$	O(#11)	$\rightarrow 0.123$
			C(#5)	$\rightarrow 0.117$
DDBAC	Cl(#1)	$\rightarrow 0.727$	C(#20)	$\rightarrow 0.148$
$D_{10}DO$	O(#11)	$\rightarrow 0.210$	H(#34)	$\rightarrow 0.833$
	O(#12)	$\rightarrow 0.210$	H(#7)	$\rightarrow 0.155$
			H(#16)	$\rightarrow 0.146$
			H(#14)	$\rightarrow 0.129$
DDBAC:$D_{10}DO$ (1:3)	Cl(#103)	$\rightarrow 0.276$	C(#122)	$\rightarrow 0.126$
	O(#45)	$\rightarrow 0.131$		
	O(#80)	$\rightarrow 0.121$		

[a] The indices of each component are labeled in Figure IV.

The results shown in Table IV.10 are also visually plotted as Fukui anionic and cationic charge distributions in Figure IV. First, it can be observed that the carbon atoms in the position numbers #5 and #6, and the oxygen atoms in the position numbers #9 and #11 calculated were cationic, while the oxygen atoms in the position numbers #13, #9, and #7 were anionic. The most suitable location for nucleophilic attack would be on the oxygen #13, which is the only oxygen not belonging to an acid group, while the most suitable location for an electrophilic attack would be on carbon #6 (most suitable to be a 'carbocation') as it is the closest carbon to both a carboxylic acid group (O#9) and the hydroxy group (O#13). Regarding the DDBAC molecule, it can be seen that the most electronegative atom in the molecule is the chloride atom with a very high Fukui value of $f^- = 0.727$ making the DDBAC molecule an excellent HBA with a strong nucleophilic attack site. Conversely, the most suitable location for an electrophilic attack would be the aromatic carbon #20 (could act as a carbocation). This group is contained within the benzyl group and is the furthest aromatic carbon from the geometrically optimized chloride anion and ammonium cation locations. However, its $f(r)$ value is still much lower than the chloride atom, and thus, the molecule can be considered as mostly a nucleophile (as observed by the less accumulated regions in yellow in Figure IV.).

Based on the $f(r)$ values of D$_{10}$DO, it can be concluded that the diol molecule is most prominently considered as an electrophile with a Fukui value of $f^- = 0.833$ on hydrogen #34. On the other hand, the molecule can also act as a nucleophile using the oxygens located on the two ends of the molecule (#11 and #12). Lastly, the geometrically optimized structure of the DDBAC:D$_{10}$DO (1:3) HES mixture can be considered as having both nucleophilic and electrophilic tendencies. The most pronounced suitable site for a nucleophilic attack would be the chloride atom (#103) with a $f^- = 0.276$. Note that the value is much lower than that of pure DDBAC due to the fact that it is being stabilized by three hydroxyl groups from the D$_{10}$DO molecule. Additionally, the HES mixture contains two other suitable sites for a nucleophilic attack, which are the electronegative oxygen atoms in the hydroxyl groups of the D$_{10}$DO molecule with positions of #45 and #80. On the contrary, the most suitable site for an electrophilic attack would be the aromatic carbon #122 (carbocation tendency), which represents the same carbon atom within the benzyl group that is furthest away from the chloride anion and ammonium cation locations. It should be noted that these Fukui results agree with those obtained from the SCDs, *σ-profiles* and *σ-potentials*, however, they still add more detailed insights from an atomic perspective.

Anionic Atoms, f^- Nucleophilic Sites	Cationic Atoms, f^+ Electrophilic Sites
Citric acid (CA)	
Dodecyldimethylbenzyl ammonium chloride (DDBAC)	
1,10-decanediol (D$_{10}$DO)	
DDBAC:D$_{10}$DO (1:3)	

Key:
Atoms: ⬤ carbon   ◯ hydrogen   🔴 oxygen   🔵 nitrogen   🟢 chloride
Clouds: 🟦 blue clouds represent the high accumulated areas, while the 🟨 yellow clouds represent less accumulated ones.
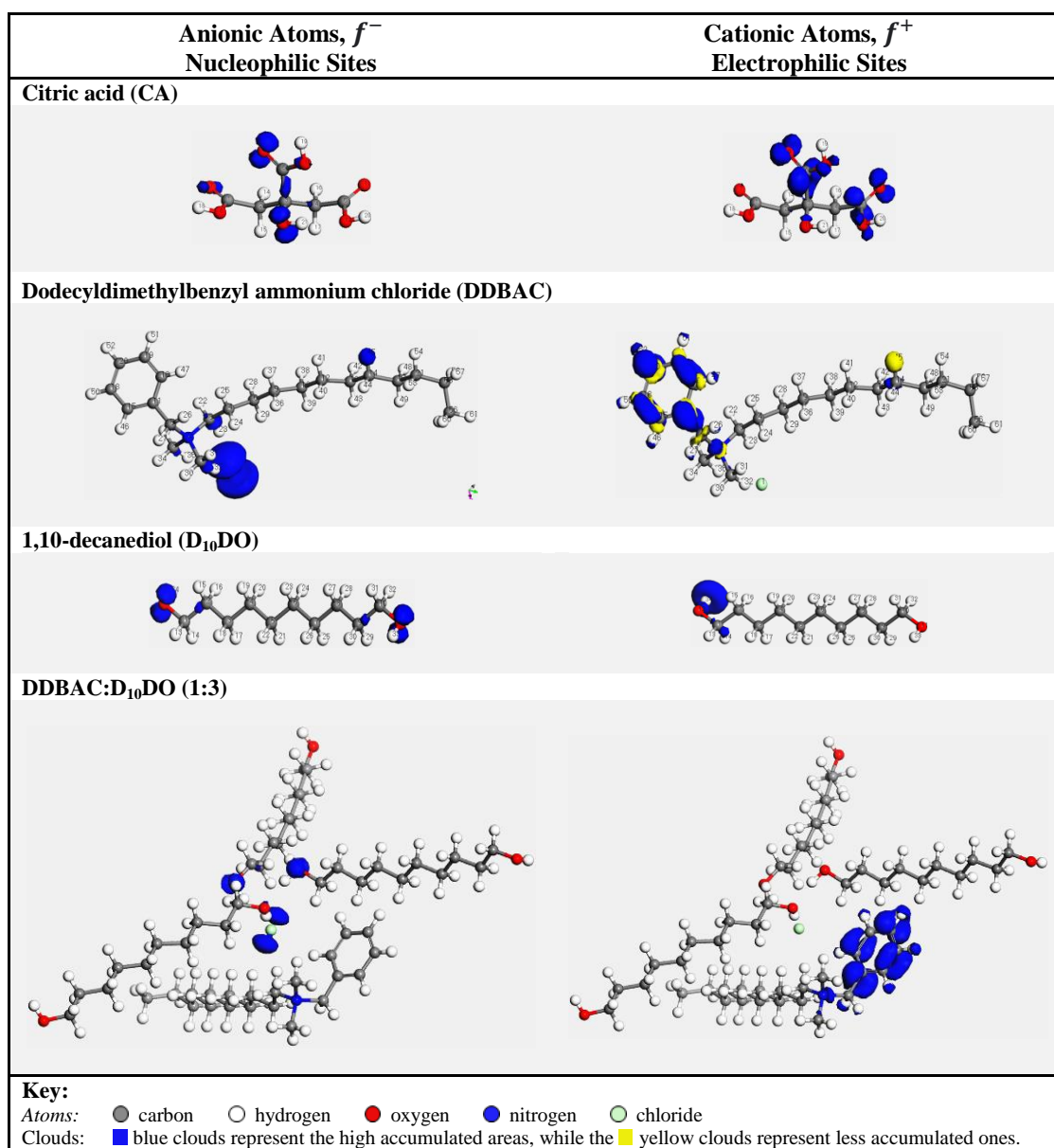
Figure IV.12. Fukui anionic and cationic charge distributions of CA, DDBAC, D$_{10}$DO, and the HES.

IV.3.3.4. Interaction Energies and Volatility of HES

The results of the interaction energies allowed to determine the most dominant type of interactions within the HES mixture. Figure IV. show that the primary interactions within the DDBAC:D$_{10}$DO (1:3) HES mixture are VAN DER WAALS' interactions with an energy value of -21.6 kcal/mol. This result was expected because, unlike hydrophilic DESs that generally depend on hydrogen bonding primarily, HESs consist of largely non-polar $-CH_3, -CH_2,$ and $-CH$ groups that primarily interact with each other through VAN DER WAALS' interactions.
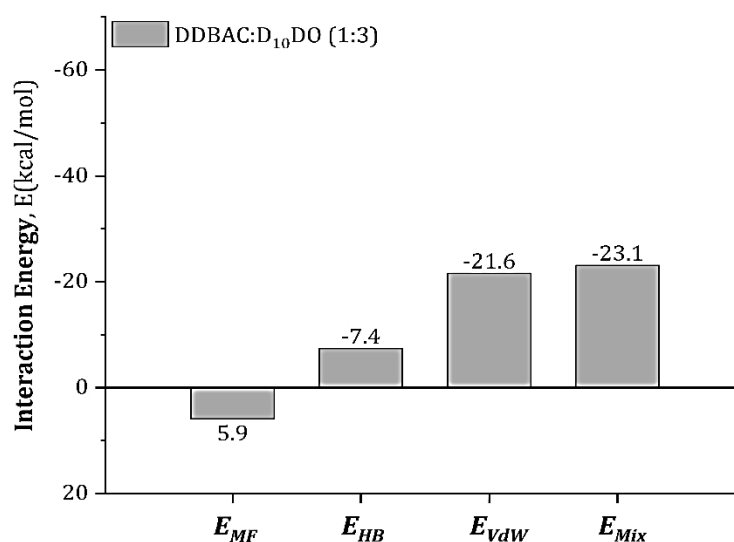
Figure IV.13. The misfits, hydrogen bonding, VAN DER WAALS, and mixture energies in kcal/mol of the DDBAC:D_{10}DO (1:3) HES mixture.

Furthermore, as a demonstration of the green character of HESs, the vapor pressure of DDBAC:D_{10}DO (1:3) (at 25.15 °C and atmospheric pressure) was found negligible (2.0×10^{-37} mbar) using COSMO*ThermX*. For the sake of comparison, the same calculation method was utilized with a widely known and commercialized organic solvent "toluene", and the vapor pressure was found to 36.6 mbar. These results were expected as the DDBAC:D_{10}DO (1:3) eutectic is a mixture of two solids at room temperature, which further demonstrates the greenness and sustainability of these novel eutectics (Dietz et al., 2019).

IV.3.3.5. Properties of the HES and CA mixture

a) Interaction Energies

The interaction energies and the total mixture energy (E_{mix}) of the HES and CA mixture are illustrated in Figure IV.. The primary interactions observed between the HES and CA are hydrogen bonding with an energy value of -16.2 kcal/mol. This result agrees with the findings obtained from the SCDs, σ-*profiles*, σ-*potentials*, and the Fukui function, where it was also found that the primary mode of interactions between the HES and the CA are through hydrogen bonds.
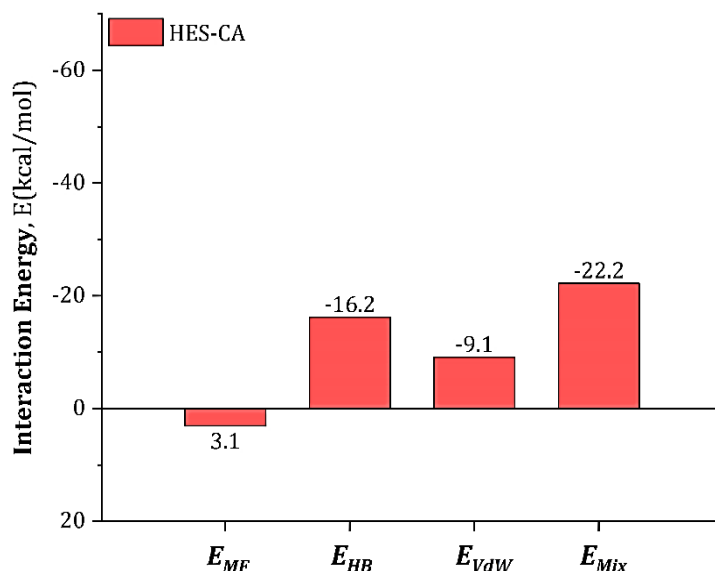
Figure IV.14. The misfits, hydrogen bonding, VAN DER WAALS, and mixture energies in kcal/mol of the HES and CA mixture.

b) Activity Coefficient at Infinite Dilution

The parameter γ_i^∞ describes the behavior of a solute molecule when completely surrounded by the molecules of the solvent (*i.e.,* a negligible concentration of solute within the solvent). The lower the infinite dilution activity coefficient, the more appropriate the solvent-solute combination. Accordingly, the infinite dilution activity coefficient ($\ln(\gamma_{CA}^\infty)$ of CA in the HES was determined using the COSMO*ThermX* software. The result obtained at 25.15 °C and atmospheric pressure was found to be $\ln(\gamma_{CA}^\infty) = 8.0 \times 10^{-12}$. The low value of $\ln(\gamma_{CA}^\infty)$ suggests that the DDBAC:D$_{10}$DO (1:3) solvent has a remarkably high affinity towards CA.

c) Solubility

The solubility of a monomer in a solvent as synthesis medium is one of the critical parameters that determines the feasibility of the synthesis process. The solubility is a measurement of the ability of a solvent to dissolve a certain amount of solute (Maleki et al., 2017). Thus, based on its fundamental importance, the solubility of CA in the DES, which is based on a solid-liquid equilibrium (SLE) calculation, was determined using the COSMO*ThermX* software at 25.15 °C and atmospheric pressure. From the results listed in Table IV.11, it can be concluded that the selected BAC-based HES is an efficient solvent for CA as the solubility of $x_{SLE} = 0.543$ was obtained. The high solubility is presumably a result of the high hydrogen bonding energy.

Table IV.11. Solubility of CA in the HES reported in weight fraction and mole fraction [a].

Parameter	Value
w_{CA-SLE}	0.209
x_{CA-SLE}	0.543

[a] The density of the solvent was calculated (875.924 kg/m^3).

d) Reactivity

The calculated quantum chemical parameters are listed in Table IV.12. From the results, it can be observed that CA has the highest tendency to react by accepting a pair of electrons (very high ω values). On the other hand, the $D_{10}DO$ is the most stable molecule in terms of its electron cloud, and thus, it would be the most probable candidate to react and donate a pair of electrons to CA in order to form the most energetically favored system. It can also be observed that the $PD_{10}CA$ molecule and the DDBAC molecule are relatively non-stable molecules, and from the findings in the previous sections it was found that the $PD_{10}CA$ has high affinity towards HBA molecules, while the DDBAC molecule has a high affinity towards HBD molecules. These are promising and facilitates their compatibility as a polymer matrix and an additive combination.

Table IV.12. The quantum chemical density functional theory parameters of DDBAC, $D_{10}DO$, CA, DDBAC:$D_{10}DO$ (1:3) HES mixture, and $PD_{10}CA$.

Parameter	DDBAC	$D_{10}DO$	CA	HES	$PD_{10}CA$
E_{HOMO} (eV)	-5.197	-6.036	-5.398	-5.559	-6.039
E_{LUMO} (eV)	-1.512	1.793	-3.741	-1.411	-1.534
ΔE_{gap} (eV)	3.685	7.829	1.657	4.148	4.505
η (eV)	1.843	3.915	0.829	2.074	2.253
μ_x (eV)	-3.355	-2.122	-4.57	-3.485	-3.787
ω (eV)	3.054	0.575	12.601	2.928	3.183

IV.3.3.6. Compatibility of PD$_{10}$CA Elastomer with DDBAC Additive

a) Interaction Energies

The interaction energies and the total mixture energy (E_{mix}) of the PD$_{10}$CA-DDBAC composite were determined using the same COSMO*ThermX* procedure applied earlier for the HES and the HES-CA mixture. The primary interactions observed between PD$_{10}$CA (polymer matrix) and DDBAC (filler) are VAN DER WAALS' interaction energies with a value of $E_{VdW} = -52.7$ kcal/mol.

The total mixture energy was also observed to be much lower than that of the HES and the HES-CA mixtures with a value of $E_{mix} = -62.2$ kcal/mol, which further confirms the compatibility between the polymer matrix and the filler (Figure IV.15).
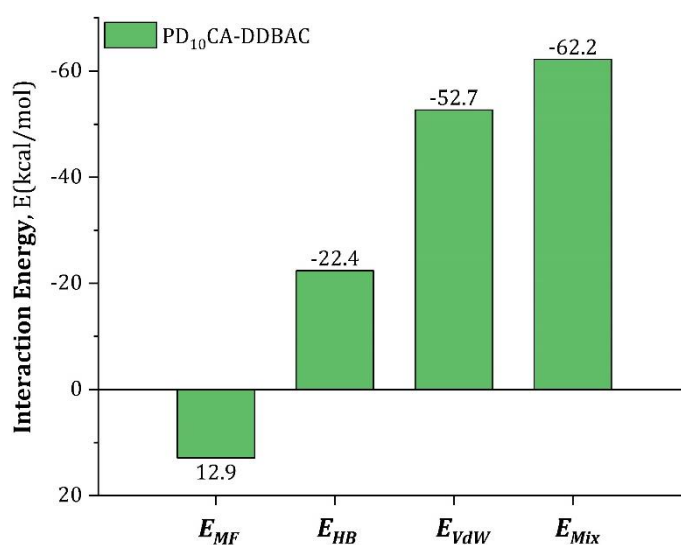
Figure IV.15. The misfits, hydrogen bonding, VAN DER WAALS, and mixture energies in kcal/mol of the PD$_{10}$CA-DDBAC composite.

b) Blend Binding Energy Distributions

The blend binding energy distribution for the polymer, the salt and the composite material are shown in Figure IV.16, and the calculated blend parameters are listed in Table IV.13 bellow. First, it can be observed from the that the combination of base-screen energies representing the PD$_{10}$CA-DDBAC composite show a more favorable distribution than the individual constituents (*i.e.,* higher peak). Additionally, from the low calculated values of χ and E_{blend}, it can be concluded that the composite at hand composed of PD$_{10}$CA as a polymer matrix and DDBAC as an additive is highly compatible. For the sake of comparison, FLORY-HUGGINS' interaction parameter calculated in this work was compared to that reported by

ABDOUNE *et al.*, where they have calculated the χ value of ten polymers consisting of polyglycols and dithymoquinone as an additive (Abdoune et al., 2019).

Their results showed that the best combination exhibited a FLORY-HUGGINS' parameter of 60.101, which is higher than that of the value calculated for the PD$_{10}$CA-DDBAC composite at $\chi = 42.750$, indicating that the continuous phase of the PD$_{10}$CA polymer well wets the non-continuous phase of DDBAC, and further demonstrates their compatibility as a polymer matrix and an additive combination.
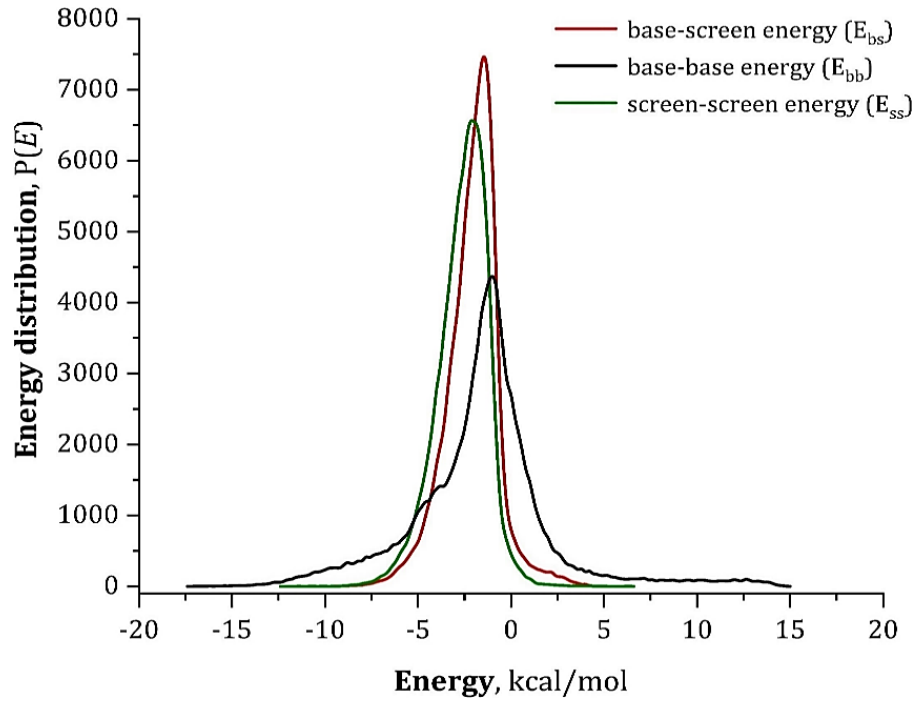
Figure IV.16. Blend binding energy distribution for pure PD$_{10}$CA (E_{bb}), DDBAC (E_{ss}), and the PD$_{10}$CA-DDBAC composite (E_{bs}).

Table IV.13. Blend binding energy and FLORY-HUGGINS interaction parameter calculated for the PD$_{10}$CA-DDBAC composite at 25.15 °C.

Parameter	Value
E_{blend} (kcal/mol)	25.316
χ	42.750

IV.4. Conclusion

This chapter reported the results obtained by COSMO-RS theory of interacting molecular surface charges based on quantum models, and Density Functional Theory (DFT) that served to predict interactions, reactivity and physicochemical properties of the studied molecules. The chapter is funded upon two parts:

The first part involved calculation results of the interaction energies, reactivity and physicochemical properties of twenty-four (24) DESs. Among the combinatory mixtures, the strongest interactions were obtained for betaine:caffeic acid DES.

In the second part, calculations demonstrated good reactivity between the benzalkonium salt as HBA and 1,10-decanediol as HBD to form the DES that served as solvent and functional monomer for the polyesterification. The vapor pressure of the DES was found negligible, confirming the non-volatility of the latter, and consolidates its low toxicity. The DES was appropriate to dissolve efficiently citric acid, this solubility being a crucial step in forming the pre-polymer. The possibility to obtain the composite relies on the interactions between poly(1,10-decanediol-citrate) ($PD_{10}CA$) and DDBAC antibacterial salt. These interactions were found strong enough favoring the formation of this composite. Besides, VAN DER WAALS' bonds were found to show the main interaction energies between the DES components, and between ($PD_{10}CA$) and the filler (DDBAC), while the DES and CA were mainly bonded through hydrogen bonding.

IV.5. References

Abdoune, Y., Benguerba, Y., Benabid, S., Khither, H., Sobhi, W., and Benachour, D. (2019). Numerical investigation of polyethylene glycol polymer (PEG) and dithymoquinone (DTQ) interaction using molecular modeling. *Journal of Molecular Liquids*, *276*, 134–140. https://doi.org/10.1016/j.molliq.2018.11.105

Adeyemi, I., Sulaiman, R., Almazroui, M., Al-Hammadi, A., and AlNashef, I. M. (2020). Removal of chlorophenols from aqueous media with hydrophobic deep eutectic solvents: Experimental study and COSMO RS evaluation. *Journal of Molecular Liquids*, *311*, 113180. https://doi.org/10.1016/j.molliq.2020.113180

Aissaoui, T., AlNashef, I. M., & Benguerba, Y. (2016). Dehydration of natural gas using choline chloride based deep eutectic solvents: COSMO-RS prediction. *Journal of Natural Gas Science and Engineering*, *30*, 571–577. https://doi.org/10.1016/j.jngse.2016.02.007

Aissaoui, T., Alnashef, I. M., Qureshi, U. A., & Benguerba, Y. (2017). Potential applications of deep eutectic solvents in natural gas sweetening for CO2 capture. *Reviews in Chemical Engineering*, *33*(6), 523–550. https://doi.org/10.1515/revce-2016-0013

Aissaoui, T., Benguerba, Y., AlOmar, M. K., & AlNashef, I. M. (2017). Computational investigation of the microstructural characteristics and physical properties of glycerol-based deep eutectic solvents. *Journal of Molecular Modeling*, *23*(10). https://doi.org/10.1007/s00894-017-3450-5

Benabid, S., Benguerba, Y., AlNashef, I. M., & Haddaoui, N. (2019). Theoretical study of physicochemical properties of selected ammonium salt-based deep eutectic solvents. *Journal of Molecular Liquids*, *285*, 38–46. https://doi.org/10.1016/j.molliq.2019.04.052

Benabid, S., Streit, A. F. M., Benguerba, Y., Dotto, G. L., Erto, A., & Ernst, B. (2019). Molecular modeling of anionic and cationic dyes adsorption on sludge derived activated carbon. *Journal of Molecular Liquids*, *289*, 111119. https://doi.org/10.1016/j.molliq.2019.111119

Dai, Y., van Spronsen, J., Witkamp, G. J., Verpoorte, R., and Choi, Y. H. (2013). Natural deep eutectic solvents as new potential media for green technology. *Analytica Chimica Acta*, *766*(2010), 61–68. https://doi.org/10.1016/j.aca.2012.12.019

Delley, B. (2000). From molecules to solids with the DMol3 approach. *Journal of Chemical Physics*, *113*(18), 7756–7764. https://doi.org/10.1063/1.1316015

Dietz, C. H. J. T., Creemers, J. T., Meuleman, M. A., Held, C., Sadowski, G., Van Sint Annaland, M., Gallucci, F., & Kroon, M. C. (2019). Determination of the Total Vapor Pressure of Hydrophobic Deep Eutectic Solvents: Experiments and Perturbed-Chain Statistical Associating Fluid Theory Modeling [Research-article]. *ACS Sustainable Chemistry and Engineering*, *7*(4), 4047–4057. https://doi.org/10.1021/acssuschemeng.8b05449

Durand, E., Lecomte, J., & Villeneuve, P. (2013). Deep eutectic solvents: Synthesis, application, and focus on lipase-catalyzed reactions. *European Journal of Lipid Science and Technology*, *115*(4), 379–385. https://doi.org/10.1002/ejlt.201200416

Eckert, F., & Klamt, A. (2002). Fast Solvent Screening via Quantum Chemistry: COSMO-RS Approach. *AIChE Journal*, *48*(2), 369–385. https://doi.org/10.1002/aic.690480220

Fischer, V. (2015). Properties and Applications of Deep Eutectic Solvents and Low-Melting Mixtures. PhD Thesis, Universität Regensburg. https://doi.org/10.5283/epub.31832

García-Argüelles, S., Serrano, M. C., Gutiérrez, M. C., Ferrer, M. L., Yuste, L., Rojo, F., & Del Monte, F. (2013). Deep eutectic solvent-assisted synthesis of biodegradable polyesters with antibacterial properties. *Langmuir*, *29*(30), 9525–9534. https://doi.org/10.1021/la401353r

García, G., Atilhan, M., & Aparicio, S. (2015). An approach for the rationalization of melting temperature for deep eutectic solvents from DFT. *Chemical Physics Letters*, *634*, 151–155. https://doi.org/10.1016/j.cplett.2015.06.017

Geerlings, P., De Proft, F., Langenaeker, W. (2003). Conceptual density theory, *Chem. Rev*. 103, 1793–1873.
https://doi.org/10.1021/cr990029p

Hizaddin, H. F. B. (2016). Selection of Ionic Liquids and Deep Eutectic Solvents via quantum chemical methods and liquid-liquid equilibria involved in the extractive denitrogenation of diesel, *Thesis for the degree of doctor of philosophy, faculty of engineering, University of Mal*. http://studentsrepo.um.edu.my/11511/1/Samsuddin.pdf

Hammond, O. S., Bowron, D. T., & Edler, K. J. (2016). Liquid structure of the choline chloride-urea deep eutectic solvent (reline) from neutron diffraction and atomistic modelling. *Green Chemistry*, *18*(9), 2736–2744. https://doi.org/10.1039/c5gc02914g

Jablonský, M., Škulcová, A., & Šima, J. (2019). Use of deep eutectic solvents in polymer chemistry–a review. *Molecules*, *24*(21), 1–33. https://doi.org/10.3390/molecules24213978

Klamt, A., Eckert, F., & Arlt, W. (2010). COSMO-RS: An alternative to simulation for calculating thermodynamic properties of liquid mixtures. *Annual Review of Chemical and Biomolecular Engineering*, *1*, 101–122. https://doi.org/10.1146/annurev-chembioeng-073009-100903

Lee, M. Y., Wang, W. L., Wu, Q. Y., Huang, N., Xu, Z. Bin, & Hu, H. Y. (2018). Degradation of dodecyl dimethyl benzyl ammonium chloride (DDBAC) as a non-oxidizing biocide in reverse osmosis system using UV/persulfate: Kinetics, degradation pathways, and toxicity evaluation. *Chemical Engineering Journal*, *352*(December 2017), 283–292. https://doi.org/10.1016/j.cej.2018.04.174

Lemaoui, T., Hatab, F. A., Darwish, A. S., Attoui, A., El, N., Hammoudi, H., Almustafa, G., Benaicha, M., Benguerba, Y., & Alnashef, I. M. (2021). *Molecular-Based Guide to Predict the pH of Eutectic Solvents : Promoting an Efficient Design Approach for New Green Solvents*. https://doi.org/10.1021/acssuschemeng.0c07367

Li, X., Choi, J., Ahn, W. S., & Row, K. H. (2018). Preparation and Application of Porous Materials based on Deep Eutectic Solvents. *Critical Reviews in Analytical Chemistry*, *48*(1), 73–85. https://doi.org/10.1080/10408347.2017.1383881

Li, X., Lee, Y. R., & Row, K. H. (2016). Synthesis of Mesoporous Siliceous Materials in Choline Chloride Deep Eutectic Solvents and the Application of These Materials to High-Performance Size Exclusion Chromatography. *Chromatographia*, *79*(7–8), 375–382. https://doi.org/10.1007/s10337-016-3051-y

Li, X., & Row, K. H. (2017). Separation of Polysaccharides by SEC Utilizing Deep Eutectic Solvent Modified Mesoporous Siliceous Materials. *Chromatographia*, *80*(8), 1161–1169. https://doi.org/10.1007/s10337-017-3336-9

Lide, D. R. (2007). CRC Handbook of Chemistry and Physics-69th Edition, CRC Press Inc., ISBN 0-8493-0369-5. https://doi.org/10.1002/jctb.280500215

Maleki, A., Kettiger, H., Schoubben, A., Jessica, M., Ambrogi, V., & Hamidi, M. (2017). PT US CR. *Journal of Controlled Release*. https://doi.org/10.1016/j.jconrel.2017.07.047

Mano, F., Aroso, I. M., Barreiros, S., Borges, J. P., Reis, R. L., Duarte, A. R. C., & Paiva, A. (2015). Production of poly(vinyl alcohol) (PVA) fibers with encapsulated natural deep eutectic solvent (NADES) using electrospinning. *ACS Sustainable Chemistry and Engineering*, *3*(10), 2504–2509. https://doi.org/10.1021/acssuschemeng.5b00613

Marczak, W., Adamczyk, N., & Łężniak, M. (2012). Viscosity of associated mixtures approximated by the Grunberg-Nissan model. *International Journal of Thermophysics*, *33*(4), 680–691. https://doi.org/10.1007/s10765-011-1100-1

Martins, M., Aroso, I., Craveiro, R., Reis, R. L., Paiva, A., & Duarte, A. R. C. (2014). Enhanced performance of supercritical fluid foaming of natural-based polymers by deep eutectic solvents. *AIChE Journal*, 2–13. https://doi.org/10.1002/aic

Mota-Morales, J. D., Gutiérrez, M. C., Sanchez, I. C., Luna-Bárcenas, G., & Del Monte, F. (2011). Frontal polymerizations carried out in deep-eutectic mixtures providing both the monomers and the polymerization medium. *Chemical Communications*, *47*(18), 5328–5330. https://doi.org/10.1039/c1cc10391a

Pearson, R. G. (1992). *The electronic chemical potential and chemical hardness*. *255*, 261–270.

Pirhadi, S., Sunseri, J., & Koes, D. R. (2016). Open source molecular modeling. *Journal of Molecular Graphics and Modelling*, *69*, 127–143. https://doi.org/10.1016/j.jmgm.2016.07.008

Rodriguez, N. R., Ferre Guell, J., & Kroon, M. C. (2016). Glycerol-Based Deep Eutectic Solvents as Extractants for the Separation of MEK and Ethanol via Liquid-Liquid Extraction. *Journal of Chemical and Engineering Data*, *61*(2), 865–872. https://doi.org/10.1021/acs.jced.5b00717

Serrano, M. C., Gutiérrez, M. C., Jiménez, R., Ferrer, M. L., & Del Monte, F. (2012). Synthesis of novel lidocaine-releasing poly(diol-co-citrate) elastomers by using deep eutectic solvents. *Chemical Communications*, *48*(4), 579–581. https://doi.org/10.1039/c1cc15284j

Shahbaz, K., Mjalli, F. S., Hashim, M. A., & Alnashef, I. M. (2011). Prediction of deep eutectic solvents densities at different temperatures. *Thermochimica Acta*, *515*(1–2), 67–72. https://doi.org/10.1016/j.tca.2010.12.022

Shahbaz, K,, Mjalli, F. S., Vakili-Nezhaad, G., AlNashef, I. M., Asadov, A., & Farid, M. M. (2016). Thermogravimetric measurement of deep eutectic solvents vapor pressure. *Journal of Molecular Liquids*, *222*, 61–66. https://doi.org/10.1016/j.molliq.2016.06.106

Tang, B., Zhang, H., & Row, K. H. (2015). Application of deep eutectic solvents in the extraction and separation of target compounds from various samples. *Journal of Separation Science*, *38*(6), 1053–1064. https://doi.org/10.1002/jssc.201401347

Wang, S., Peng, X., Zhong, L., Jing, S., Cao, X., Lu, F., & Sun, R. (2015). Choline chloride/urea as an effective plasticizer for production of cellulose films. *Carbohydrate Polymers*, *117*, 133–139. https://doi.org/10.1016/j.carbpol.2014.08.113

Warrag, S. E. E., Adeyemi, I., Rodriguez, N. R., Nashef, I. M., Van Sint Annaland, M., Kroon, M. C., and Peters, C. J. (2018). Effect of the Type of Ammonium Salt on the Extractive Desulfurization of Fuels Using Deep Eutectic Solvents. *Journal of Chemical and Engineering Data*, *63*(4), 1088–1095. https://doi.org/10.1021/acs.jced.7b00832

Warrag, S. E. E., Darwish, A. S., Adeyemi, I. A., Hadj-Kali, M. K., Kroon, M. C., & Alnashef, I. M. (2020). Extraction of pyridine from n-alkane mixtures using methyltriphenylphosphonium bromide-based deep eutectic solvents as extractive denitrogenation agents. *Fluid Phase Equilibria*, *517*, 112622. https://doi.org/10.1016/j.fluid.2020.112622

Zhang, Q., De Oliveira Vigier, K., Royer, S., & Jérôme, F. (2012). Deep eutectic solvents: Syntheses, properties and applications. *Chemical Society Reviews*, *41*(21), 7108–7146. https://doi.org/10.1039/c2cs35178a

General Conclusion

Nowadays, deep eutectic solvents are widely investigated due to their importance as environmentally-friendly media, liquid solvents at room temperature, also for their low cost and easy preparation. In polymer technology, the use of DESs is advantageous since they play multiple roles in green synthesis processes, reducing the number of reagents such as catalyst and polymerization initiator and enhancing the product yield besides their contribution in greener processes.

The aim of the present study was to compute the interaction energies, and reactivity between the reagents during a DES-assisted polycondensation for a green synthesis of a biodegradable polyester with antibacterial activity, and predict the properties of the DES-based composite.

The computational modeling was carried out in two parts. The first part was was dedicated to the design and modeling of a series of DESs with the aim to provide knowledge on these solvent unwell known, particularly in polymer science. A series of 24 DESs were prepared by mixing three quaternary ammonium salts namely, choline chloride, tetra methyl ammonium chloride and betaine with a series of hydrogen-bond donors. Molecular structures and *in-silico* calculations of the interaction energies, reactivity and physicochemical properties of the DESs was performed using COSMO-RS theory of interacting molecular surface charges based on quantum models (QM), and Density Functional Theory (DFT).

Sigma-profiles and sigma-potential results revealed that betaine/caffeic acid pairing is the most promising combination, which was confirmed by calculated values of activity coefficient, reactivity and interaction energies. Results obtained for the density calculation for this combination were very encouraging. However, the viscosity estimation cannot be relied on due to the lack of accuracy of the computation program. Based on the results of this work, the weakness in calculating viscosity by means of COSMO*thermX* software supports the perspective to make more effort in developing a new viscosity QSPR model for the DES structures.

In the second part, a computational study focusing on the molecular level interactions and mechanisms was conducted to evaluate the feasibility of preparing a biodegradable poly(diol-citrate) (PDCA) polyester filled with a benzalkonium chloride (BAC) salt as antimicrobial agent using hydrophobic eutectic solvent (HES) assisted polycondensation. The diol selected was 1,10-decanediol ($D_{10}DO$) as hydrogen bond donor (HBD), while the selected BAC was dodecyldimethylbenzyl ammonium chloride (DDBAC) as hydrogen bond acceptor (HBA). The results of the computational model showed that the HES and the $PD_{10}CA$ interacted with DDBAC primarily through VAN DER WAALS' interactions, while CA

interacted with DDBAC primarily through hydrogen bonding. The solubility activity coefficient study and the low value of FLORY-HUGGINS parameter suggest that the HES is an excellent solvent for CA. From the Fukui function indices and the σ-profile curves, it has been found that the CA molecule exhibited a high electrophilicity and a strong HBD tendency. Additionally, the strong HBA character of DDBAC as filler combined with the HBD character of $PD_{10}CA$ elastomer create an excellent dynamic between the filler and the prepared $PD_{10}CA$ matrix, which was demonstrated through the low mixing energy and the low FLORY-HUGGINS parameter of the composite.

Based on the theoretical calculations, it was found that DDBAC-based HESs may be considered as potential solvents for PDCAs with antimicrobial properties. Nonetheless, we believe that an experimental study aimed at estimating the antimicrobial activity of the DDBAC embedded $PD_{10}CA$ composite films is of paramount importance in order to drive the HES-assisted PDCA synthesis towards an industrial reality enabling their use in various applications such as food tray coating to slower the decomposition of food and thus, ensure longer conservation time.

Appendix

Appendix

Table A.1. Fukui indices of CA.

Atom	$f^{(-)}$	$f^{(+)}$	$\Delta f = f^{(+)} - f^{(-)}$	Atom	$f^{(-)}$	$f^{(+)}$	$\Delta f = f^{(+)} - f^{(-)}$
C (1)	0.015	0.01	-0.005	O (12)	0.009	0.052	0.043
C (2)	-0.011	-0.01	0.001	O (13)	0.209	0.037	-0.172
C (3)	-0.032	-0.011	0.021	H (14)	0.042	0.029	-0.013
C (4)	0.001	-0.007	-0.008	H (15)	0.044	0.034	-0.01
C (5)	0.006	0.117	0.111	H (16)	0.038	0.047	0.009
C (6)	0.08	0.169	0.089	H (17)	0.045	0.056	0.011
O (7)	0.100	0.032	-0.068	H (18)	0.022	0.012	-0.01
O (8)	0.027	0.013	-0.014	H (19)	0.045	0.042	-0.003
O (9)	0.202	0.141	-0.061	H (20)	0.014	0.033	0.019
O (10)	0.059	0.061	0.002	H (21)	0.043	0.022	-0.021
O (11)	0.041	0.123	0.082				

Table A.2. Fukui indices of DDBAC.

Atom	$f^{(-)}$	$f^{(+)}$	$\Delta f = f^{(+)} - f^{(-)}$	Atom	$f^{(-)}$	$f^{(+)}$	$\Delta f = f^{(+)} - f^{(-)}$
Cl (1)	0.727	0.008	-0.719	H (32)	0.023	0.011	-0.012
N (2)	-0.014	-0.023	-0.009	H (33)	0.021	0.011	-0.01
C (3)	0.005	-0.011	-0.016	H (34)	0.023	0.016	-0.007
C (4)	-0.009	-0.007	0.002	H (35)	0.023	0.013	-0.01
C (5)	-0.008	0.016	0.024	H (36)	0.004	0.002	-0.002
C (6)	-0.003	0.000	0.003	H (37)	0.005	0.002	-0.003
C (7)	0.000	0.001	0.001	H (38)	0.002	0.001	-0.001
C (8)	-0.003	-0.01	-0.007	H (39)	0.002	0.001	-0.001
C (9)	-0.002	-0.001	0.001	H (40)	0.001	0.000	-0.001
C (10)	-0.001	0.000	0.001	H (41)	0.001	0.000	-0.001
C (11)	-0.006	0.096	0.102	H (42)	0.001	0.000	-0.001
C (12)	-0.001	0.000	0.001	H (43)	0.000	0.000	0.000
C (13)	0.000	0.000	0.000	H (44)	0.000	0.000	0.000
C (14)	0.000	0.000	0.000	H (45)	0.000	0.000	0.000
C (15)	0.001	0.064	0.063	H (46)	0.004	0.064	0.06
C (16)	0.000	0.070	0.070	H (47)	0.003	0.061	0.058
C (17)	0.000	0.000	0.000	H (48)	0.000	0.000	0.000
C (18)	0.003	0.054	0.051	H (49)	0.000	0.000	0.000
C (19)	0.003	0.050	0.047	H (50)	0.003	0.061	0.058
C (20)	0.003	0.148	0.145	H (51)	0.003	0.060	0.057
C (21)	0.000	0.000	0.000	H (52)	0.003	0.076	0.073
H (22)	0.033	0.012	-0.021	H (53)	0.000	0.000	0.000
H (23)	0.009	0.010	0.001	H (54)	0.000	0.000	0.000
H (24)	0.014	0.009	-0.005	C (55)	0.000	0.000	0.000
H (25)	0.022	0.005	-0.017	C (56)	0.000	0.000	0.000
H (26)	0.012	0.045	0.033	H (57)	0.000	0.000	0.000
H (27)	0.015	0.048	0.033	H (58)	0.000	0.000	0.000
H (28)	0.011	0.005	-0.006	H (59)	0.000	0.000	0.000
H (29)	0.010	0.004	-0.006	H (60)	0.000	0.000	0.000
H (30)	0.027	0.015	-0.012	H (61)	0.000	0.000	0.000
H (31)	0.026	0.014	-0.012				

Table A.3. Fukui indices of $D_{10}DO$.

Atom	$f^{(-)}$	$f^{(+)}$	$\Delta f = f^{(+)} - f^{(-)}$	Atom	$f^{(-)}$	$f^{(+)}$	$\Delta f = f^{(+)} - f^{(-)}$
C (1)	-0.009	0.000	0.009	H (18)	0.018	0.025	0.007
C (2)	-0.009	-0.071	-0.062	H (19)	0.014	0.009	-0.005
C (3)	-0.004	-0.007	-0.003	H (20)	0.014	0.008	-0.006
C (4)	-0.003	-0.005	-0.002	H (21)	0.012	0.004	-0.008
C (5)	-0.002	-0.002	0.000	H (22)	0.012	0.006	-0.006
C (6)	-0.002	-0.001	0.001	H (23)	0.012	0.003	-0.009
C (7)	-0.003	-0.001	0.002	H (24)	0.012	0.002	-0.010
C (8)	-0.004	0.000	0.004	H (25)	0.014	0.002	-0.012
C (9)	-0.009	-0.001	0.008	H (26)	0.014	0.001	-0.013
C (10)	-0.008	0.000	0.008	H (27)	0.019	0.001	-0.018
O (11)	0.210	-0.002	-0.212	H (28)	0.018	0.001	-0.017
O (12)	0.210	-0.198	-0.408	H (29)	0.036	0.001	-0.035
H (13)	0.043	0.048	0.005	H (30)	0.031	0.002	-0.029
H (14)	0.071	0.129	0.058	H (31)	0.072	0.002	-0.070
H (15)	0.036	0.036	0.000	H (32)	0.043	0.001	-0.042
H (16)	0.031	0.146	0.115	H (33)	0.046	0.008	-0.038
H (17)	0.019	0.021	0.002	H (34)	0.045	0.833	0.788

Table A.4. Fukui indices of HES.

Atom	$f^{(-)}$	$f^{(+)}$	$\Delta f = f^{(+)} - f^{(-)}$	Atom	$f^{(-)}$	$f^{(+)}$	$\Delta f = f^{(+)} - f^{(-)}$
C (1)	-0.008	-0.001	0.007	H (83)	0.023	0.001	-0.022
C (2)	-0.001	0.000	0.001	H (84)	0.019	0.000	-0.019
C (3)	-0.001	0.000	0.001	H (85)	0.009	0.000	-0.009
C (4)	-0.001	0.000	0.001	H (86)	0.01	0.000	-0.01
C (5)	0.000	0.000	0.000	H (87)	0.005	0.000	-0.005
C (6)	0.000	0.000	0.000	H (88)	0.005	0.000	-0.005
C (7)	0.000	0.000	0.000	H (89)	0.003	0.000	-0.003
C (8)	0.000	0.000	0.000	H (90)	0.003	0.000	-0.003
C (9)	0.000	0.000	0.000	H (91)	0.002	0.000	-0.002
C (10)	0.000	0.000	0.000	H (92)	0.002	0.000	-0.002
O (11)	0.000	0.000	0.000	H (93)	0.001	0.000	-0.001
O (12)	0.024	0.000	-0.024	H (94)	0.001	0.000	-0.001
H (13)	0.018	0.001	-0.017	H (95)	0.001	0.000	-0.001
H (14)	0.014	0.001	-0.013	H (96)	0.001	0.000	-0.001
H (15)	0.010	0.001	-0.009	H (97)	0.000	0.000	0.000
H (16)	0.006	0.000	-0.006	H (98)	0.000	0.000	0.000
H (17)	0.004	0.000	-0.004	H (99)	0.000	0.000	0.000
H (18)	0.004	0.000	-0.004	H (100)	0.000	0.000	0.000
H (19)	0.002	0.000	-0.002	H (101)	0.000	0.000	0.000
H (20)	0.002	0.000	-0.002	H (102)	0.030	0.006	-0.024
H (21)	0.001	0.000	-0.001	Cl(103)	0.276	0.002	-0.274
H (22)	0.001	0.000	-0.001	N (104)	-0.002	-0.021	-0.019
H (23)	0.001	0.000	-0.001	C (105)	0.008	-0.007	-0.015
H (24)	0.001	0.000	-0.001	C (106)	-0.003	-0.008	-0.005
H (25)	0.000	0.000	0.000	C (107)	-0.003	0.028	0.031
H (26)	0.000	0.000	0.000	C (108)	-0.001	-0.001	0.000
H (27)	0.000	0.000	0.000	C (109)	-0.002	-0.004	-0.002
H (28)	0.000	0.000	0.000	C (110)	-0.001	-0.010	-0.009
H (29)	0.000	0.000	0.000	C (111)	-0.001	-0.001	0.000
H (30)	0.000	0.000	0.000	C (112)	-0.001	-0.001	0.000
H (31)	0.000	0.000	0.000	C (113)	0.003	0.083	0.080
H (32)	0.000	0.000	0.000	C (114)	0.000	0.000	0.000
H (33)	0.000	0.000	0.000	C (115)	0.000	0.000	0.000
H (34)	0.008	0.001	-0.007	C (116)	0.000	0.000	0.000
C (35)	0.000	0.000	0.000	C (117)	0.004	0.057	0.053
C (36)	0.000	0.000	0.000	C (118)	-0.011	0.08	0.091
C (37)	0.000	0.000	0.000	C (119)	0.000	0.000	0.000
C (38)	0.000	0.000	0.000	C (120)	0.004	0.064	0.060
C (39)	0.000	0.000	0.000	C (121)	0.000	0.028	0.028
C (40)	-0.001	0.000	0.001	C (122)	0.000	0.126	0.126
C (41)	-0.002	0.000	0.002	C (123)	0.000	0.000	0.000
C (42)	-0.004	-0.002	0.002	H (124)	-0.009	-0.005	0.004
C (43)	-0.007	0.001	0.008	H (125)	0.015	0.019	0.004
C (44)	-0.016	-0.001	0.015	H (126)	0.012	0.011	-0.001

O (45)	0.131	0.002	-0.129	H (127)	0.007	0.006	-0.001
O (46)	0.000	0.000	0.000	H (128)	0.004	0.052	0.048
H (47)	0.000	0.000	0.000	H (129)	0.005	0.042	0.037
H (48)	0.000	0.000	0.000	H (130)	0.006	0.004	-0.002
H (49)	0.000	0.000	0.000	H (131)	0.006	0.006	0.000
H (50)	0.000	0.000	0.000	H (132)	0.005	0.015	0.010
H (51)	0.000	0.000	0.000	H (133)	0.004	0.015	0.011
H (52)	0.000	0.000	0.000	H (134)	0.004	0.017	0.013
H (53)	0.001	0.000	-0.001	H (135)	-0.004	0.003	0.007
H (54)	0.001	0.000	-0.001	H (136)	0.007	0.018	0.011
H (55)	0.001	0.000	-0.001	H (137)	0.006	0.021	0.015
H (56)	0.001	0.000	-0.001	H (138)	0.004	0.002	-0.002
H (57)	0.002	0.000	-0.002	H (139)	0.002	0.002	0.000
H (58)	0.002	0.000	-0.002	H (140)	0.001	0.001	0.000
H (59)	0.004	0.001	-0.003	H (141)	0.001	0.001	0.000
H (60)	0.004	0.001	-0.003	H (142)	0.001	0.001	0.000
H (61)	0.007	0.001	-0.006	H (143)	0.001	0.000	-0.001
H (62)	0.006	0.000	-0.006	H (144)	0.000	0.000	0.000
H (63)	0.016	0.002	-0.014	H (145)	0.000	0.000	0.000
H (64)	0.019	0.002	-0.017	H (146)	0.000	0.000	0.000
H (65)	0.034	0.002	-0.032	H (147)	0.000	0.000	0.000
H (66)	0.048	-0.003	-0.051	H (148)	0.004	0.065	0.061
H (67)	0.018	0.000	-0.018	H (149)	0.006	0.058	0.052
H (68)	0.000	0.000	0.000	H (150)	0.000	0.000	0.000
C (69)	-0.017	-0.001	0.016	H (151)	0.000	0.000	0.000
C (70)	-0.005	0.000	0.005	H (152)	0.004	0.066	0.062
C (71)	-0.002	0.000	0.002	H (153)	0.006	0.063	0.057
C (72)	-0.002	0.000	0.002	H (154)	0.004	0.08	0.076
C (73)	-0.001	0.000	0.001	H (155)	0.000	0.000	0.000
C (74)	0.000	0.000	0.000	H (156)	0.000	0.000	0.000
C (75)	0.000	0.000	0.000	C (157)	0.000	0.000	0.000
C (76)	0.000	0.000	0.000	C (158)	0.000	0.000	0.000
C (77)	0.000	0.000	0.000	H (159)	0.000	0.000	0.000
C (78)	0.000	0.000	0.000	H (160)	0.000	0.000	0.000
O (79)	0.001	0.000	-0.001	H (161)	0.000	0.000	0.000
O (80)	0.121	0.000	-0.121	H (162)	0.000	0.000	0.000
H (81)	0.032	0.001	-0.031	H (163)	0.000	0.000	0.000
H (82)	0.038	0.001	-0.037				

120

الملخص:

تم تصميم المذيبات سهلة الانصهار حسابيًا (*In-silico*) باستخدام مجموعات من ثلاثة أملاح أمونيوم رباعي (رباعي ميثيل كلوريد الأمونيوم (TMAC) وكلوريد الكولين (ChCl) و(البيتايين) كمستقبلات رابطة الهيدروجين (HBAs) مع (السوربيتول ، الجلسرين ، اليوريا ، الإيثيلين جلايكول ، الجلوكوز، حمض الخليك، حمض الكافيين و 1،2-بيوتانيديول) المانحة لرابطة الهيدروجين (HBDs). تم التنبؤ بآليات التفاعل بين HBAs و HBDs و تم حساب طاقات التفاعل عن طريق نموذج الفرز الشبيه بالموصل لنظرية المذيبات الحقيقية (COSMO-RS). أظهرت النتائج أن نظام الاقتران الأنسب هو البيتايين : حمض الكافيك، والذي يقدم أقوى التفاعلات الجزيئية.

بعد ذلك، أجريت دراسة نظرية على المكونات المشاركة في التخليق الأخضر لبوليستر بولي (ديكان-سيترات) (PD₁₀CA). تتضمن العملية كلوريد دوديسيلدي ميثيل بنزيل أمونيوم (DDBAC) كمكون HBA من DES، مع 1،10 - ديكانيديول مثل HBD (مونومر) و حمض الستريك كمونومر مشترك. بعد البلمرة، كان DDBAC بمثابة مادة مالئة. تم تنفيذ التفاعلات الجزيئية بين مكونات DES (HBA و HBD) وحمض الستريك في DES ، و DDBAC مع PD₁₀CA ، والخصائص الفيزيائية والكيميائية للبوليمر باستخدام نظرية COSMO-RS و DFT داخل برنامج .COSMO*therm* أظهرت النتائج أن تفاعل DDBAC مع DDO و PD₁₀CA مع DDBAC هو بشكل أساسي روابط VAN DER WAALS ، بينما يتفاعل CA بشكل أساسي من خلال الترابط H . تؤكد هذه التفاعلات أيضًا الاقتران المناسب لـ HBA-HBD ، وحشو المصفوفة ، والمذيب المذاب ، على التوالي.

الكلمات المفتاحية :

المذيبات المنصهرة بعمق، التخليق الأخضر، البلمرة، الأسترة، مفعول مضاد للبكتيريا.

Abstract:

Deep eutectic solvents (DESs) were computationally designed (*in-silico*) using combinations of three quaternary ammonium salts (tetramethyl ammonium chloride (TMAC), choline chlorine (ChCl) and betaine) as hydrogen-bond acceptors (HBAs) with (sorbitol, glycerol, urea, ethylene glycol, glucose, acetic-acid, caffeic acid and 1,2-butanediol) hydrogen-bond donors (HBDs). The interaction mechanisms between the HBAs and HBDs were predicted and interaction energies were calculated by means of Conductor-like Screening Model for Real Solvents (COSMO-RS) theory. The results showed that the most appropriate pairing system was Betaine: Caffeic acid DES, presenting the strongest molecular interactions.

Then, a theoretical study was conducted on the components involved in the green synthesis of poly(1,10-decane-citrate) polyester ($PD_{10}CA$). The process involves dodecyldimethylbenzylamonium chloride (DDBAC) as HBA component of the DES, with 1,10-decanediol as HBD (monomer) and citric acid as co-monomer. After polymerization, the DDBAC served as filler. The molecular interactions between the DES components (HBA and HBD), citric acid in the DES, and DDBAC with $PD_{10}CA$, and the polymerphysicochemical properties were implemented *in-silico* using COSMO-RS and DFT program within COSMO*therm* software. The results showed that the interaction of DDBAC with DDO, and $PD_{10}CA$ with DDBAC, are mainly VAN DER WAALS' bonds, while CA interacts mainly through H-bonding. These interactions also confirm the appropriate pairing of HBA-HBD, matrix-filler, and solvent-solute, respectively.

Keywords:

Résumé:

Des solvants eutectiques profonds (SEP) ont été conçus par ordinateur (*in-silico*) en utilisant des combinaisons de trois sels d'ammonium quaternaire (chlorure de tétraméthylammonium (TMAC), chlorure choline (ChCl) et bétaïne) comme accepteurs de liaisons hydrogènes (notés HBA) avec huit donneurs de liaison hydrogène (sorbitol, glycérol, urée, éthylène glycol, glucose, acide acétique, acide caféique et 1,2-butanediol) (HBD). Les mécanismes d'interaction entre les HBA et les HBD ont été prédits et les énergies d'interactions ont été calculées au moyen de la théorie du modèle de criblage de type conducteur pour les solvants réels (COSMO-RS). Les résultats ont montré que le système d'appariement le plus approprié était (la bétaïne : acide caféique) présentant les interactions moléculaires les plus fortes.

Ensuite, une étude théorique a été menée sur les composants impliqués dans la synthèse verte du poly(1,10-décanediol-citrate) ($PD_{10}CA$). Le procédé implique le chlorure de dodécyldiméthylbenzylamonium (DDBAC) comme composant HBA du DES, avec le 1,10-décanediol comme HBD (monomère) et l'acide citrique comme co-monomère. Après polymérisation, le DDBAC a servi de charge conférant au polymère une activité bactéricide. Les interactions moléculaires entre les composants des SEP (HBA et HBD), l'acide citrique dans le SEP, et le DDBAC avec $PD_{10}CA$, et les propriétés physicochimiques du polymère ont été implémentées *in silico* à l'aide de la théorie COSMO-RS et DFT en utilisant le logiciel COSMO*therm*. Les résultats ont montré que l'interaction du DDBAC avec le DDO, et du $PD_{10}CA$ avec le DDBAC, sont principalement des liaisons de VAN DER WAALS, tandis que CA interagit principalement par liaison H. Ces interactions confirment également l'appariement approprié de HBA-HBD, matrice-charge et solvant-soluté, respectivement.

Mots-clés:

Solvant eutectique profond, Synthèse verte, Polyestérification, activité anti-bactérienne.